

EVOLUTION OF TALC- AND CARBONATE-BEARING ALTERATIONS IN
ULTRAMAFIC ROCKS ON LEKA (CENTRAL NORWAY)

MASTER OF SCIENCE THESIS

ANDERS BJERGA



Department of Earth Science

University of Bergen

February 2014

“If you free yourself from the conventional reaction to a quantity like a million years, you free yourself a bit from the boundaries of human time. And then in a way you do not live at all, but in another way you live forever.”

- John McPhee

ABSTRACT

The thesis focuses on several low-angle fracture zones within the ultramafic section of the Leka Ophiolite Complex, central Norway, along which the original lithology has been completely serpentinized and carbonated. The alteration zones have a core made up of talc-carbonate bearing rocks surrounded by serpentine-carbonate bearing rocks with a sharp contact towards the country rock peridotites. Mineral assemblages of the alterations are controlled by the temperature, pressure, X_{CO_2} and the chemical composition of the protolith. The study is based on petrographic and geochemical analysis of samples from three different alteration zones. To assess the metamorphic evolution of the study area, forward modeling has been carried out using the thermodynamic software *Perple_X*. Modeling of mineral equilibrium in the $SiO_2 - MgO - FeO - Fe_2O_3 - CaO - H_2O - CO_2$ system is used to constrain the conditions during complete serpentinization and carbonation of partly altered peridotites. Conditions during alteration of the country rock peridotites was constrained in the $SiO_2 - MgO - FeO - Fe_2O_3 - CaO - H_2O$ system.

The partly altered peridotites consist of the mineral assemblage olivine - clinopyroxene - serpentine - magnetite - brucite and formed at temperatures $< 400^\circ C$ by infiltration of pure H_2O fluids. Completely serpentinized rocks with the mineral assemblage serpentine - magnesite - magnetite - dolomite formed at temperatures $< 510^\circ C$ and low X_{CO_2} (≤ 0.05) by the breakdown of the minerals in the partly altered peridotites. Talc-carbonate rocks formed at static conditions by the breakdown of the serpentine in the previously formed serpentinite rock to form the assemblage talc - magnesite - magnetite - dolomite at temperatures $< 550^\circ C$ and higher concentrations of X_{CO_2} . Carbon isotope values determined for dolomite from carbonate lenses within the talc-carbonate rock yield $\delta^{13}C$ values of ~ 5 , indicative of a mantle source for the carbon required for the carbonation. Oxygen isotope values $\delta_{SMOW}^{18}O$ of $\sim 10.8 - 11.3\text{‰}$ together with initial $^{87}Sr/^{86}Sr$ values between 0.7029 - 0.7063, suggest dehydration of rocks with mantle affinity as a source for the fluids.

The combination of radiogenic- and stable isotopes leads to the interpretation that the source of fluids for the hydration and carbonation of the peridotites is the dehydration of partly hydrated ultramafic rocks. The dehydration most likely occurred during the post-Caledonian extension in the Devonian. Assuming that the temperature conditions estimated for the formation of the talc-carbonate rocks represent minimum temperatures of the fluids at their origin, it is shown that the temperatures are high enough to trigger dehydration reactions of hydrous peridotites occurring in deeper parts of the ophiolite complex. The buoyant fluids could have moved up through the fracture network and reacted with the rocks at shallower depths. High pressure gradients during fluid flow may have resulted in enhanced permeability through hydrofracturing.

ACKNOWLEDGMENTS

I very much want to thank my supervisors Jiří Konopásek and Rolf Birger Pedersen from the University of Bergen for allowing me to learn and progress in my own way and tempo, and for excellent guidance along the way. I also want to thank Jiří for the opportunity I got to participate in the electron microprobe analysis in Brno, Czech Republic. I appreciate all the hours you have put into correcting my texts and giving me constructive feedback on my work. Rolf Birger Pedersen I want to thank for initiating the project, and his excellent knowledge of the geology in central Norway, and especially of the Leka Ophiolite Complex. I am also grateful for all the opportunities Rolf have given me during the master thesis through two cruises to the Jan Mayen and as an assistant during a geochemical field course. To both: I have learned a lot from our discussions and I am honored to have worked with you both.

Invaluable help was given by Irina Maria Dumitru in the making of the thin sections and in the preparation of the sample material for the chemical analysis. I appreciate all your help and your enthusiastic attitude. Yuval Ronen is appreciated for excellent guidance with the strontium isotope analysis and help with writing the sample preparation. Egil Erichsen was very helpful with the scanning electron microscope. Ole Tumyr is thanked for the XRF-analyses. I also want to thank Radek Škoda at the Masaryk University, Brno, for running the electron microprobe. Nicola McLoughlin is thanked for learning me how to take pictures with the petrographic microscope. I want to thank Jostein Hiller and Anne Brit Normann for their hospitality during my stay at Leka.

I also want to thank my fellow students at the University of Bergen. I especially want to thank Hallgeir Sirevaag for reading through, and giving valuable feedback on my field descriptions, and also for giving me invaluable help with \LaTeX . Karen Cecilie Johannessen was very helpful and read through my whole thesis, providing several improvements of the language. Kristian Agasøster Haaga is thanked for all the hours we spent in the basement of UiB, cutting and milling the samples.

All the people I have lived with during my years in Bergen is especially appreciated for their optimism and all the good times. It is a privilege to have so many good friends, and I want to thank you all.

My family is valued beyond measure. Kirsti, Brigit and Mette, thank you for helping and supporting me during my years in Bergen.

Bergen, 5 February 2014



Anders Bjerga

CONTENTS

1	INTRODUCTION	1
1.1	Aim	1
2	REGIONAL GEOLOGY	3
2.1	General Setting	3
2.2	Central Norway	3
2.3	Helgeland Nappe Complex	3
2.4	Post-Caledonian Extension	5
2.5	Leka Ophiolite Complex	6
2.5.1	General Geology	7
2.6	Relevant Lithologies	9
2.6.1	Mantle Tectonite	9
2.6.2	Layered Ultramafics	11
3	FIELD DESCRIPTIONS	13
3.1	Overview and Introduction	13
3.2	Partly Altered Peridotites	14
3.3	Alteration Zones	14
3.3.1	Serpentinite	18
3.3.2	Talc-Carbonate Rocks	18
3.4	Age Relations	19
4	METHODS	23
4.1	Fieldwork and Sampling	23
4.2	Petrographic Thin Sections	23
4.3	Major Element Analysis	24
4.3.1	Sample Preparation	24
4.4	Radiogenic Isotope Analysis	25
4.4.1	Chemical Separation and Analysis	25
4.5	Stable Isotope Analysis	25
4.6	Mineral Analysis	26
5	RESULTS	27
5.1	Sample Descriptions	27
5.1.1	Partly Altered Peridotites from the Mantle Tectonite	27
5.1.2	Partly Altered Peridotites from the Cumulate Section	30
5.1.3	Serpentinite	32
5.1.4	Talc-carbonate Group One	35
5.1.5	Talc-carbonate Group Two	39
5.2	Whole-Rock Geochemistry	39
5.2.1	Partly Altered Peridotites	39
5.2.2	Serpentinite	42
5.2.3	Talc-Carbonate Rocks	42
5.3	Stable Isotopes	43
5.4	Strontium Isotopes	43
6	METAMORPHIC EVOLUTION	45
6.1	Introduction and Background	45
6.1.1	General Assumptions	45

6.2	Thermodynamic Modeling of Partial Alteration of Peridotite	46
6.3	Thermodynamic Modeling of the Serpentinite Assemblage	48
6.4	Thermodynamic Modeling of Talc-Carbonate Group One	49
7	INTERPRETATION AND DISCUSSION	55
7.1	Geochemistry of the Alteration	55
7.2	Partly Altered Peridotites	55
7.3	Formation of Serpentinite	56
7.4	Conditions During Talc-Carbonate Alteration	57
7.5	Possible Fluid Sources	58
7.6	Evolution of the Alteration	59
8	CONCLUSIONS	67
	Appendices	82
A	MICROPROBE RESULTS	83
B	SAMPLE LOCALITIES	95

INTRODUCTION

Numerous bodies of ultramafic rocks have been observed within the Scandinavian Caledonides and most of these bodies have been mineralogically and/or texturally modified by metamorphism on the ocean-floor or during the Caledonian orogeny (e.g., Bucher, 1988). Serpentinization and carbonation of ultramafic rocks involve the replacement of anhydrous primary minerals such as olivine and clinopyroxene by serpentine, talc and carbonate minerals (e.g., magnesite, dolomite and calcite) in which H₂O and CO₂ are chemically bound within the crystal structure. The reactions are driven primarily by the instability of mineral assemblages with respect to the infiltrating fluids (O'Hanley, 1996; Bucher and Grapes, 2011). The metamorphic reactions associated with infiltration of fluids, thus represent a step wise conversion from thermodynamically unstable primary phases to a secondary, thermodynamically stable mineral assemblage (Giggenbach, 1981). The process of serpentinization and carbonation of ultramafic rocks has been studied extensively in a variety of tectonic settings (Naldrett, 1966; Griffiths, 1972; Barnes et al., 1973; Evans and Trommsdorff, 1974; Trommsdorff and Evans, 1974; Evans, 1977; Fyon et al., 1983; Bohlke, 1989; Pohl, 1990; Schandl and Naldrett, 1992; Halls and Zhao, 1995; Hansen et al., 2005; Robinson et al., 2005; Sântti et al., 2006; Lindahl and Nilsson, 2008; Escayola et al., 2009; Bedard and Escayola, 2010; Hövelmann et al., 2011; Klein and Garrido, 2010, 2011; Beinlich et al., 2012; Paukert et al., 2012; Klein and McCollom, 2013; Schwarzenbach et al., 2013).

After the early experimental works by Johannes (1967), Greenwood (1967) and Johannes (1969) to establish the reaction curves for the system MgO – SiO₂ – H₂O – CO₂, the application of equilibrium thermodynamics in retrieving information about temperature, pressure and fluid compositions associated with metamorphism of ultramafic rocks have been extensively utilized (c.f., Spear, 1995; Evans et al., 2013). In addition, a large amount of isotope studies on serpentinized and carbonated peridotites show that isotopic constraints provide a useful tool in interpreting the source of the fluids responsible for alteration (c.f., O'Hanley, 1996 and references therein). The carbon source is commonly the most difficult to constrain, and has typically been assigned to dehydration reactions of carbonate-bearing sediments, seawater or magmatic degassing (O'Hanley, 1996).

The presence of permeable zones that can act as pathways for altering fluids have been proposed to be one of the main factors controlling the amount of carbonation exerted to bodies of peridotite (Ash and Arksey, 1990; Halls and Zhao, 1995; Hansen et al., 2005; Escayola et al., 2009; Harlov and Austrheim, 2013; Schwarzenbach et al., 2013). During progressive metamorphism of hydrous rocks in the crust, a free fluid phase is formed through devolatilization reactions and the fluids can move upwards due to buoyancy (e.g., Connolly, 2010; Jamtveit and Austrheim, 2010). If more fluids are produced than can escape from the rock, the forces caused by the fluid pressure gradients can exceed the confining stress and the tensile strength. This can lead to hydrofracturing of the rocks, accompanied by an increase in the permeability of the rock subjected to fracturing (Spear, 1995; Flekkø y et al., 2002; Fossen, 2011).

1.1 AIM

The current study describes the petrological and chemical evolution of zones of completely serpentinized and carbonated peridotites located within the Leka Ophiolite Complex (LOC) cropping out on the island

of Leka, Nord-Trøndelag, Norway. The investigated rocks provide a fossil analogue to carbonation of ultramafic rocks in a hydrothermal system, and complement on a series of recent articles (Austrheim and Prestvik, 2008; Iyer et al., 2008a; Okland et al., 2012; Plümper et al., 2012) investigating alteration of the ultramafic rocks on Leka. Forward modeling of the observed mineral assemblages in the SiO_2 - MgO - FeO - Fe_2O_3 - CaO - H_2O - CO_2 system is used to constrain the temperature and composition of the infiltrating fluids. Field relationships combined with radiogenic and stable isotopic data are used to constrain the timing of the alteration and to elucidate possible fluid sources.

REGIONAL GEOLOGY

2.1 GENERAL SETTING

The Scandinavian Caledonides represent an Early Paleozoic collision belt comprising numerous north-south trending tectonic elements of different lithologies and origin that have been through a wide range of metamorphism and tectonic events (Roberts, 2003; Corfu et al., 2007). During the collision between Laurentia and Baltica, the Baltoscandian margin was subducted in a westward direction which have led to the presence of ultra-high pressure eclogite facies parageneses in the western part of the Western Gneiss Region (Griffin et al., 1985; Dobrzhinetskaya et al., 1995). The tectonic units have been grouped into four tectonostratigraphic groups based on their relative position in the nappe stack, namely: Lower, Middle, Upper and Uppermost Allochthon (Fig. 1; Roberts and Gee, 1985). The autochthonous basement consists of the Precambrian Baltic Shield covered by Late Precambrian to Ordovician sediments (Rey et al., 1997; Corfu et al., 2007). The Lower and Middle Allochthons are composed of sedimentary rocks that were deposited along the continental margin of Baltica, in addition to slices of Precambrian basement rocks (Stephens, 1988). The Upper Allochthon consist of medium to high-grade metasedimentary rocks overlain by low-grade ophiolites, island-arc magmatic rocks and sedimentary successions that may have been derived, in part, from the Laurentian side of the Iapetus (Stephens and Gee, 1985; Pedersen et al., 1988; Stephens and Gee, 1989; Roberts, 2003). The Uppermost Allochthon mainly comprise ophiolites, granitoids and metasediments (Stephens and Gee, 1985). Carbon and strontium chemostratigraphy of carbonate formations suggests that the Uppermost Allochthon are a fragment of Laurentian affinity (Melezhik et al., 2002; Roberts et al., 2002; Yoshinobu et al., 2002; Roberts et al., 2007; McArthur et al., 2013).

2.2 CENTRAL NORWAY

All four allochthonous nappes are present in the central Norway. The eastern part of central Norway consists of rocks with Baltic affinity belonging to the Lower and Middle allochthon, in addition to rocks that formed in the ancient Iapetus ocean, belonging to the Upper Allochthon (Stephens and Gee, 1985; Grenne et al., 1999; Roberts et al., 2002; Roberts, 2003; Barnes et al., 2007). The western part of central Norway is dominated by rocks formed in a continental-margin setting, making up the Uppermost Allochthon (Roberts et al., 2007). Correlation of meta-igneous, and metasedimentary rocks from Leka Ophiolite Complex (LOC) with rocks from similar islands (e.g., Rødøy and Boldvær; McArthur et al., 2013) suggests that the LOC, currently situated on an island exposed to the Atlantic Ocean (Fig. 1 A), belongs to the Sauren – Torghatten Nappe of the Helgeland Nappe Complex (HNC).

2.3 HELGELAND NAPPE COMPLEX

The Helgeland Nappe Complex is the structurally highest nappe complex of the Uppermost Allochthon in the northern central Scandinavian Caledonides, and consist of at least five poly-deformed nappe units that have not undergone ultra-high-pressure (UHP) metamorphism, separated by east-dipping

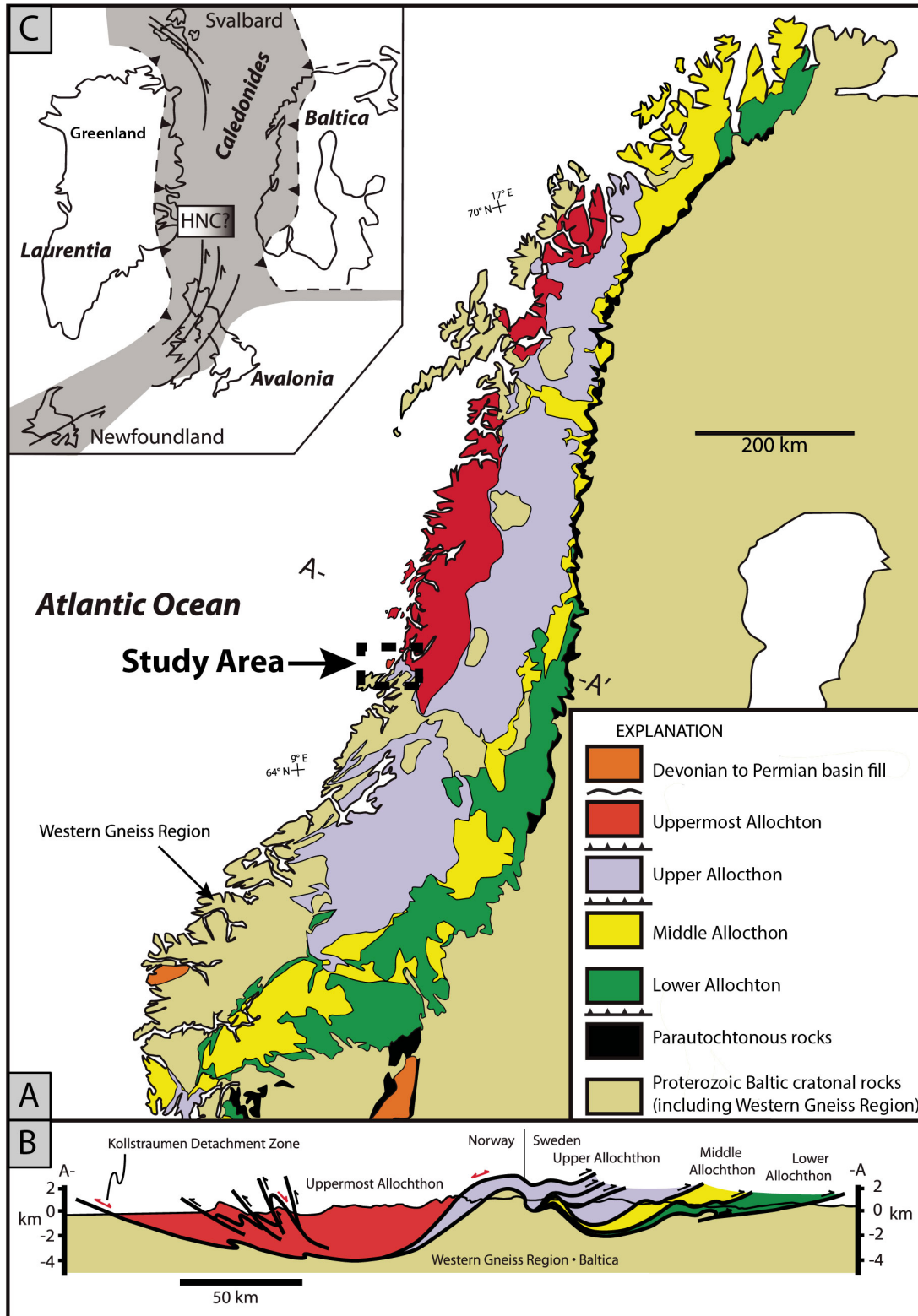


Fig. 1: A) Simplified tectonostratigraphical map displaying the major units of the Scandinavian Caledonides. The study area belongs to the Helgeland Nappe Complex (HNC) of the Uppermost allochthon and its location is marked (Gee and Sturt, 1985; Barnes et al., 2007; McArthur et al., 2013). Outboard terranes (Upper and Uppermost Allochthon) consists of oceanic-arc systems, metamorphic complexes and exotic continental crust. The Upper and Uppermost Allochthons are separated by major thrust faults. B) Simplified geological cross section across the central Caledonides along the profile A - A' marked in A), which outline the general structural style within the Uppermost Allochthon. C) Sketch map of the North-Atlantic Caledonides during the final convergence and collision of Laurentia, Baltica and Avalonia continental terranes in mid-Silurian time. Possible location of the rocks belonging to the HNC is marked. Modified from Barnes et al. (2007).

shear zones (Barnes et al., 2007; Nordgulen et al., 2008, 2011). Emplacement of the nappes occurred during the Silurian – Devonian phase of the Caledonian orogeny (Stephens and Gee, 1989; Thorsnes et al., 1991). The five nappes within the HNC, from structurally lowest to highest are the Horta nappe, Sauren-Torghatten, Lower, Middle and the Upper nappe. The nappes have been divided into two groups (c.f., McArthur et al., 2013) in which the first group (Lower and Upper nappe) consists of migmatitic gneisses, calc-silicate rocks and marbles with no exposed depositional basement (Thorsnes et al., 1991; Barnes et al., 2007). The second group consists of meta-conglomerates, marbles, calc-silicate schists and pelitic schists belonging to the Middle nappe and the Sauren-Torghatten nappe (Yoshinobu et al., 2002).

The nappes have generally undergone amphibolite facies metamorphism, as evident from the presence of migmatites (Barnes et al., 2007), and are discontinuously deposited on ultramafic and mafic rocks (Thorsnes et al., 1991; Heldal, 2001). All the nappes are intruded by plutonic rocks of varying composition. Some plutonic rocks that intrude the HNC have been dated to similar ages as regional migmatitic rocks, suggesting that they formed in the collisional stage (Reid, 2004).

2.4 POST-CALEDONIAN EXTENSION

In the Early Devonian, a change in the regional tectonic regime from a compressional setting to a tensional setting, led to widespread extensional tectonics in the western Caledonides (Fossen, 1992; Fossen and Rykkelid, 1992). Mica $^{40}\text{Ar}/^{39}\text{Ar}$ thermochronology of mylonites from the base of the Jotun Nappe Complex suggests that the transition from the Caledonian thrusting to the post-Caledonian orogenic collapse occurred between 408 and 402 Ma (Fig. 4 in; Fossen and Dunlap, 1998). This late- to post-orogenic extension of the Caledonian nappe stack led to significant movement along detachment zones, exhumation of high-pressure rocks and the formation of post-orogenic extensional basins (Fig. 1; Norton, 1986; Seranne and Seguret, 1987; Andersen and Jamtveit, 1990; Fossen, 1992; Fossen and Dunlap, 1998; Osmundsen et al., 1998; Fossen, 2000; Eide et al., 2005; Steltenpohl et al., 2009; Fossen, 2010; Nordgulen et al., 2011; Souche et al., 2012). Fossen (1992) recognized two types of orogenic extension in the southern Norway. In the early stages of the orogenic collapse, the deformation occurred as backsliding of the orogenic wedge along preexisting thrust sheets (Mode I extension; Fig. 2 B). The backsliding was followed by crustal collapse and the formation of high-angle listric faults (Mode II extension; Fig. 2 C).

In the central Norway, the extension led to denudation of metamorphic core-complexes in the footwalls of major extensional faults (Osmundsen et al., 2005). Braathen et al. (2000) suggested that the main structural style north for the Møre-Trøndelag fault zone have been domal uplift. Titus et al. (2002) noticed that the LOC is situated within a pull-apart geometry, and suggested that the exposed central Norway basement window to the north is bound by sinistral faults associated with the LOC, while the south side is bound by the margin-parallel Møre-Trøndelag fault zone (Fig. 3). The northern part of the central Norway basement window is bound by the Kollstraumen detachment (Fig. 3). Extensional movement of the Kollstraumen detachment is constrained by U-Pb ages of titanite and monazite from syn-extensional felsic dykes, and is inferred to have occurred after 402 – 401 Ma (Kendrick et al., 2004). Extensional movement on the opposing Høybakken detachment which display a well developed top-to-the WSW fabric, is indicated by hornblende and mica $^{40}\text{Ar}/^{39}\text{Ar}$ thermochronology ages of ~400 and 390 Ma, respectively (Kendrick et al., 2004).

The Devonian basins in western Norway are associated with low-to moderate angle normal faults (Osmundsen et al., 1998; Osmundsen and Andersen, 2001) and display a continuous section from undeformed sediments at the top to ductile shearing at the base involving both the Devonian metasediments and the basement rocks (Seranne and Seguret, 1987). Metamorphism of the Devonian

basins are interpreted to be synkinematic with the extensional tectonics (Seranne and Seguret, 1987; Seguret et al., 1989; Fossen, 2000; Souche et al., 2012).

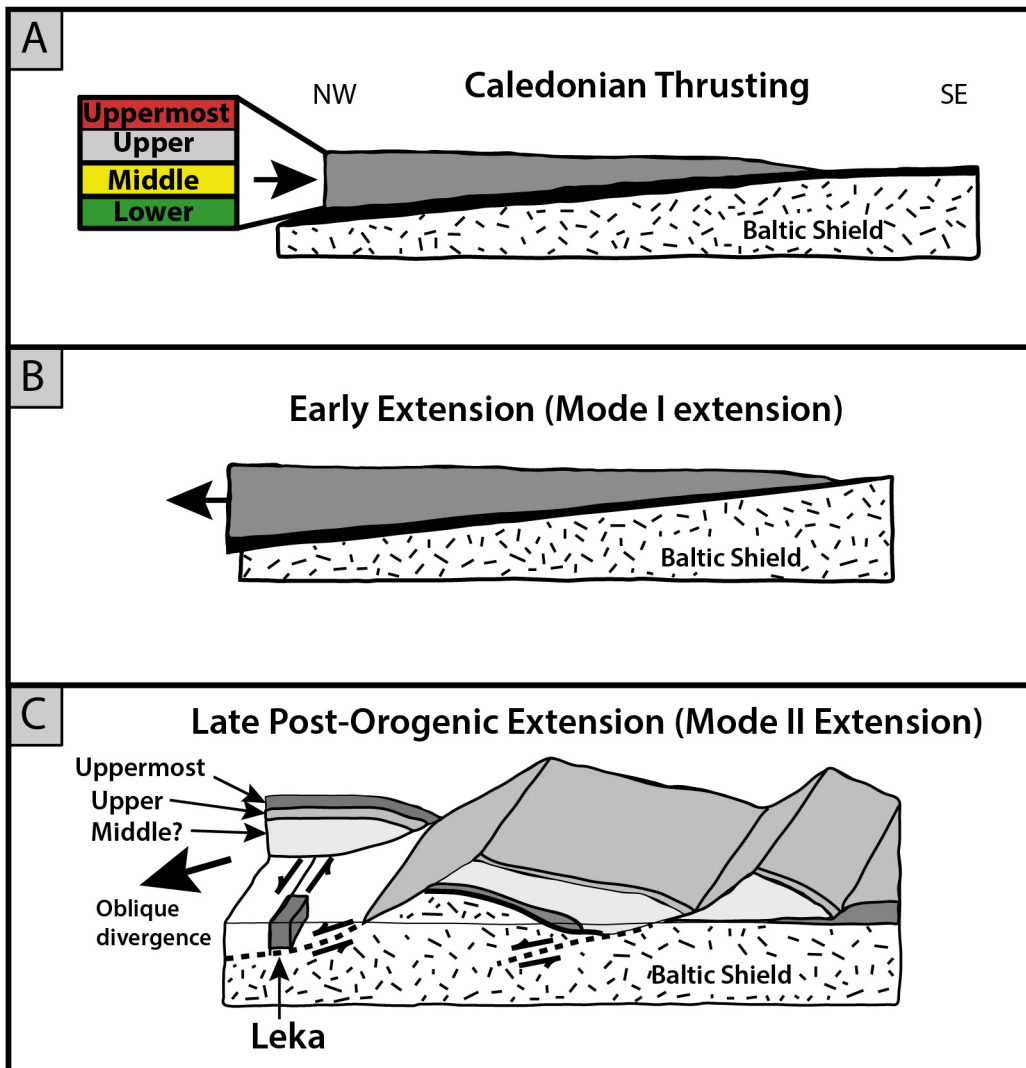


Fig. 2: Schematic drawing of the inferred development of the Scandinavian Caledonides. A) Thrusting of the Allochthons during continent–continent collision during the Scandian phase. B) Reactivation of thrust sheets during extension tectonics in Ordovician (Mode I extension), with backsliding of the orogenic wedge. C) Strike-slip partitioning during oblique divergence. Formation of high-angle, listric normal faults (mode II), with transcurrent motion occurring on cost-parallel strike-slip faults. Figure redrawn and modified from Titus et al., 2002 (from Fossen, 1992).

2.5 LEKA OPHIOLITE COMPLEX

The Leka Ophiolite Complex (LOC) is situated on the island of Leka (~90 km²), Nord-Trøndelag, Norway, north of the Western Gneiss Region and is a member of the oldest generation of ophiolites within the Norwegian Caledonides. The complex belongs to the Upper or Uppermost Allochthon of the Scandinavian Caledonides and has one of the largest, and best preserved ultramafic sections in Scandinavia (Prestvik, 1972; Furnes et al., 1988; Pedersen et al., 1988). U–Pb zircon dating of quartz–keratophyres (a leucocratic sodic felsic quartz–albite–phyric volcanic rock; Schermerhorn, 1973) from the upper plutonic zone of the LOC gave a crystallization age of 497 ± 2 Ma, which is similar to

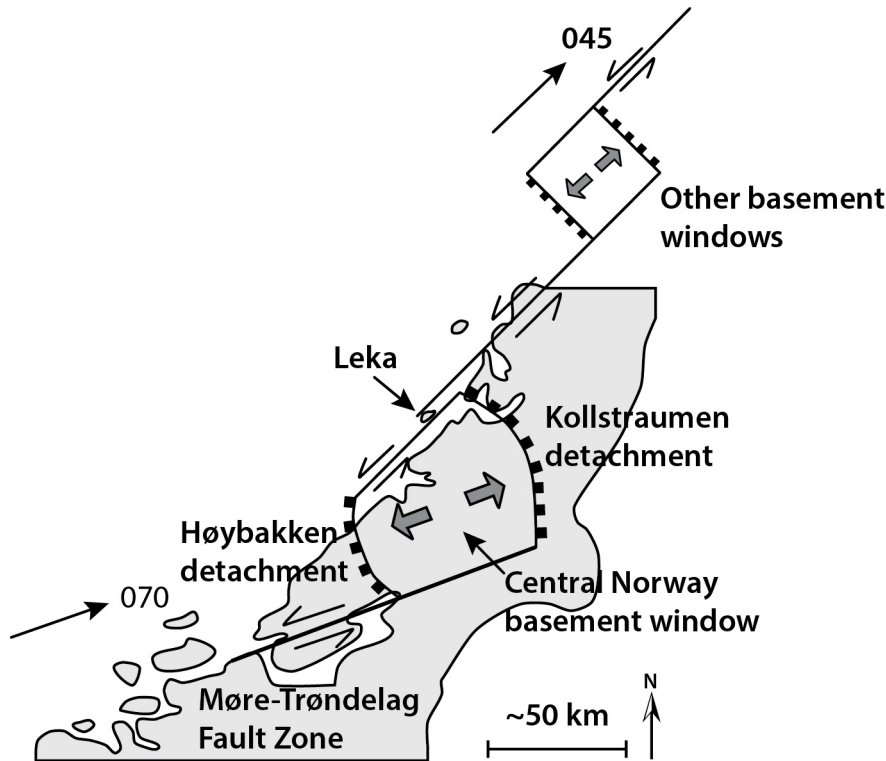


Fig. 3: Illustration showing the central Norway basement window bound by the Kollstraumen detachment and the Høybakken detachment. Braathen et al. (2000) have suggested that domal uplifting is responsible for the presence of basement gneisses north of the Møre-Trøndelag Fault Zone. Titus et al. (2002) suggests that the exposed central Norway basement window to the north is bound by sinistral faults associated with the LOC while the south side is bound by the margin-parallel Møre-Trøndelag fault zone. Redrawn after Titus et al. (2002).

the magmatic age of the Karmøy Ophiolite Complex (493 ± 7 Ma, southwestern Norway), Betts Cove (489 ± 3 Ma, Newfoundland, Canada) and Pipestone Pond-Coy Pond Complexes (Newfoundland; Dunning and Krogh, 1985; Dunning and Pedersen, 1988; Tollo, 2010).

On the basis of geochemical data, the inferred crystallization sequence (ol-sp-cpx-opx-pl) from the mantle cumulates, and the extensive serpentinization of the ultramafic rocks, it has been proposed that the evolution of the LOC started at a spreading ridge above a subduction zone and evolved towards an oceanic crust (Furnes et al., 1988; Dilek et al., 1998). Obduction and emplacement of the ophiolite complex probably occurred during the oblique convergence between Baltica and Laurentia during the Scandian phase (Roberts and Gee, 1985; Stephens and Gee, 1985; Roberts, 2003). The adjacent mainland mostly consists of structurally lower amphibolite-grade basement gneisses of the Northern Vestranden region, and the contact with the LOC is not exposed. Due to the lack of continuity between the gneisses and the LOC it has been proposed that the contact between these are tectonic (Furnes et al., 1988; Titus et al., 2002). Gravity measurements show that the ophiolite complex has a rhombochasm geometry with steep walls and a flat bottom currently located at a depth of ~6 – 7 km (Sindre and Pedersen, 1990; Titus et al., 2002).

2.5.1 General Geology

In the LOC all the principal components of a typical ophiolite can be observed, this includes a lower, strongly deformed harzburgite unit (representing the depleted upper mantle), ultramafic cumulates, layered metagabbros, metabasalt dykes and pillow lavas (Prestvik, 1980; Furnes et al., 1988). The

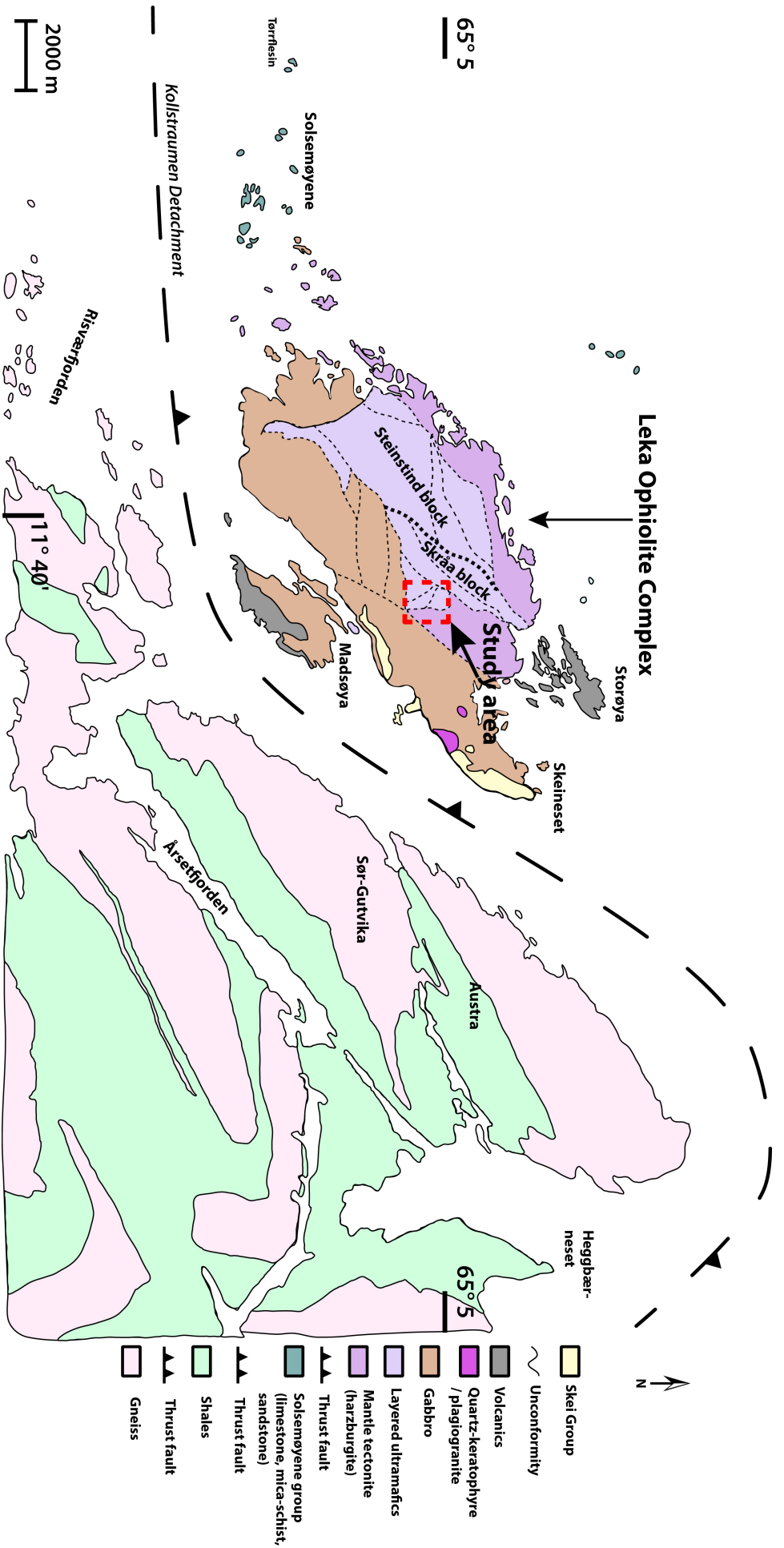


Fig. 4: Simplified geological map showing the regional geology and the Leka Ophiolite Complex (LOC) belonging to the Upper or Uppermost Allochthon of the Scandinavian Caledonides. Unconformably overlying the LOC is the sedimentary Skel group while layered ultramafics, mantle tectonites, gabbros and volcanic rocks make up the almost complete ophiolite sequence of the LOC. The Solsemøyene Group is found on islands to the west for the LOC, they are not associated with the ophiolite complex and their exact stratigraphic position is not known. Due to the lack of continuity between the nearby islands and the LOC, all the contacts have been interpreted as tectonic (Titus et al., 2002). Rocks from the adjacent mainland consists of shales and amphibolite-grade gneisses belonging to structurally lower positions (Middle Allochthon, Lower Allochthon and Parautochthon) within the Caledonian nappe stack and their contact to the LOC is interpreted as tectonic. The Kollstrømmen detachment zone is a regional, mainly ductile, late orogenic extensional shear zone that marks the termination of the central Norway basement window in the north (Braathen et al., 2000). The location of the study area is marked and a more detailed map is shown in Fig. 7. The figure is based on data from Furnes et al. (1988), Titus et al. (2002) and the geological survey of Norway.

structurally lowest part of the LOC is represented by the harzburgites, which are exposed in the northern part of the island where they are in tectonic contact with the metagabbros. Trace element analysis of pillow lavas and basalt dikes mainly shows Island Arc Tholeiitic (IAT) to Mid-Ocean Ridge Basalt (MORB) affinity, although rocks with Within-Plate Basalts (WPB) and boninitic affinity are also present (Furnes et al., 1988; Tveit, 1989).

The rocks at Leka have been weakly metamorphosed at greenschist facies, with some evidence of relic amphibolite facies minerals in the gabbroic rocks and in the mantle tectonite (Prestvik, 1972; Dunning and Pedersen, 1988; Albrektsen, 1990). During the Caledonian obduction, the mafic and ultramafic rocks were folded into two open synclines with several tight folds within the ultramafic units indicating moderate-scale ductile deformation (Dunning and Pedersen, 1988; Titus et al., 2002; Maaløe, 2005). Later brittle deformation has led to the formation of faults on different scales. Two distinct fault sets can be observed: NE-SW trending larger/longer faults and a NW-SE trending set with smaller/shorter faults (Titus et al., 2002). The largest faults have separated the LOC into different blocks (Fig. 4; Prestvik, 1972; Furnes et al., 1988).

A sedimentary succession consisting of conglomerates, sandstones, mica-schists and limestones named the Skei group lies unconformably on the metagabbros. The NW-SE trending faults observed within the gabbro are not observed in the Skei group, and it is inferred that the first orogenic events began prior to the sedimentation (Furnes et al., 1988). Sr and C isotopic compositions of marbles indicate deposition during Ordovician time (Barnes et al., 2007). An Ordovician age is also supported by detrital zircon data (McArthur, 2007 in Nordgulen et al., 2011). Zircon data from some cobbles in the Skei group are also similar to that of the Lower Nappe metasandstones, suggesting that some of the material making up the conglomerates could have been derived from the exposed Lower Nappe rocks (Barnes et al., 2007). The Skei Group has been folded and strongly deformed, as evident from markedly elongated pebbles in polymict conglomerate (Prestvik, 1974; Sturt et al., 1985).

2.6 RELEVANT LITHOLOGIES

Understanding the composition of the partly altered ultramafic rocks of the Leka Ophiolite Complex is crucial for the characterization of the alteration of these rocks. In the following sections, detailed description and geochemistry of peridotites from previous works are presented.

2.6.1 *Mantle Tectonite*

The mantle tectonite represents the lowest structural level exposed within the LOC and consists predominantly of harzburgites with dunite bodies of variable size and veins of pyroxenite (Fig. 5). Foliation in the harzburgite is imperfect and defined by 2–10 mm thick bands of aligned and/or flattened minerals. The harzburgite has a strong compositional banding, which is cut by dikes and veins of dunite and pyroxenite which underwent ductile deformation (Albrektsen, 1990; Albrektsen et al., 1991). In the lower part of the tectonite the orientation of the fabric in the harzburgite is variable due to the open folding of the rocks. Towards the cumulate section, structural features such as banding and foliation become increasingly parallel with the boundary to the cumulate layers (Furnes et al., 1988; Maaløe, 2005). The boundary between the harzburgite tectonite and the layered dunites is marked by an unconformity (Furnes et al., 1988).

Bands of clinopyroxenite and/or orthopyroxenite and olivine websterite commonly occur within the tectonite. These bands are unevenly distributed and mainly occur in the western part of the LOC. Towards the cumulate section, the harzburgite tectonite becomes progressively more dunitic in composition.

The contact between the cumulates and the tectonite is difficult to identify, but the appearance of chromite layers and variations in the Fo content of olivine crystals have been utilized to mark the transition (Furnes et al., 1988; Pedersen, 1992)

The mineral assemblages of the harzburgites from Lauvhatten mantle complex (defined by Albrektsen, 1990) consists of olivine, primary and secondary clinopyroxene, Cr-spinel, ferritchromite, magnetite and serpentine ± brucite/clinochlore (Albrektsen, 1990; Iyer et al., 2008a). Olivine composition range between Fo₈₈ and Fo₉₂ which are the common values for abyssal and alpine peridotites (Mackenzie, 1960; Green, 1964; Loney et al., 1971; Furnes et al., 1991; Arai, 1994). Olivine in dunites in the mantle tectonite shows marginally higher Fo compositions (Fo_{89–93}) than the country rock peridotites. Clinopyroxene composition is primarily Cr-rich diopside with CaO content ranging from ~20.4 to 24.4 wt.%, MgO from 16.7 – 23.6 wt.% and FeO in the range of 1.9 – 3.4 wt.% (Furnes et al., 1991).

Harzburgite tectonite, eastern part

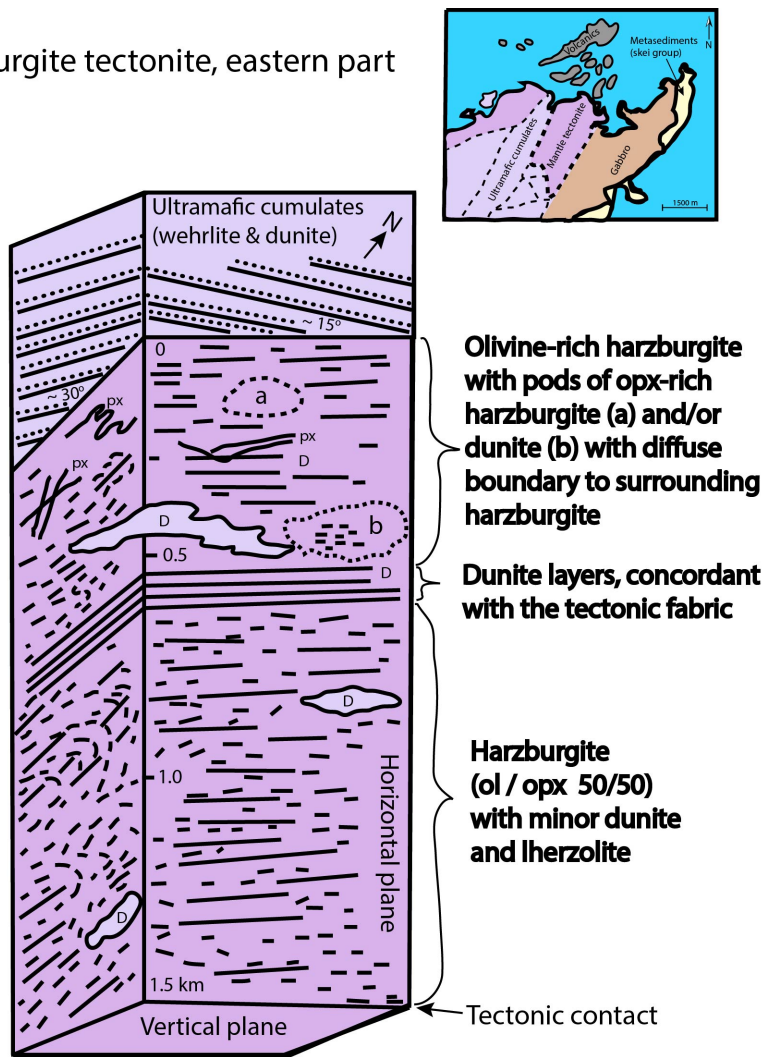


Fig. 5: Schematic illustration of internal lithological and structural relationships within the harzburgite tectonite and the relationship between the tectonite and the ultramafic cumulates. The thickness of the harzburgite tectonite is around 1.5 km. The inset map shows the area which the illustration is based upon. Important lithological and structural relationships observed are folded orthopyroxene veins, clinopyroxene veins and irregular bodies of dunite cutting the harzburgite tectonite and the typical fabric in the harzburgite tectonite (defined by flattened and/or stretched orthopyroxene crystals). Redrawn and modified after Furnes et al. (1988).

2.6.2 Layered Ultramafics

The layered series of the LOC consists of well preserved and exposed dunites, wehrlites and pyroxenites with sub-vertical layering (Fig.5). In the lower part of the layered series thick sub-zones (up to hundreds of meters wide) of olivine cumulates interlayered with similar sized zones of olivine-pyroxene cumulates dominate. Within some subzones, macrorhythmic units can be observed and these are defined by olivine adcumulates (i.e., ~100 – 93% accumulated magmatic crystals in a finer grained groundmass) at the base. In the macrorhythmic units, clinopyroxene and sporadically orthopyroxene appear upwards in the units and their content increase until it reaches cotectic proportions with olivine, although zones may also be incomplete (Pedersen et al., 1993). The macrorhythmic units are commonly enriched in chromite close to the base of the units and have been mapped laterally for nearly 3 km by Pedersen et al. (1993).

Within the dunites, meter sized lens-shaped pods of wehrlites are exposed (Iyer et al., 2008a). Locally, centimeter to tens of centimeter thick orthopyroxene dikes with variable orientation crosscut the dunites and wehrlites (Iyer et al., 2008a). The olivine in the dunite has a Mg-rich composition varying from Fo_{89} to Fo_{93} with clearly visible changes in the weathering color accompanying the compositional differences (Furnes et al., 1991; Pedersen et al., 1993).

Dunites are composed of olivine, serpentine \pm brucite, Cr-spinel and magnetite, while the wehrlites are made up of primary and secondary clinopyroxene, olivine, serpentine \pm brucite/clinocllore, Cr-Al spinel, ferritchromite and magnetite (Iyer et al., 2008a). Olivine composition in the layered ultramafics ranges from Fo_{84} to $Fo_{92.5}$ (Furnes et al., 1991; Pedersen et al., 1993). Clinopyroxene in the layered ultramafics has SiO_2 content between 51 – 55 wt.% and Al_2O_3 ranging from 1–5.5 wt.% (Furnes et al., 1991). The observed clinopyroxene composition plots in the diposide field of the pyroxene classification, and represents a cumulus phase coexisting with olivine with a Fo composition of 82–87. Phase calculations based on bulk-rock chemistry by Iyer et al. (2008a) indicates that orthopyroxene was a minor phase in the dunites.

FIELD DESCRIPTIONS

3.1 OVERVIEW AND INTRODUCTION

The study area (0.8 x 0.8 km) is located in the Skråa block of the Leka Ophiolite Complex, which comprises rocks from the cumulate section and is in tectonic contact with rocks from the mantle tectonites to the northeast (Fig. 7). All the rocks in the study area are serpentinized to variable degrees. Small chemical differences (see chapter 5) between the country rocks (i.e., mantle tectonite and cumulates) makes it convenient to label both as partly altered peridotites. In all of the exposed partly altered peridotites there are abundant low-angle fracture zones along which the original lithologies have been completely serpentinized and locally altered to talc-carbonate bearing rocks (Fig. 9). Because the weathering skin of the lithologies in the area is largely dependent on the mineral assemblage, it is in some places possible to observe pronounced color changes indicating a change in the mineral assemblage (marked with arrows in Fig. 6). The morphology of the field area is dominated by cliffs and hills, with excellent exposure of the rocks.

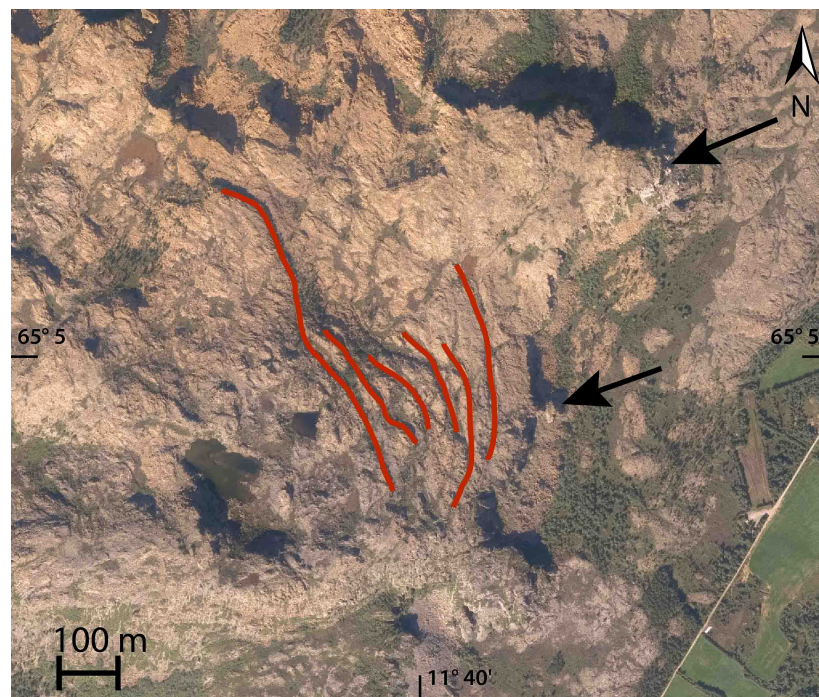


Fig. 6: Aerial photograph of the study area at Leka with macro-scale faults marked in red. Only the most obvious faults relevant to this study are included in this picture. The general direction for these faults is NW-SE. Noticeable color differences indicating changes in mineral assemblage are indicated by arrows.

3.2 PARTLY ALTERED PERIDOTITES

The study area consists of partly altered peridotites from the mantle tectonite representing the lowest structural level of the LOC and partly altered peridotites from the cumulate section (Fig. 4; Furnes et al., 1988; Albrektsen et al., 1991). All the peridotites have been serpentinized to various degrees (10–90%; Albrektsen, 1990; Pedersen et al., 1993; Iyer et al., 2008a) and are therefore referred to as partly altered peridotites. Partly altered peridotites from the cumulate section mainly composed of olivine, clinopyroxene and serpentine minerals (see chapter 5) make up most of the study area, while a small amount of partly altered peridotite from the mantle tectonite is exposed in the north-eastern part. The direct contact between the mantle cumulates and the mantle tectonite is not exposed in the field area and is inferred based on the appearance of chromite layers (Furnes et al., 1988; Pedersen et al., 1993).

The cumulate section consists of 10–30 meter thick zones of partly altered peridotite with mostly dunitic composition, interlayered with subzones consisting of partly altered peridotites and pyroxenites. Layers with gray weathering color (Fig. 8 A and B) are rich in clinopyroxene and identified as wehrlite and pyroxenites (Furnes et al., 1988). Macrorhythmic units composed of interlayered wehrlites, pyroxenites and peridotites are observed within the subzones. In the cumulate section, the olivine composition fluctuates between Fo_{85} to Fo_{93} which leads to a color difference in the weathering skin (Pedersen, 1992; Pedersen et al., 1993). Compositional layering in the field is commonly laterally continuous over a few meters (Fig. 8 C). Ductile folded, cross-cutting pyroxene veins are common in the partly altered peridotites (Fig. 8 D). Differential weathering has resulted in relief between the pyroxene-rich parts and the more olivine-rich parts. Locally, polygonal domains have formed in the pyroxene veins (Fig. 13 D). The formation of these domains has been assigned to serpentinization processes by Iyer et al. (2008b). They propose that the observed fracturing pattern is the result of the reaction-assisted fracturing due to volume change. Such reaction-assisted fracturing is supposed to enhance the rate of hydration by producing fresh reactive surfaces and new pathways for infiltrating fluids (Jamtveit et al., 2000; Fletcher et al., 2006). Local shear zones are observed within the partly altered peridotites (Fig. 8 F), these have been interpreted as post-dating the folding of the rocks. The partly altered peridotite from the cumulate section contains of disseminated grains of chromite and thin bands of chromite occur locally.

3.3 ALTERATION ZONES

A distinct set of large, sub-horizontal, NW-SE trending faults occurs within the partly altered peridotites, along which there is a macroscopically visible replacement of the original mineralogy (Fig. 9). The alteration zones are represented by rocks in which the mineral assemblages of the partly altered peridotites (olivine, clinopyroxene, serpentine, brucite and Cr-spinel) has been altered to serpentine, carbonate and talc (see chapter 5). The vertical thickness of the alteration zones is commonly in the range of 1 to 5 meters, but reaches up to 12 meters. The alteration has created sharp reaction fronts between the macroscopically altered rocks and the partly altered peridotites that can usually be followed laterally for meters to tens of meters (Fig. 9). The exposed rocks in the alteration zones show little evidence for any major deformation. The core of the alteration zone is made up of talc-carbonate rock symmetrically surrounded by layers of the carbonate bearing serpentinite. The serpentinite show sharp contacts with the talc-carbonate and the partly altered peridotites. A schematic drawing of the alteration zone is shown in Fig. 10.

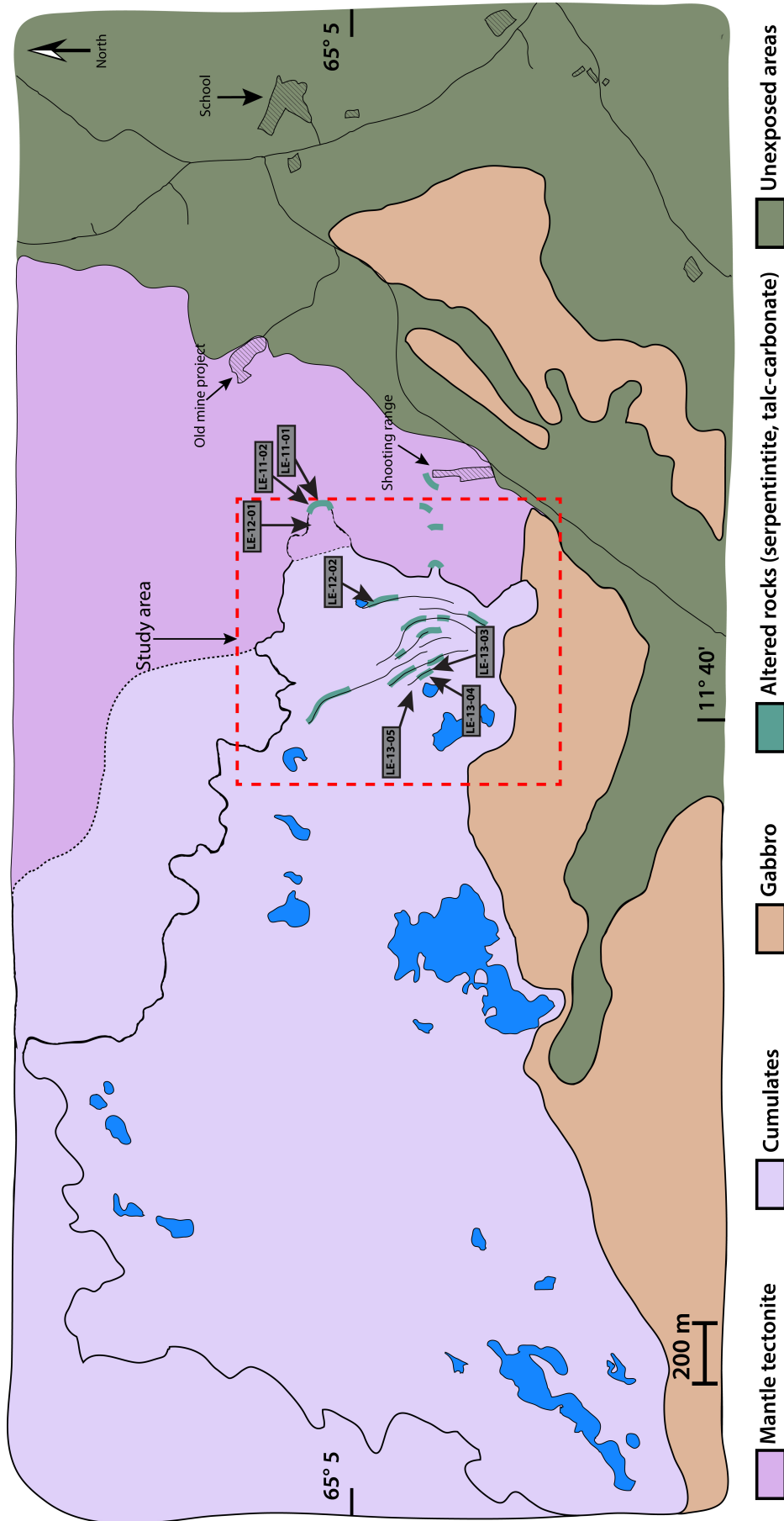


Fig. 7: Simplified geological map of the study area with sample locations. Localities where there is macroscopically visible alteration of the partly altered peridotites is marked. Formation of the talc-carbonate rocks and serpentinites are mainly observed within clearly visible fracture zones. The relevant macro-scale faults are marked within the study area. The contact between the partly altered peridotites from the mantle tectonite and the partly altered peridotites from the cumulate section are tectonic and marked by an unconformity.

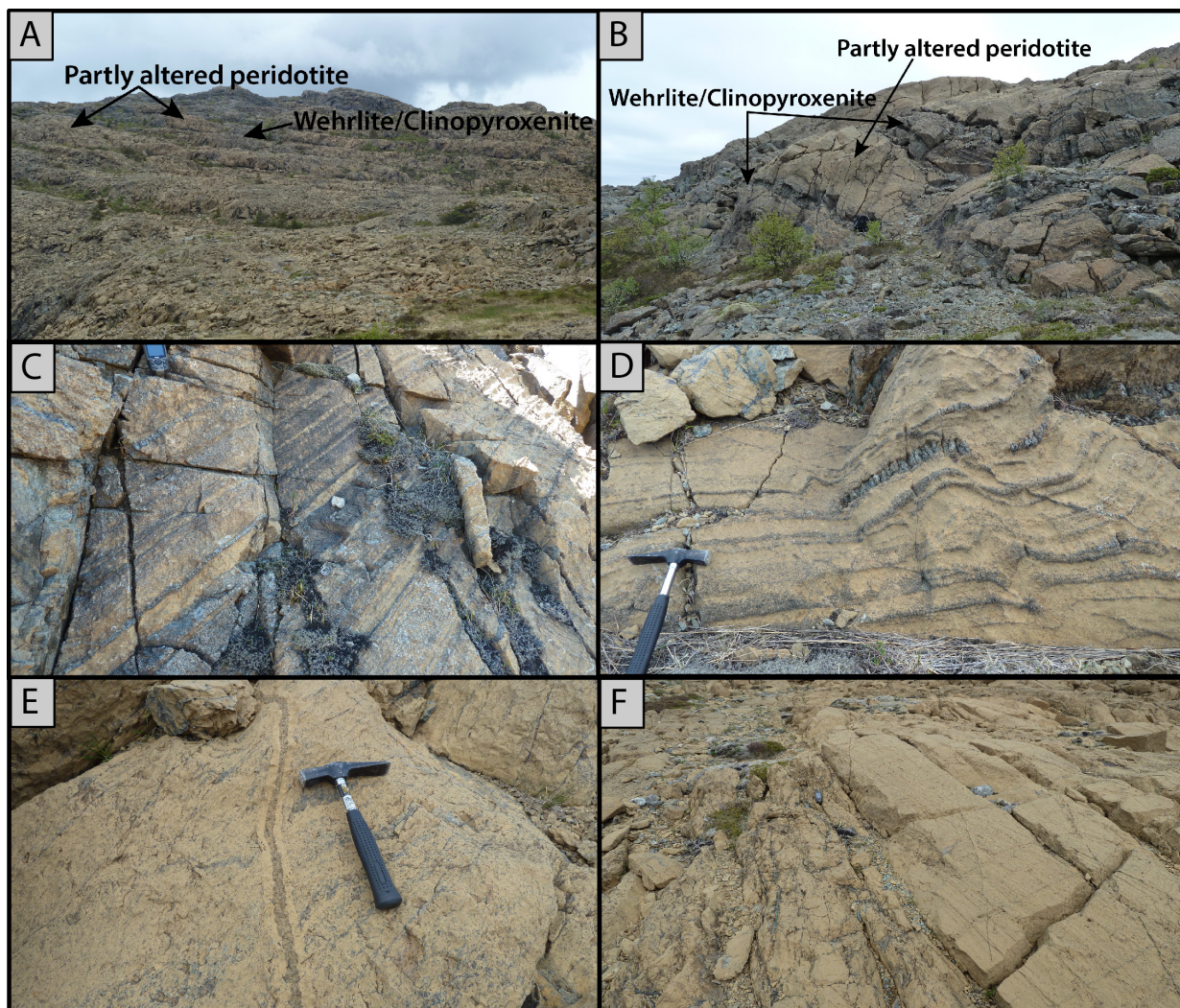


Fig. 8: A) Macrorhythmic layering of the rocks in the cumulate section. Lighter, yellowish areas are partly altered peridotites from the cumulate section, while gray areas consist of wehrlites, pyroxenites and lherzolites. B) Closer view of the macrorhythmic units with repeated successions of dunite, wehrlite and pyroxenites. The contact between the different units are generally sharp. C) Modal layering in the partly altered peridotites. The modal layering is defined by modal variations in olivine, clinopyroxene, orthopyroxene and chromite (Pedersen et al., 1993). Due to differential weathering of olivine (yellow weathering color) and serpentinized pyroxene, small topographic reliefs have been created between zones with higher and lower concentrations of olivine. D) Cross-cutting and folded pyroxene veins in the partly altered peridotites. These veins are a result of high-temperature, ductile shear deformation, possibly occurring in a late magmatic stage (Pedersen, 1992). E) Vein of dunite with a pyroxene-rich core. The foliation of the partly altered peridotite gradually disappears towards the vein. F) Local shear-zone in the partly altered peridotites from the cumulate section. Thin bands of chromite can be seen on the right-hand side of the shear-zone. Serpentinization appears to be more extensive in the shear-zone compared to the adjacent rocks.

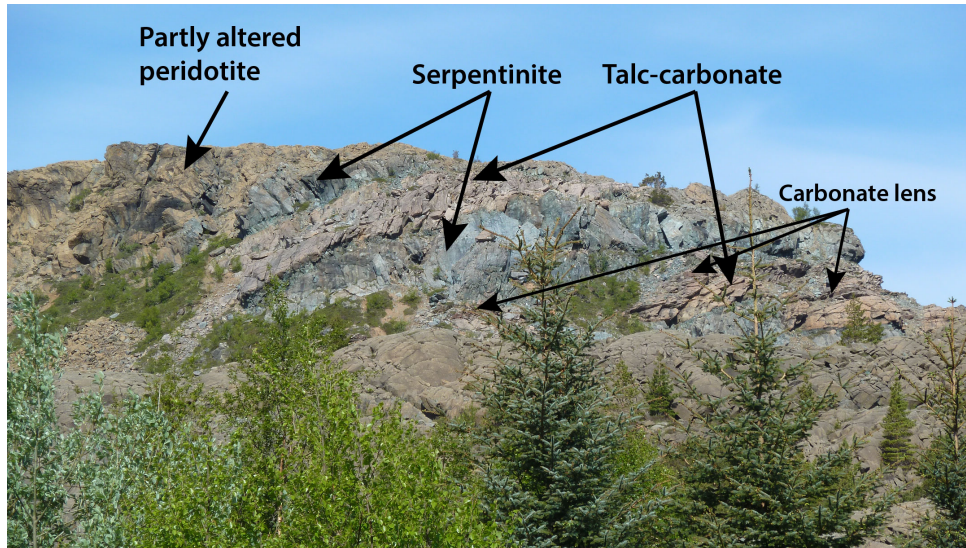


Fig. 9: Talc-carbonate rocks symmetrically surrounded by carbonate-bearing serpentinite. Sharp contacts are observed between the alteration zones and the partly altered peridotites. The carbonate lenses on the picture is ~0.5 - 1 m thick.

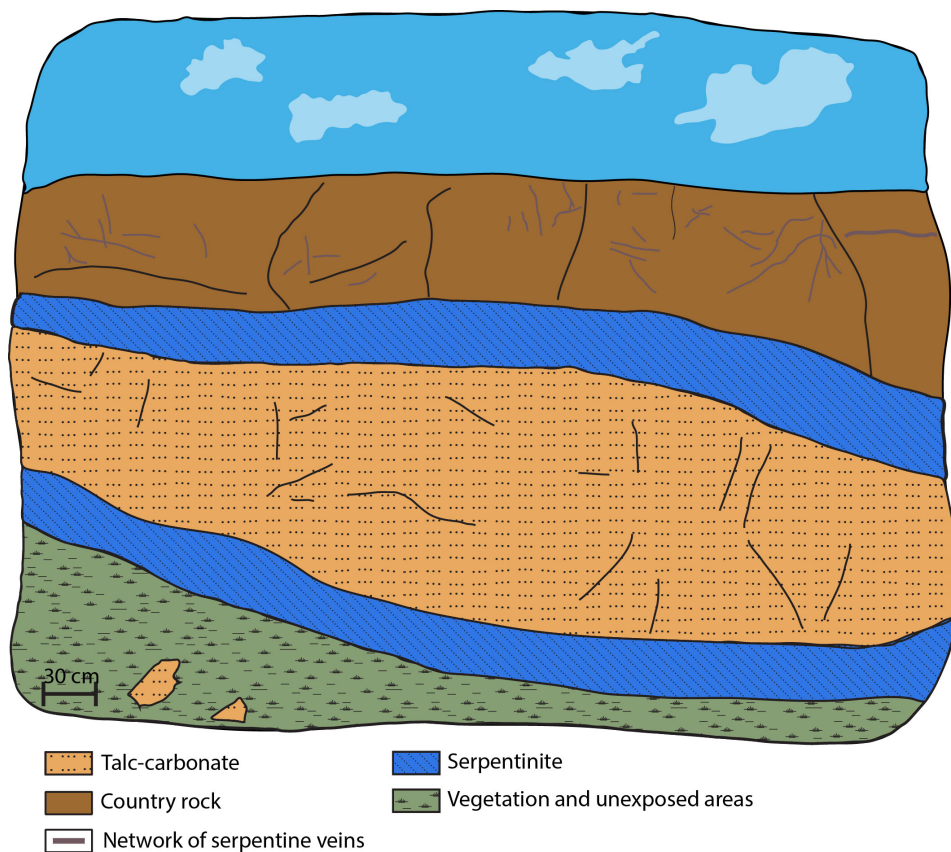


Fig. 10: Schematic drawing illustrating the observed zoning in the alteration zones, with the serpentinite forming rims along the margins of the talc-carbonate rock within the fracture zones.

3.3.1 *Serpentinite*

Serpentinite is associated with the major NE-SW trending low-angle faults, and it almost always forms sharp contacts with the partly altered peridotites and the talc-carbonate rock (Fig. 11). The serpentinite is composed of serpentine, carbonate and spinel minerals, and varies in vertical thickness from 0.5 m to 5 m. The serpentinite has a high tendency to fracture and break loose as blocks during weathering. As a consequence, only the uppermost part of the simplified sequence illustrated in Fig. 10 is usually exposed. Drilling performed in the area has shown that the simplified sequence is a general pattern for most of the alteration zones (Olerud, 1990). The serpentinite is locally brecciated, sheared and contains sheared veins of fibrous serpentine. The serpentinite assemblage has a characteristic blue/green color which makes identification in the field relatively straightforward. It usually lacks internal structure and is very fine grained.



Fig. 11: Photograph from the study area showing the sharp reaction fronts between the different lithologies. The partly altered peridotite is in the upper part of the picture, serpentinite in the middle (characteristic blue/green color) and talc-carbonate at the bottom. Note the sharp alteration front between the serpentinite and the talc-carbonate rock which reflect the breakdown of serpentine to talc-carbonate assemblage.

3.3.2 *Talc-Carbonate Rocks*

The talc-carbonate rock consists mainly of talc, carbonate and spinel minerals. Size and thickness of the talc-carbonate lenses varies considerably, with thickness ranging from 1 m to 12 m. Within the talc-carbonate rock, sets of 1-4 cm thick, sub-horizontal talc \pm carbonate veins occur (Fig. 12 A). Relatively thick lenses (~0.4 to 1.5 m thick) of coarse grained dolomite commonly associated with talc, have been developed (Fig. 12 F). Locally, patches of serpentinite can be observed within the talc-carbonate (Fig. 12 A). Talc \pm carbonate veins with ~50 cm wide reaction halos are observed cross-cutting the serpentinite. The talc-carbonate bearing rocks commonly have an orange to pink weathering color while fresh surfaces of the rock commonly display green/blue colors. The weathering surface shows preserved structures, indicating that the mineralogical changes took place at static

conditions (Fig. 12 B and C). Locally, concentric structures are observed on the weathering surface (Fig. 12 D). A blue-colored variety (sample LE-13-03), was observed only in one locality, in sharp contact with the pink-colored talc-carbonate rock (Fig. 12 E). The talc-carbonate is generally very fine grained and lacks internal texture.

3.4 AGE RELATIONS

To understand the evolution of the study area, it is important to establish a relative age relationship between the different lithologies and the veins within them. Three aspects of the relative age relations are considered; the relationship between the different veins, the age relations between the vein development and the activity in the alteration zones and the age relation between the different mineral assemblages in the alteration zone. From oldest to youngest the relative age relations are inferred to be:

1. A network of thin, fine grained serpentine veins with varying orientation (Fig. 13 A).
2. Steeply dipping serpentine veins with a light blue/green color (Fig. 13 C), commonly crosscut by:
3. Thick (~5 cm) sub-horizontal serpentine veins, commonly with a green core and a dark rim (Fig. 13 A and B), probably formed at the same time as a set of thinner, sub-horizontal serpentine veins (Fig. 13 A and C). It is likely that the serpentinite rock formed contemporaneously with, or shortly after the sub-horizontal serpentine veins, no cross-cutting relationship between these have been observed.
4. Formation of the talc-carbonate, sub-horizontal talc \pm carbonate veins (Fig. 12 A) and the carbonate lens.
5. A set of very fine grained, steeply dipping serpentine veins, which clearly crosscuts the rocks from the alteration zones, in addition to the talc and carbonate veins (Fig. 13 D-F).

The age relations are shown schematically in Fig. 14.

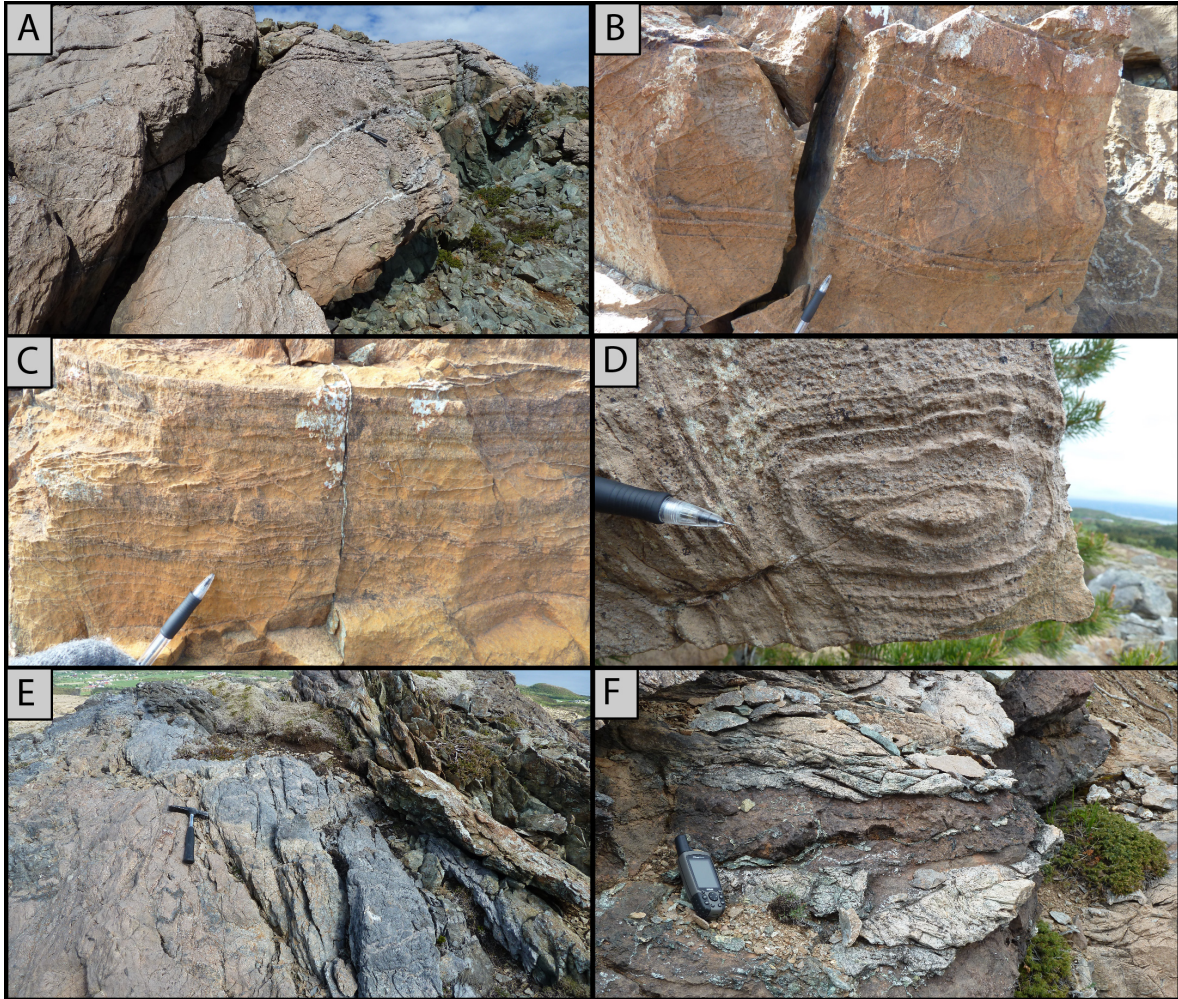


Fig. 12: A) Talc-carbonate rock with sub-horizontal veins consisting of talc \pm carbonate. Darker areas in the talc-carbonate rock is serpentinite that has not been fully converted to talc-carbonate assemblage. The observed texture on the weathering skin is inherited from the layering of the protolith peridotite and indicate that the mineralogical changes took place during static conditions. Note the talc-carbonate reaction halo around the pure talc-vein cross-cutting the serpentinite. B and C) Well preserved ghosts of igneous structures visible on the weathering surface of the talc-carbonate rock. Also note the vertical fine-grained vein of serpentine cutting through the talc-carbonate rock in C. D) Concentric structures on weathered surface in the talc-carbonate rock. E) Blue talc-carbonate rock in sharp contact with the pinkish talc-carbonate rock. The different mineralogy and color is related to differences in the protolith. The protolith for the pink/orange talc-carbonate rock was a partly altered peridotite while for the bluish talc-carbonate the protolith was probably a pyroxenite. Note that these rocks appear to be deformed. F) Carbonate lens (brown) in the talc-carbonate rock dissected by a network of very fine grained, green serpentine veins. Formation of the carbonate lenses is inferred to have occurred contemporaneously with, or shortly after, the formation of the alteration zones.

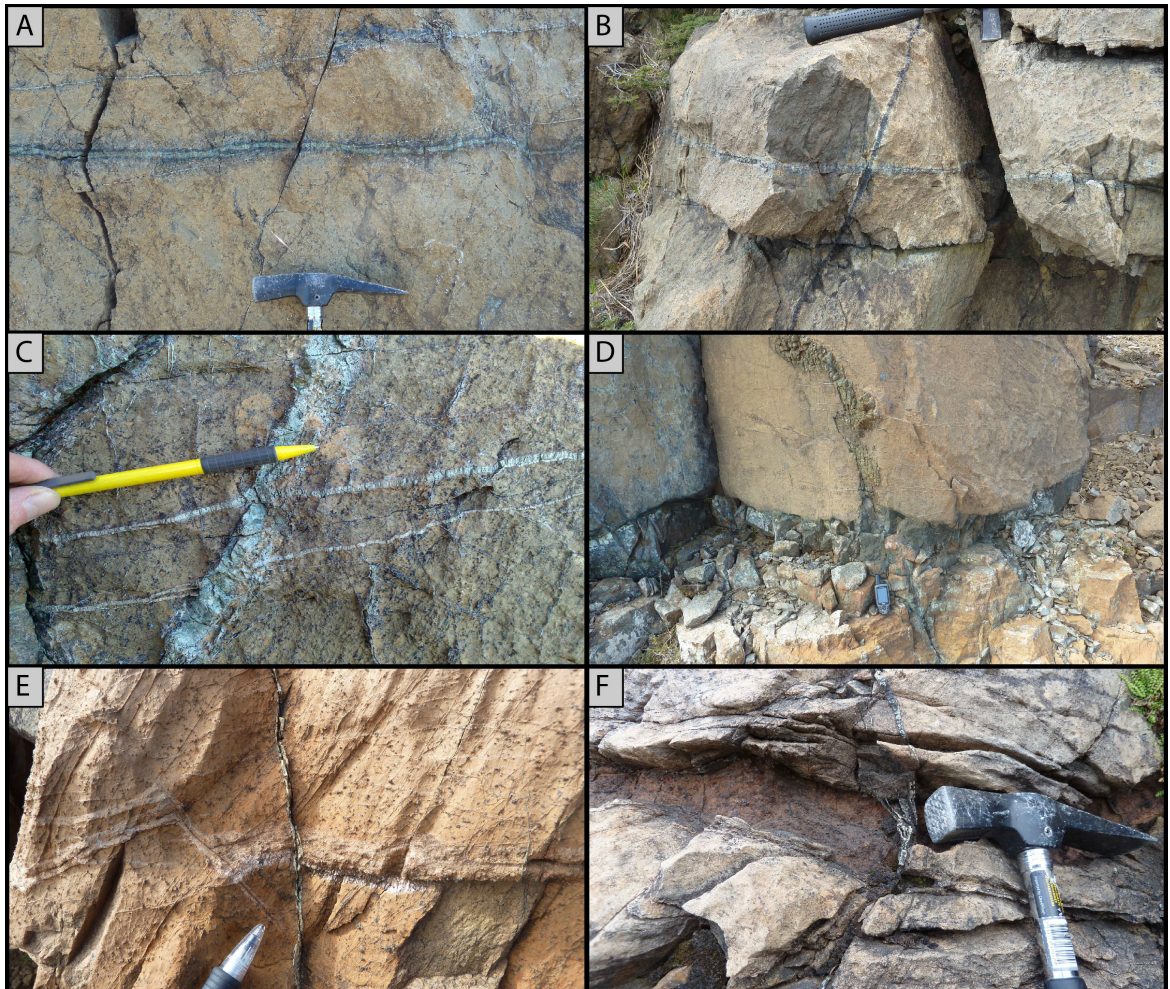


Fig. 13: A) Two sets of sub-horizontal serpentine veins in the partly altered peridotite. These sub-horizontal veins are commonly seen to crosscut the network of serpentine veins which are interpreted to be the oldest set of serpentine veins. B) Sub-horizontal serpentine veins cutting through a steeply dipping serpentinized pyroxene vein in the partly altered peridotites. Note the blue color in the sub-horizontal veins compared with the darker color in vertical. C) Two sub-horizontal serpentine veins clearly cross-cutting a near vertical serpentine vein and a network of serpentine veins in the partly altered peridotite. D) A vertical pyroxene vein cutting through the partly altered peridotite. In the lower part of the picture a fine grained serpentine vein cuts through the talc-carbonate rock. Formation of the polygonal domains seen in the pyroxene vein has been assigned to serpentinization processes by Iyer et al. (2008b). E and F) A very fine grained serpentine vein cross-cutting a talc vein and a carbonate vein in the talc-carbonate rock. The very fine grained serpentine vein is thus interpreted to represent the latest vein forming event in the study area.

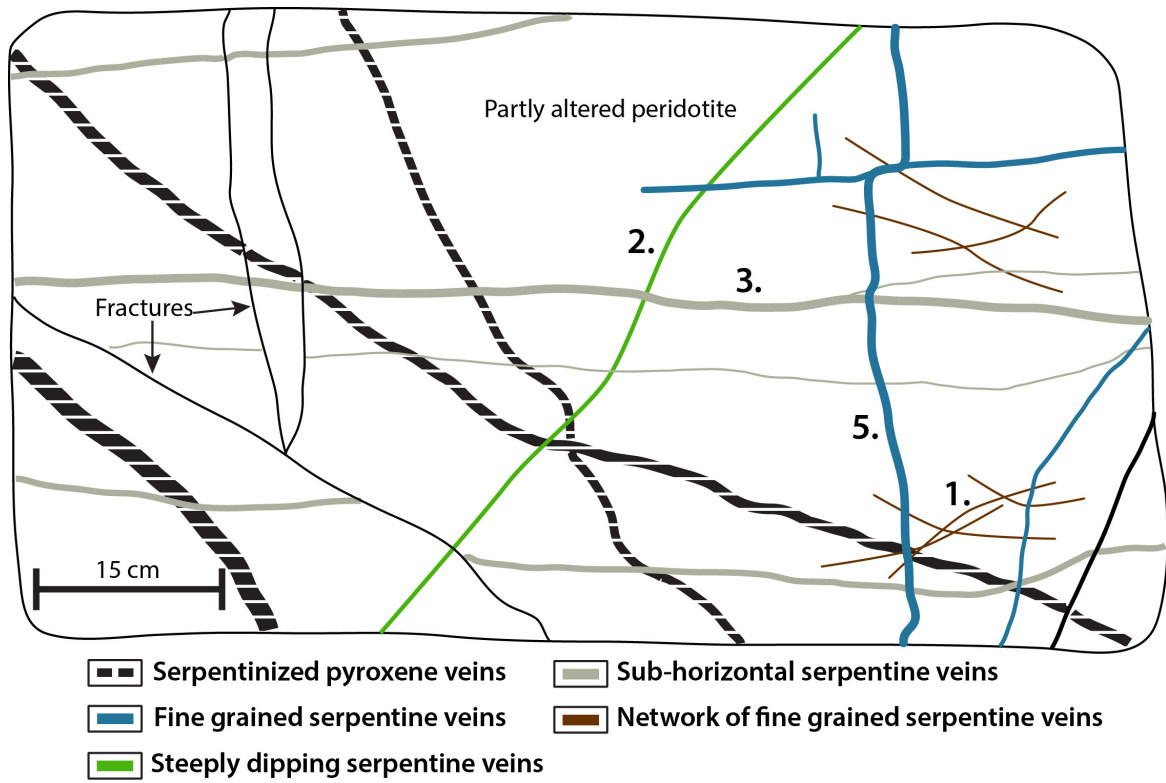


Fig. 14: A schematic drawing of cross-cutting relationships as they are observed in the study area. The numbers correspond to the age relations discussed in the text. The talc-carbonate rocks (not shown in this figure) probably formed shortly after the sub-horizontal serpentine veins and the serpentinite.

METHODS

4.1 FIELDWORK AND SAMPLING

Samples were collected during two periods of fieldwork, 2 weeks during the summer of 2012, and 4 days in October 2012. A total of 30 samples was collected, of which seven were used for the whole-rock major element and isotope analysis. Nine samples were chosen for the analysis of mineral chemistry. Sample locations are depicted in Fig. 7. To minimize the contamination, a large amount (1 – 3 kg) of each sample was used for the analyses of whole-rock major element and the isotope analysis. Weathered rock surfaces were removed in the field and only fresh pieces of the rocks were sampled. GPS locations for the analyzed samples used in the study are given in Appendix B.

Table 1: *Overview of different methods and software used*

Method/Software	Aim
Optical microscopy	Identification of mineral assemblages and micro textures, determination of mineral modes
Electron microprobe	Analysis of mineral composition
X-ray fluorescence (XRF)	Measurement of the whole-rock chemical composition
Perple_X	Modeling of conditions during formation of the observed mineral assemblages
Sr isotope analysis	Identification of the fluid source
Oxygen isotopes	Estimates of the equilibration temperature between the sample and the altering fluids
Carbon isotopes	Identification of the source for the CO ₂

4.2 PETROGRAPHIC THIN SECTIONS

The raw material for the petrographic thin sections was cut with a diamond saw in the basement of the University of Bergen (UiB). Samples were marked and put in plastic bags to avoid breakage and erosion of markings. Subsequently, the rock chips grinded manually on a Struers grinder with two diamond discs. After grinding on the medium coarse disc, the rock chips were transferred to the fine-grinding lap and one of the faces was smoothed out, flattened, and scratches were removed. Subsequently, the smoothed rock chips were glued to a glass slide. Polishing of the samples was done on a semi-automatic Struers instrument DP-U2 at the thin-section laboratory of the University of Bergen.

Table 2: Comparison of major element standard values measured at Department of Earth Science (UiB) with values from GeoReM (Jochum et al., 2005). BCR2 is a basalt powder standard (using the recommended values by Plumlee, 1998). MRG1 is a gabbro powder standard (using the recommended values by Govindaraju, 1994). All reference values are available on the GeoReM website; <http://georem.mpch-mainz.gwdg.de/>.

Oxide wt.%	SiO ₂	Al ₂ O ₃	Fe ₂ O ₃	MgO	CaO	Na ₂ O	K ₂ O	TiO ₂	MnO	P ₂ O ₅
BCR2 average	54,56	13,47	13,96	3,62	7,13	3,25	1,84	2,14	0,22	0,36
Reference material	54,10	13,50	13,80	3,59	7,12	3,16	1,79	2,26	0,20	0,35
% deviation	0,85	-0,26	1,15	0,74	0,19	2,69	2,79	-5,16	10,00	1,43
MRG1 average	40,31	8,39	18,33	13,73	14,84	0,85	0,28	3,69	0,19	0,07
Reference material	39,12	8,47	17,94	13,55	14,70	0,74	0,18	3,77	0,17	0,08
% deviation	3,04	-0,94	2,19	1,34	0,97	14,86	53,33	-2,23	11,76	-12,50

4.3 MAJOR ELEMENT ANALYSIS

Whole-rock major element concentrations were analyzed by standard X-ray fluorescence spectroscopy (XRF) procedures, using a Phillips PW1404 in the XRF-laboratory at the University of Bergen. Concentrations of major elements were determined using the glass beads. During the XRF-analysis two standard beads (BCR2 and MRG1) were run after every seventh unknown sample for the quality control purpose. For most major-elements (SiO₂, Al₂O₃, Fe₂O₃, MgO, CaO) the error is equal to, or less than 3%. (Tab. 2). The concentrations of K₂O, Na₂O, MnO and P₂O₅ were low in all the samples and could not be determined with certainty by the XRF analysis. In addition, all the samples were analyzed for FeO (titration) and CO₂ (15% HClO₄ leach) at ACME Analytical Laboratories (Canada).

4.3.1 Sample Preparation

Samples for major element analysis were crushed two times in a jaw crusher in the crushing room of the University of Bergen (Fig. 15 A), leaving a coarse-grained gravel of the sample. Subsequently, the coarse-grained sample material was finely ground using an agate mill (Fig. 15 B). Milling time varied from 7 to 10 minutes, depending on the minerals present in the individual samples.

Loss on ignition (LOI) was determined by heating of the samples to ~1000°C for approximately 2 hours in a Carbolite ELF 11/14B muffle furnace located in the mineral preparation laboratory (clean lab) of the University of Bergen. The mass difference before and after ignition represents the amount of volatile elements stored in the mineral phases in the rock sample.

4.3.1.1 Preparing Glass Tablets for Major-Element Analysis

6,72 g of dried flux (spectromelt A-10, lithium tetraborate, Li₂B₄O₇) were mixed together with 0,96 g of milled rock powder. The lithium tetraborate flux reduces the temperature and time necessary for melting of the sample. The mixed powder was put in platinum cups and mounted on top of gas torches in a fusion furnace (Claisse, model fluxy). A collector, in which the molten material cools was placed on top of the cups. During heating, the platinum cups are rotated to homogeneously heat the sample. When the material is melted, it is automatically dropped into the collector. The process is fully automatic with a running time of around 30 minutes for production of three glass disks.

4.4 RADIOGENIC ISOTOPE ANALYSIS

Strontium and rubidium isotopes were measured utilizing the thermal-ionization mass spectrometer (TIMS) Finnigan MAT 262 (upgraded in 2008 with QHV 2 High voltage supply and RunIt26X software from Spectromat) with 13 sample magazine at the Department of Earth Science, University of Bergen (Fig. 15 C).

4.4.1 Chemical Separation and Analysis

Samples weighing ca 0.2 g were weighed accurately in 25 ml PFA Savillex beakers and digested in concentrated hydrofluoric acid (HF) on a heating plate at 135°C for 48 hours. The HF supernatant was evaporated to dryness and the solid residue was subsequently hydrolyzed in a weak solution of nitric acid (HNO₃) on a heating plate at sub-boiling conditions. The nitrate salt residue was then dried and completely dissolved in ca 5 ml 2N HNO₃. The solution was weighed and fractions containing ~20% of the total solution were recovered and weighed accurately. An accurately weighed portion of Rb-Sr spike, enriched in ⁸⁴Sr and ⁸⁷Rb was added to the fractions. The fractions were used to determine rubidium and strontium concentrations. The remaining fractions (~ 80%) were used to determine ⁸⁷/⁸⁶Sr ratios.

Strontium from both fractions was separated by specific extraction chromatography on Sr-spec resin, using a modified version of the method described by Deniel and Pin (2001). The strontium eluate was collected in 2 ml micro-centrifuge tubes and dried. The mobile phase that exits the column (effluent) was collected as well, but only for the 20% fraction. This effluent, which also contains the rubidium, was dried in Savillex beakers and the residue dissolved in 0.3 ml hydrochloric acid (HCl). Rubidium was separated from this residual effluent by ion chromatography on Biorad resin AG 50W-X8 in purposely-prepared 0.75 ml micro-columns.

Both elements were loaded on double filaments for analysis. Strontium was analyzed in dynamic mode while rubidium was analyzed in static mode. Strontium isotope ratios were corrected for mass fractionation using a ⁸⁸Sr/⁸⁶Sr ratio of 8.375209. Repeated measurements of the SRM 987 standard at the time of analysis yielded an average ⁸⁷Sr/⁸⁶Sr ratio of 0.710235 ± 0.000009, 2σ (n = 10).

The chemical processing was carried out in a clean-room environment using reagents purified by sub-boiling point distillation in a Teflon cupola by Pico Trace, Germany.

4.5 STABLE ISOTOPE ANALYSIS

Stable isotope analysis was conducted at the Bjerknes Center, University of Bergen. Powdered sample material were reacted with H₃PO₄ at 70°C in individual reaction chambers using a MAT Kiel III carbonate preparation device. The reaction chambers were subsequently checked for complete reaction. Isotope ratios were measured on a Finnigan MAT 252 mass spectrometer with dual inlet. The data were calibrated to Vienna Pee Dee Belemnite (VPDB) scale and the long term standard deviation was measured with the NSB-19 standard to be ≤ ± 0.08 for δ¹⁸O and ≤ ± 0.03 for δ¹³C. The oxygen data are reported as δ¹⁸O (SMOW) and the carbonate data as δ¹³C (VPDB). The relationship between δ¹⁸O (PDB) and δ¹⁸O (SMOW) is:

$$\delta^{18}O(SMOW) = 1,03091 * \delta^{18}O(PDB) + 30,91 \quad (1)$$

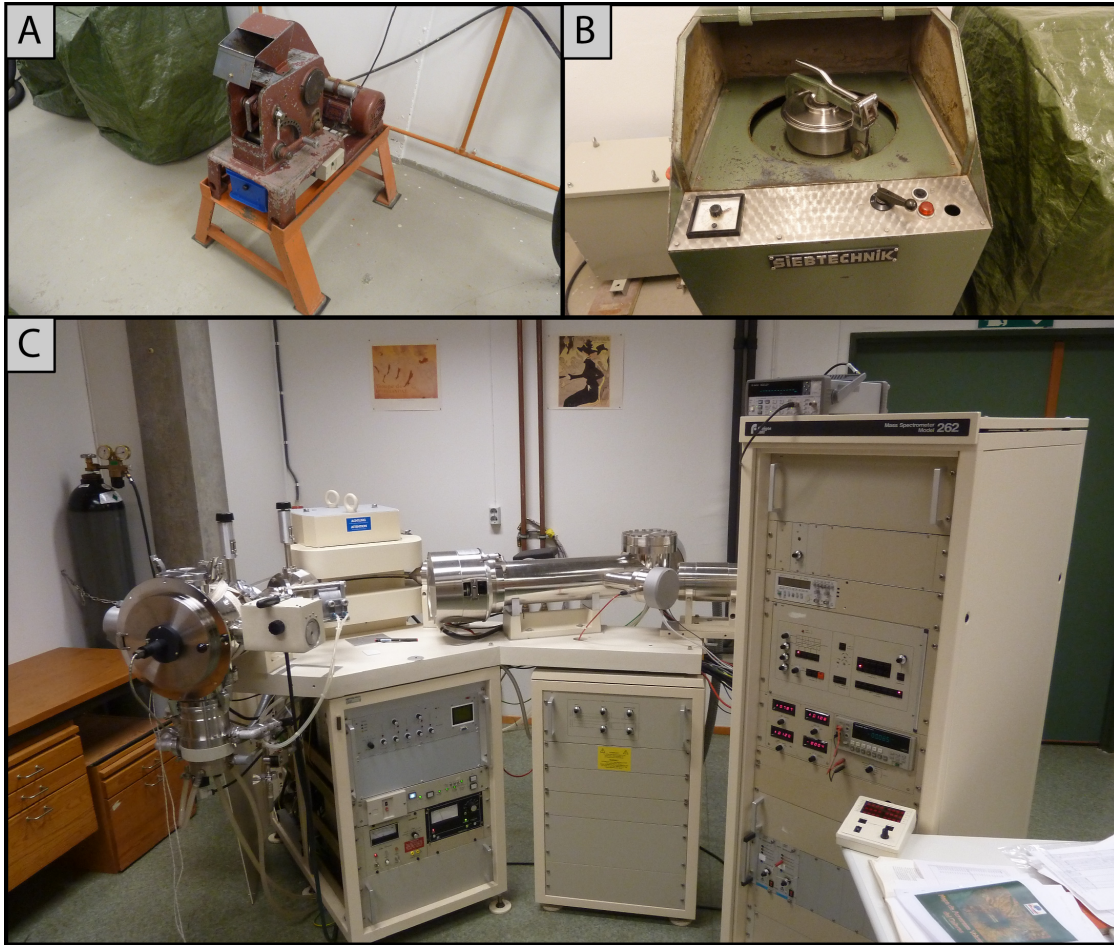


Fig. 15: A) Jaw crusher located at the University of Bergen. The jaw crusher was used to crush the samples into a coarse-grained fraction. Between the individual samples, all the parts of the jaw crusher were cleaned with water and alcohol. B) Roller for milling of the coarse grained sample material. An agate ring is placed inside the holder to finely ground the material. C) Finnigan MAT 262 mass spectrometer used for strontium and rubidium analysis, located at the Department of Earth Science, University of Bergen.

4.6 MINERAL ANALYSIS

Mineral chemistry was determined in nine representative samples, using the electron microprobe analysis (EMPA). A Cameca SX100 microprobe at the Masaryk University in Brno with operating conditions of 15 keV accelerating voltage and a beam current of 10 nA for micas, carbonates and spinels and 20 nA for olivine and pyroxene was used to analyze the minerals. The used beam diameter was 1 μm for spinel, 4 μm for olivine and pyroxene, 5 μm for micas and 7 μm for carbonates. Polished thin sections coated with carbon were used for the analysis. The mineral analysis are presented as oxide-weight percent (wt.%) and atom-per-formula-unit (a.p.f.u).

A field emission scanning electron microscope (FE-SEM) equipped with an energy dispersive spectrometer (EDS) system located at the analytical electron microscopy laboratory at the University of Bergen was utilized to identify brucite in the partly altered peridotites and dolomite in the carbonate lens.

RESULTS

5.1 SAMPLE DESCRIPTIONS

The investigated partly altered peridotites consist of variable amounts of olivine, serpentine, clinopyroxene and spinel-group minerals. Rocks from the alteration zones contain variable amounts of serpentine, talc, carbonate, ferritchromite and magnetite. Petrographic investigations of nine thin sections revealed the relationship between the primary minerals and the alteration products. Mineral compositions for all phases are plotted in the Si - Mg + Fe - Ca ternary diagram Fig. 16 and listed in Appendix A. All mineral abbreviations are from Whitney and Evans (2009).

5.1.1 Partly Altered Peridotites from the Mantle Tectonite

The investigated partly altered peridotites from the mantle section on Leka are represented by sample LE-12-01 (see Fig. 7 for sample location). The sample is composed of the minerals olivine (40-50%), clinopyroxene, spinel, serpentine (40-50%), magnetite ± carbonate. Olivine grains are highly fractured and range in size from 1,5 to 2,5 mm. Approximately 50% of the olivine has been replaced by fine grained serpentine minerals (Fig. 17). Ferritchromite is opaque and occurs as 0.1 - 0.8 mm long, elongated anhedral to subhedral crystals. Magnetite occurs as fine grained, equidimensional, opaque grains in areas where there has been extensive serpentinization. The original texture has been almost

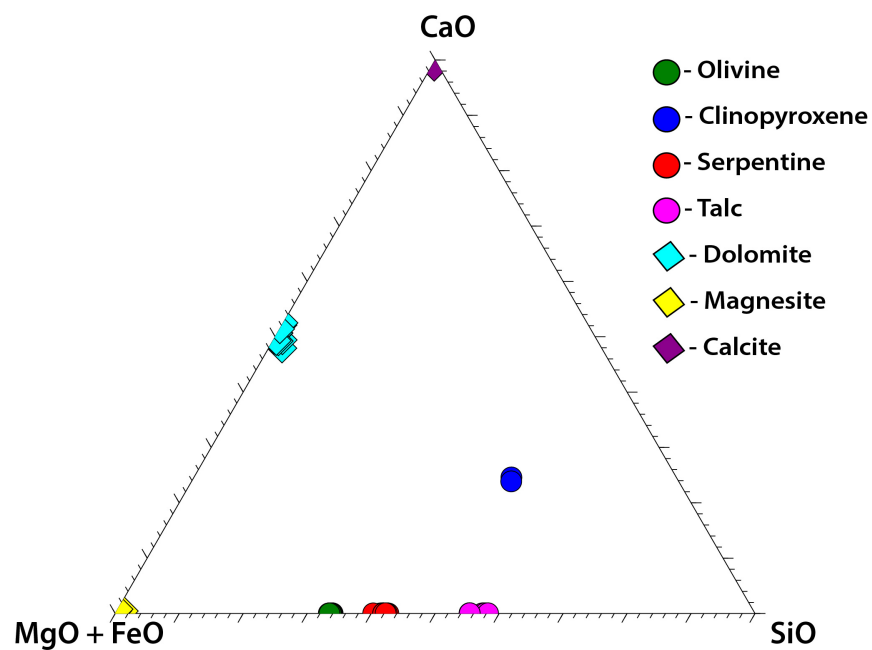


Fig 16: Mineral compositions plotted in the ternary Si - Mg + Fe - Ca system. The diagram shows that there are small variations in the mineral compositions.

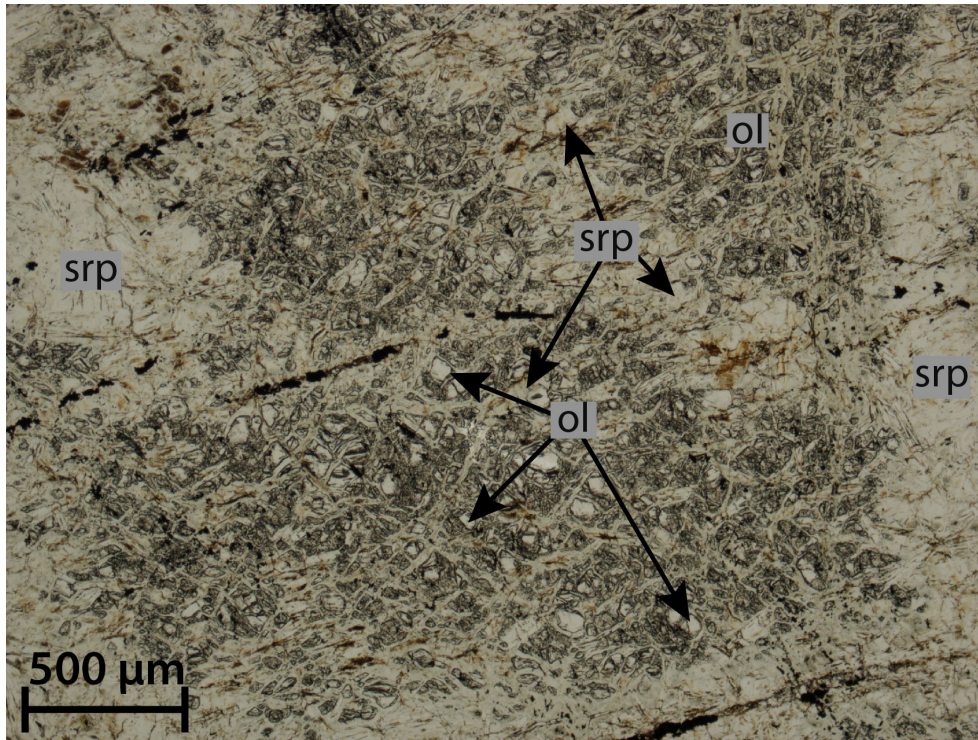


Fig 17: Photomicrograph of partly altered peridotite sample LE-12-01 showing highly fractured, coarse grained olivine being replaced by fine grained bladed crystals of serpentine. Olivine is ubiquitously seen to be dissected by a network of serpentine veins, indicating that the serpentine forms after olivine. Taken in plane polarized light (PPL).

completely obliterated during serpentinization. The original minerals are not seen in contact with each other due to extensive replacement by serpentine minerals along grain rims and fractures.

5.1.1.1 *Olivine*

The olivine composition in the partly altered peridotite is relatively homogenous, with Mg# [i.e., atomic $Mg^{2+}/(Mg^{2+} + Fe^{2+})$] of 0.90. The concentration of CaO, TiO_2 and Cr_2O_3 is low (≤ 0.02 wt.%) while NiO show concentrations between 0.37 and 0.42 wt.%.

5.1.1.2 *Clinopyroxene*

Clinopyroxene (Fig. 18) is augitic in composition with Si and Mg content of 1.90 – 1.91 and 0.92 – 0.94 atoms per formula unit (a.p.f.u) respectively. The concentration of Ca is between 0.91 and 0.94 a.p.f.u and the Al content is 0.11 a.p.f.u. Na_2O and FeO contents are low with 0.28 – 0.32 wt.% and 2.19 – 2.20 wt.% respectively. Cr_2O_3 and Na_2O concentrations are between 0.95 and 1.00 wt.% and 0.28 – 0.32 wt.% respectively.

5.1.1.3 *Spinel*

Spinel in the partly altered peridotite is identified as ferritchromite with a Cr# [i.e., atomic $Cr/(Cr + Al)$] of 0.98 and a $Fe^{3+}\#$ [i.e., atomic $Fe^{3+}/(Fe^{3+} + Cr + Al)$] of 0.56. The Mg content is 0.13 a.p.f.u. MnO and NiO concentrations are 0.74 and 0.43 wt%, respectively, while TiO_2 , Al_2O_3 , CaO, K_2O and Na_2O show low concentrations (≤ 0.35 wt.%).

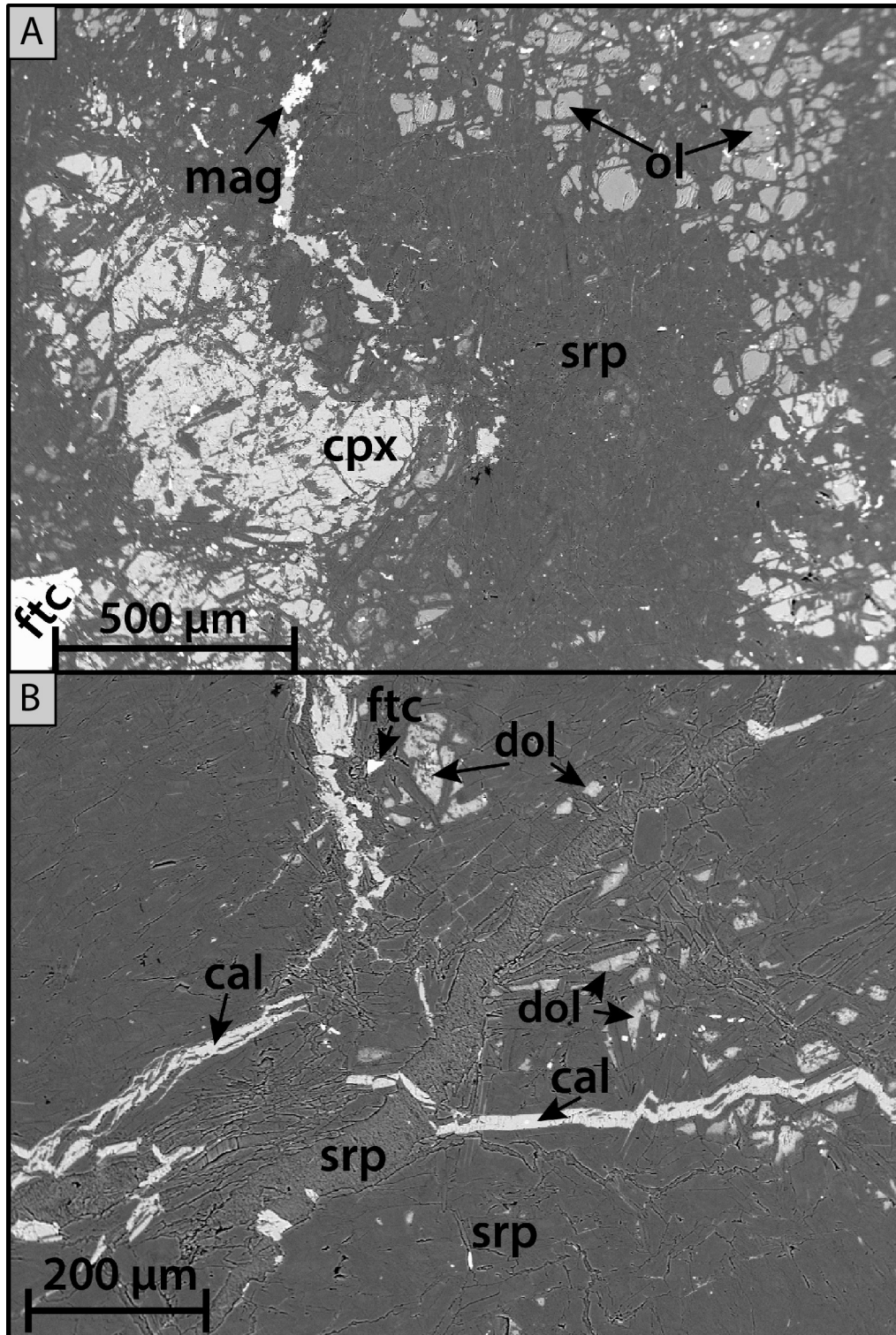


Fig 18: BSE images of partly altered peridotite sample LE-12-01 from the mantle tectonite. A) The primary peridotite minerals clinopyroxene (cpx) and olivine (ol) are replaced by serpentine (srp) and magnetite (mag). Primary Cr-spinel has been replaced by ferritchromite (ftc). Replacement of clinopyroxene and olivine by serpentine occurs along grain margins and fractures. The contacts between the primary minerals are not observed because of the replacement of the minerals by serpentine. B) Dolomite (dol) in the matrix is overgrown by bladed crystals of serpentine. This indicates that there might have been dolomite present in the partly altered peridotites prior to the first serpentinization event. A calcite (cal) vein crosscuts a vein of serpentine and is interpreted as a late feature.

5.1.1.4 *Serpentine*

Serpentine in the partly altered peridotite from the mantle section occurs in the matrix and in veins (Fig. 18 B). Vein forming serpentine has higher Fe content (0.24 to 0.27 a.p.f.u) and shows lower Mg# (0.91 – 0.92) than the serpentine minerals in the matrix, which have Fe content of 0.09 to 0.12 a.p.f.u and display a Mg# between 0.96 and 0.97. Si content in the vein serpentine is 2.02 – 2.03 a.p.f.u which is slightly lower than in the matrix serpentine (2.05 – 2.09 a.p.f.u). Both the serpentine in the veins and the serpentine in the matrix show low concentrations of Al₂O₃ (≤ 1.3 wt.%) and TiO₂ (≤ 0.02 wt.%).

5.1.1.5 *Carbonate Minerals*

Dolomite is observed in the matrix of sample LE-12-01 being penetrated by blades of serpentine (Fig. 18 B). This indicates that there might have been dolomite present in the rock prior to the first serpentinization. Pure calcite (0.99 Ca a.p.f.u) occurs in a vein crosscutting a vein of serpentine (Fig. 18 B).

5.1.2 *Partly Altered Peridotites from the Cumulate Section*

The partly altered peridotites belonging to the cumulate section of the Skråa block are represented by the samples LE-13-01, LE-13-02 and LE-13-05. They consist of olivine (70 – 80%), spinel, serpentine and magnetite and differ from the partly altered peridotites from the mantle tectonite by a higher amount of primary olivine and lack of clinopyroxene. Olivine is the most abundant mineral and is commonly better preserved in the partly altered peridotites from the cumulate section than in the partly altered peridotites from the mantle tectonite.

Olivine occurs as 0.6 – 1.2 mm large, highly fractured subhedral to euhedral crystals. Serpentine occurs as fine grained bladed crystals in the matrix and in veins, and forms a mesh texture with olivine. Serpentine commonly shows interpenetrating needle texture (Fig. 19 A).

Primary spinel is usually altered to ferritchromite and makes up approximately 3 – 5% of the total rock volume. In sample LE-13-05, spinel occurs as 0.1 – 0.3 mm large, sub-hedral to anhedral crystals while grains up to 0.8 mm large are observed in sample LE-13-01. Primary Cr-spinel appears dark red to dark brown while altered spinels are opaque. Fine grained magnetite occurs in all the samples and is locally very abundant. Sample LE-13-05 has a notable amount of spinel (~7 – 8 % of the rock volume; Fig. 19 B).

Veins composed of serpentine and carbonate are observed in sample LE-13-01 (Fig. 19 A). Blocky crystals of carbonate, identified as dolomite, occur in veins together with fibrous serpentine in sample LE-13-02 (Fig. 19 B). The observed carbonate varies in size (from < 0.1 to 0.15 mm) and color and has developed anhedral to subhedral crystals. Detailed investigation of the veins containing the blocky carbonate reveals an ataxial growth pattern (c.f., Passchier and Trouw, 2005).

5.1.2.1 *Olivine*

The minerals in the samples LE-13-02 and LE-13-05 were chosen for microprobe analysis. Olivine from these samples shows relatively homogenous compositions with Mg# ranging from 0.90-0.93. Olivine from both samples is poor in CaO, Cr₂O₃ and TiO₂ with < 0.1 wt.%. FeO content in olivine from LE-13-02 and LE-13-05 is 0.15 to 0.20 a.p.f.u and 0.13 – 0.15 a.p.f.u, respectively. Olivine in

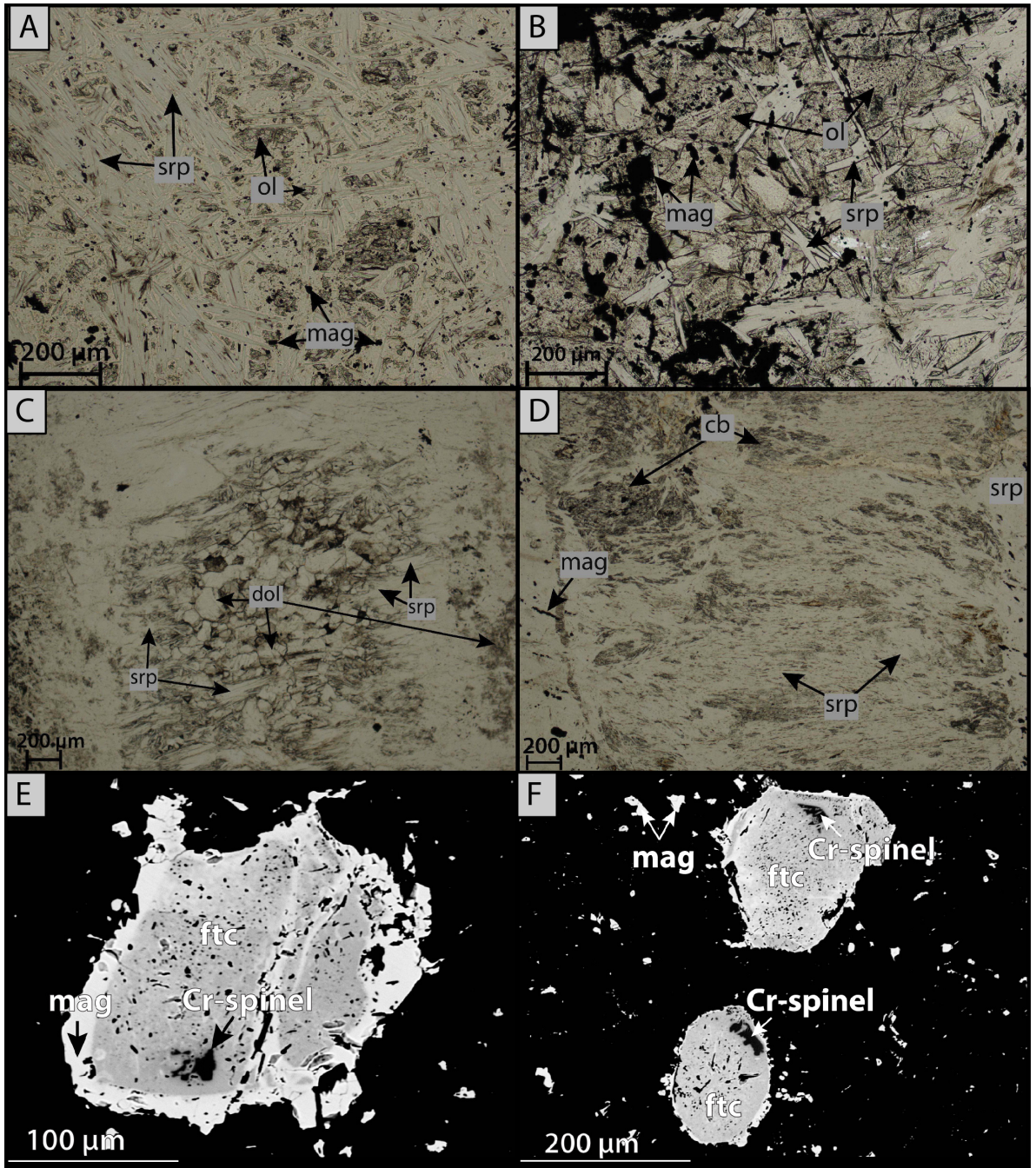


Fig 19: Photomicrographs and backscatter electron (BSE) images of the partly altered peridotites from the cumulate section. Pictures A-D are seen with PPL. A) Bladed crystals of serpentine (srp) and remnants of olivine (ol) in sample LE-13-01. Blades of serpentine overgrowing grains of olivine suggests that serpentine grew from the olivine. B) Serpentine and high concentration of magnetite forming after olivine in sample LE-13-05. Bladed crystals of serpentine clearly penetrate the olivine crystal. C) Vein with an ataxial growth pattern (c.f., Passchier and Trouw, 2005) in sample LE-13-02. Dolomite is present as blocky crystals while serpentine (srp) occurs as elongated crystals perpendicular to the vein walls and overgrows the crystals of dolomite. D) Ataxial vein of serpentine (srp) and carbonate (cb) in sample LE-13-01. Serpentine crystals occur as fibers perpendicular to the walls together with interstitial carbonate. E) Primary Cr-spinel altered to ferritchromite (ftc) in sample LE-13-05. Note the high abundance of Cr-spinel inclusions within the ferritchromite. F) Ferritchromite replacing primary Cr-spinel in sample LE-13-05. Note the high concentration of magnetite in the matrix.

LE-13-02 shows higher concentrations of NiO (0.20 – 0.30 wt.%) than in sample LE-13-05 (0.09–0.10 wt.%). Olivine in LE-13-05 contains 0.38 – 0.42 wt.% of MnO, whereas the concentration in olivine from LE-13-02 is lower (0.19 – 0.23 wt.%).

5.1.2.2 *Spinel*

Spinel was analyzed in sample LE-13-05 and identified as Cr-spinel, ferritchromite and magnetite. Primary Cr-spinel is commonly altered to ferritchromite and rimmed by pure magnetite (Fig. 19 E). The primary Cr-spinel is characterized by a moderate Cr# of 0.54 and a low Fe³⁺# of 0.07. A high ZnO content of 1.11 – 1.37 wt.% is observed in Cr-spinel in sample LE-13-05. ZnO values of > 0.5 wt.% are considered unusually high (e.g., Groves et al., 1983 in Wylie et al., 1987).

Ferritchromite has a Cr# of 0.97 and a Fe³⁺# of 0.50. The concentration of MnO is higher (2.4 wt.%) compared to the Cr-spinel (1.04 wt.%) and the Mg content is 0.25 a.p.f.u.

Magnetite commonly forms rims around primary Cr-spinels and ferritchromite (Fig. 19 E) and occurs as smaller grains within the serpentine and olivine matrix (Fig. 20 B and C). The magnetite has near endmember composition (Fe³⁺# = 0.97) with a low concentration of Cr₂O₃ (1.7 wt.%). MnO and MgO show concentrations of 0.2 and 1.4 wt.% respectively. Al₂O₃, TiO₂ and NiO show low concentrations (wt% ≤ 0.1).

5.1.2.3 *Serpentine*

Serpentine occurs as the matrix mineral and is also present in veins together with carbonate. In sample LE-13-02, serpentine in the matrix in the veins both have similar composition with Mg# of 0.97 – 0.98. Aluminum content is low, ranging from 0.08 – 0.09 a.p.f.u. Some measured serpentines with a lower Mg# (0.95), and a higher NiO (0.21 wt.%) concentration may be intergrown with brucite, which have been described from similar rocks on Leka by Iyer et al. (2008a).

5.1.2.4 *Carbonate Minerals*

Carbonate in the partly altered peridotites from the cumulate section is represented by dolomite. It is observed in veins together with serpentine in both samples LE-13-01 and LE-13-02 (Fig. 20 D). In sample LE-13-01 the Mg content range from 0.97 to 0.98 a.p.f.u with a Ca content of 0.98 a.p.f.u. The dolomite in sample LE-13-02 have Mg and Ca contents of 0.96 and 1.01 a.p.f.u, respectively. Mg/Ca in the dolomite ranges from 0.68 to 0.71. This is higher than for stoichiometric dolomite (0.64) and it reflects a limiting mixing with the magnesite endmember.

5.1.3 *Serpentinite*

Serpentinites are represented by the samples LE-11-02 and S0402, and composed of serpentine (~80%), carbonate (~15%) and spinel. Sample LE-11-02 does not show any fabric (Fig. 21 A), while sample S0402 represents a local shear zone at the bottom of the alteration sequence (Fig. 21 C). Serpentine minerals in both samples vary in color from colorless to pale green and form interpenetrating bladed crystals. Fine-grained anhedral to sub-hedral carbonate grains form acicular crystals in sample LE-11-02 (Fig. 21 B and D). Vein-forming carbonate is overgrown by bladed serpentine (Fig. 21 E). Spinel in the serpentinite is usually altered to ferritchromite and magnetite (Fig. 21 F).

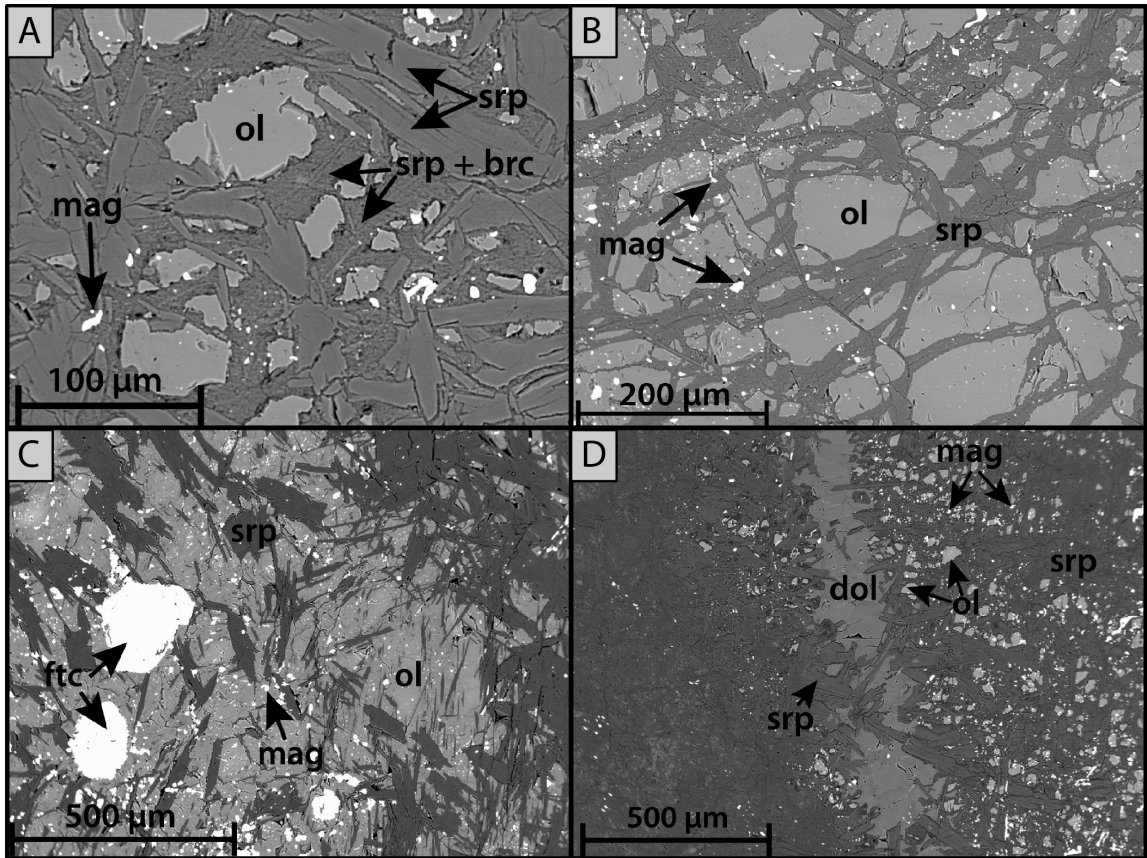


Fig 20: BSE images from the partly altered peridotite of the cumulate section. Images A,B and D) are from sample LE-13-02 and C) is from sample LE-13-05. A) Olivine (ol), serpentine (srp) and serpentine intergrown with brucite (srp + brc). The presence of brucite in the partly altered peridotites has been used as an argument for the low temperatures of the serpentinization (Johannes, 1968; Iyer et al., 2008a). B) Serpentine forming along cracks in olivine (mesh texture). Note the high concentration of fine-grained magnetite (mag) in this sample. C) Bladed crystals of serpentine (srp) replacing olivine (ol). A high abundance of fine-grained magnetite (mag) and subhedral grains of ferritchromite (ftc) occur in this sample. D) Dolomite (dol) vein overgrown by bladed crystals of serpentine (srp). Magnetite (mag) and relics of olivine (ol) are present in the serpentine matrix.

5.1.3.1 Serpentine

The analyzed serpentine from the matrix shows some variability in the chemistry with Mg# ranging from 0.92 to 0.95 and Fe content of 0.15 to 0.23 a.p.f.u. The Mg# of serpentine is lower in the serpentinite than in the partly altered peridotites. Al and Mn content is low (≤ 0.08 a.p.f.u). NiO content ranges from 0.14 to 0.27 wt.% and Cr₂O₃ concentrations range from < 0.10 to 0.25 wt.%.

5.1.3.2 Carbonate

Carbonate in the serpentinite is identified as magnesite with Mg# of 0.93 to 0.95 and Fe content of 0.05 to 0.07 a.p.f.u. Concentrations of MnO and CaO are between 0.51 – 0.68 wt.% and 0.11 – 0.17 wt.%, respectively.

5.1.3.3 Spinel

Two investigated spinels in sample LE-11-02 are identified as ferritchromite with a high Cr# (0.99 – 1.00). The ferritchromite show different degrees of alteration, which is evident by the Fe³⁺# of 0.53

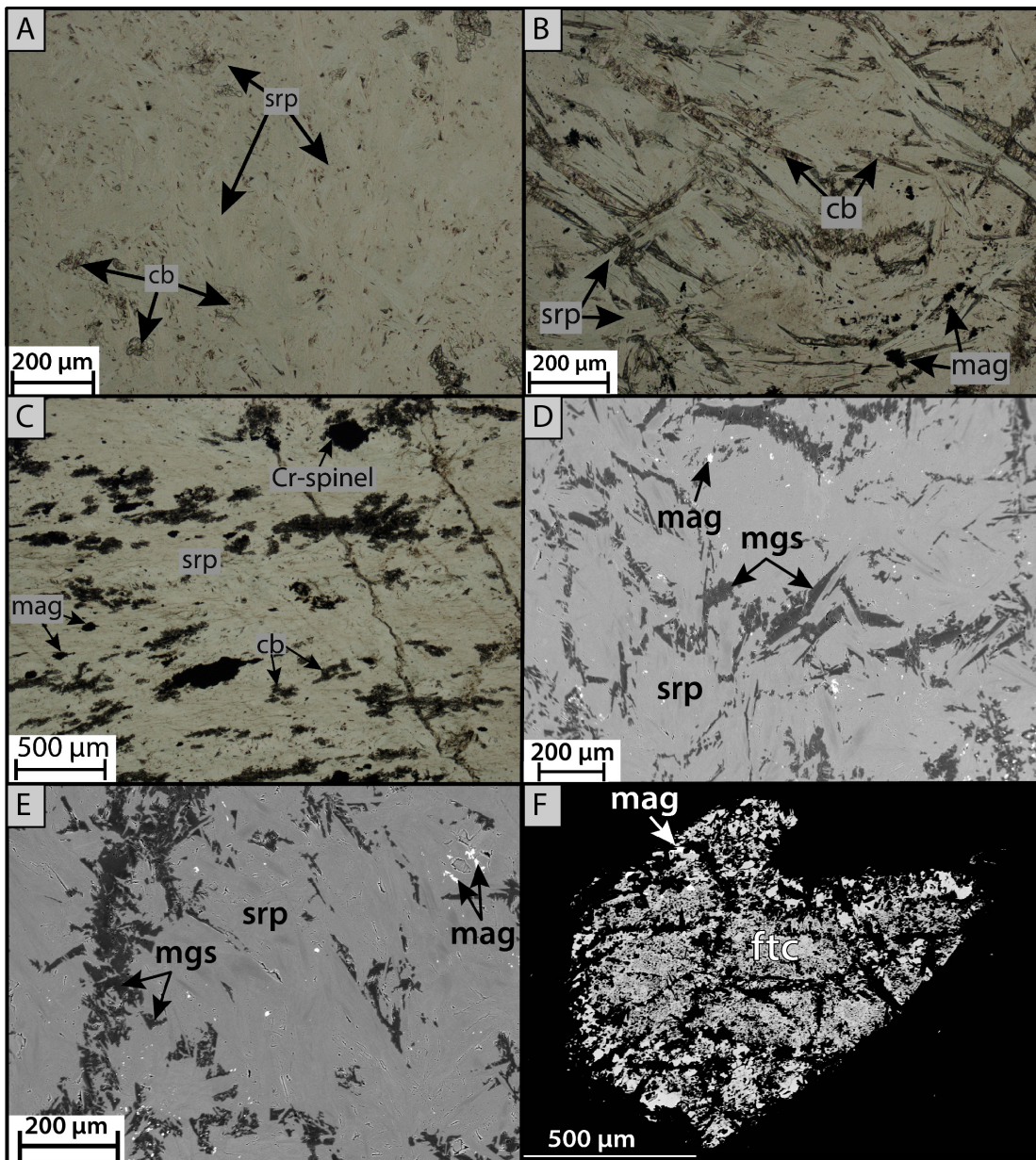


Fig 21: Photomicrographs and BSE images from serpentinite sample LE-11-02. The figures A to C were taken in PPL. Picture C is from sample S0402. A) Lack of fabric in serpentinite sample LE-11-02. Serpentine minerals form bladed crystals varying in color from colorless to pale green. Carbonate forms fine-grained, equidimensional to elongated anhedral crystals. B) Acicular carbonate and green to colorless serpentine in sample LE-11-02 C) Locally developed shear zone at the bottom of the alteration sequence manifested by stretched serpentine and carbonate in sample S0402. D) Magnesite (mgs) forming elongated/acicular crystals in the matrix of the serpentinite. E) Vein of magnesite (mgs) overgrown by serpentine (srp). The primary peridotite texture is completely obliterated. F) Zoned crystal of ferritchromite, with magnetite forming at the outermost rims.

and 0.73 (with higher number indicating higher degree of alteration). In the least altered ferritchromite, ZnO and MnO concentrations are higher (0.41 wt.% and 0.60 wt.%, respectively) when compared to the more altered ferritchromite with ZnO of 0.18 wt.% and MnO of 0.33 wt.%. NiO shows higher concentrations in the most altered ferritchromite (0.31 wt.%) compared to the least altered one (0.14 wt.%).

5.1.4 *Talc-carbonate Group One*

Difference in chemistry and field occurrence makes allows the distinction between two groups of talc-carbonate rocks. Talc-carbonate group one (represented by samples LE-11-01, LE-12-02, LE-13-04) has a pink/orange weathering surface (Fig. 12 A) and a whole-rock chemistry that resembles that of the partly altered peridotites. Talc-carbonate group two (represented by sample LE-13-03) has a blue weathering surface (Fig. 12 D), a whole-rock chemistry resembling that of an orthopyroxenite (Fig. 26) and a higher modal content of dolomite.

Talc-carbonate of the group one (TCG1) is composed of talc (45 – 55%), carbonate (40 – 50%), spinel, \pm serpentine, \pm chlorite. The original peridotite texture has been completely obliterated. Talc and carbonate occur in approximately similar proportions in all the investigated samples of the group one (Fig. 23 A).

In sample LE-11-01, talc forms bladed crystals (~0.1 – 0.3 mm in length) which make up the fine-grained, colorless to pale green matrix together with ~0.1 – 0.2 mm large, subhedral crystals of carbonate (Fig. 22). Talc and carbonate are finer-grained in the samples LE-12-02 and LE-13-04 compared to the sample LE-11-01 (Fig. 23). Relics of serpentine are enclosed in magnesite are observed in the sample LE-13-04 (Fig. 24). Very fine-grained serpentine occurs as a vein mineral in sample LE-12-02 (Fig. 23 A). Spinel in all the samples forms 0.1 – 0.5 mm large, subhedral to anhedral crystals. Chlorite commonly replace spinel in sample LE-12-02 (Fig. 23 A and B, and Fig. 25 C and D).

5.1.4.1 *Talc*

Talc is ubiquitous in all the investigated talc-carbonate samples and has a near endmember composition with Mg# ranging between 0.94 and 0.96. Fe content is higher in sample LE-12-02 (0.43 – 0.45 a.p.f.u) compared to sample LE-11-01 and LE-13-04 (0.29 – 0.39 a.p.f.u). Ni content ranges from 0.10 to 0.39 wt.%. The concentration of CaO, MnO, Al₂O₃ and Cr₂O₃ is low (< 0.15 wt.%).

5.1.4.2 *Carbonate Minerals*

Carbonate identified as dolomite and magnesite is present in all the samples. Dolomite in samples LE-11-01 and LE-13-04 is almost pure endmember characterized by a Mg# of 0.96 to 0.97 and 0.94, respectively. Ca content is between 0.96 and 1.02 a.p.f.u. Fe content is low (\leq 0.06 a.p.f.u).

A compositional zoning represented by dolomite enclosed in magnesite rimmed with iron-rich magnesite is observed in sample LE-11-01 (Fig. 25 A and B). Magnesite has Mg# between 0.95 and 0.97. Iron-rich magnesite has Mg# of 0.84 and 0.90. Higher concentrations of MnO are observed in the magnesite (0.70 – 0.84 wt.%) compared to the iron-rich magnesite (0.04 – 0.14 wt.%). CaO concentration ranging from 0.15 to 0.22 wt.% and 0.21 to 0.49 wt.% is observed in the magnesite and iron-rich magnesite, respectively.

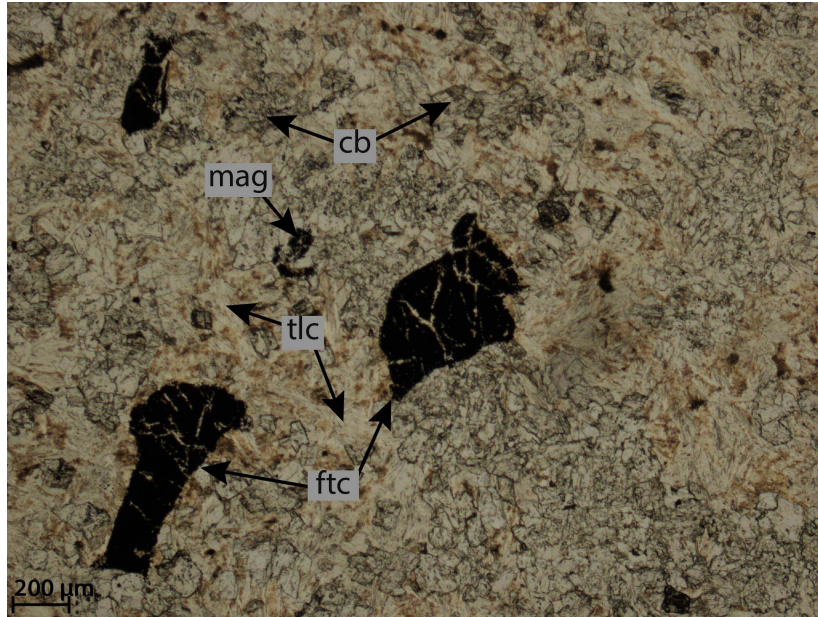


Fig 22: Photomicrograph of sample LE-11-01 taken in PPL. Bladed crystals of talc (tlc) ~0.1 – 0.3 mm large, form the matrix together with the fine-grained subhedral carbonate (cb). Ferritchromite (ftc) is present as ~0.1 – 0.3 mm large, subhedral crystals. Only a small amount of magnetite (mag) is present in this sample.

5.1.4.3 *Serpentine*

Vein-forming serpentine in sample LE-12-02 is characterized by a lower Mg# (0.87 – 0.89) compared to the serpentine minerals in the partly altered peridotite and in the serpentinite. Al_2O_3 and Cr_2O_3 concentrations are between 1,28 and 3,82 wt.% and 0.02 and 0.27 wt.%, respectively. Serpentine enclosed in magnesite crystals in sample LE-13-04 has a Mg# of 0.89 and Al_2O_3 content of 1.20 wt.%.

5.1.4.4 *Chlorite*

Chlorite in sample LE-12-02 is classified as type I ($X_{\text{Mg}} + X_{\text{Fe}} \geq X_{\text{Al}} + X_{\text{vacancy}}$) Mg-chlorites after the classification scheme of Zane and Weiss (1998) and Zane et al. (1998), with Mg# of 0.81 and Al content of 3.08 to 3.09 a.p.f.u. The chlorite is rich in chromium with Cr_2O_3 concentrations ranging from 1.22 to 1.49 wt.% and has a Ni content of 0.12 to 0.13 wt.%. CaO and MnO show low concentrations (≤ 0.05 wt.%).

5.1.4.5 *Spinel*

In sample LE-11-01, ferritchromite shows a high Cr# (0.99 to 1,00) and relatively high Fe^{3+} # (0.76 to 0.82). In sample LE-12-02, ferritchromite has high Cr# (0.98-0.99) and moderate Fe^{3+} # (0.49 – 0.61). The concentration of ZnO ranges from 0.12 to 0.43 wt.%.

In sample LE-13-04, the core of a zoned Cr-spinel (Fig. 25 F) has a #Cr of 0.49, Fe^{3+} # of 0.07 and ZnO of 0.61 wt.% while the rim has a Cr# of 0.99 and a Fe^{3+} # of 0.58.

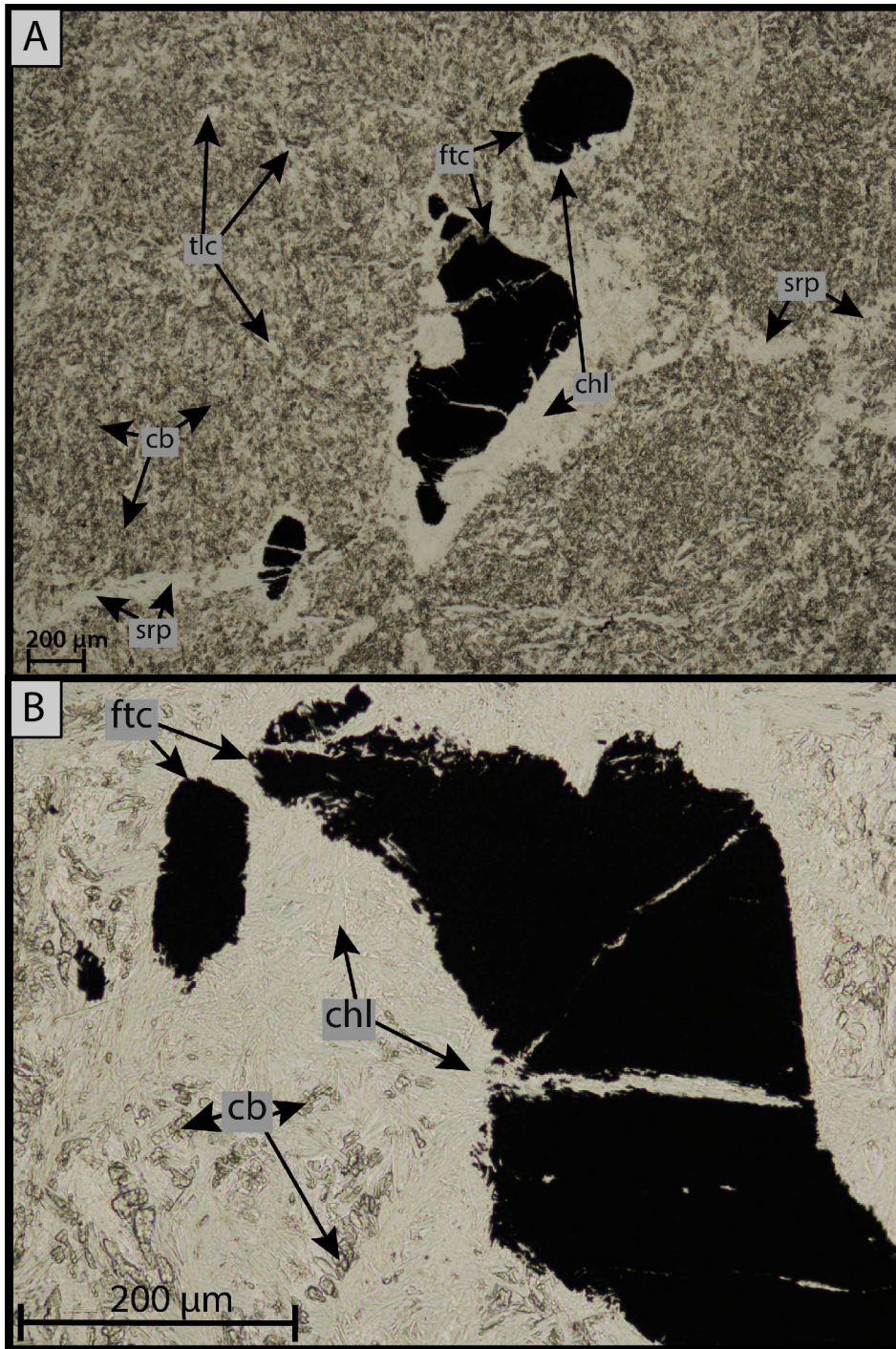


Fig 23: Photomicrographs of partial replacement of spinel in talc-carbonate rock sample LE-12-02. Spinel is replaced by chlorite (chl) along the rims and in fractures. Carbonate (cb) occurs as a fine-grained anhedral to subhedral crystals. A) Fine-grained talc (tlc) and carbonate occur in the sample in an approximately ~1 to 1 ratio together with heterogeneously distributed spinel. Serpentine forms fine-grained veins cutting the talc-carbonate matrix. B) Bladed crystals of chlorite penetrating carbonate (cb) crystals and replacing spinel along the rims and in fractures.

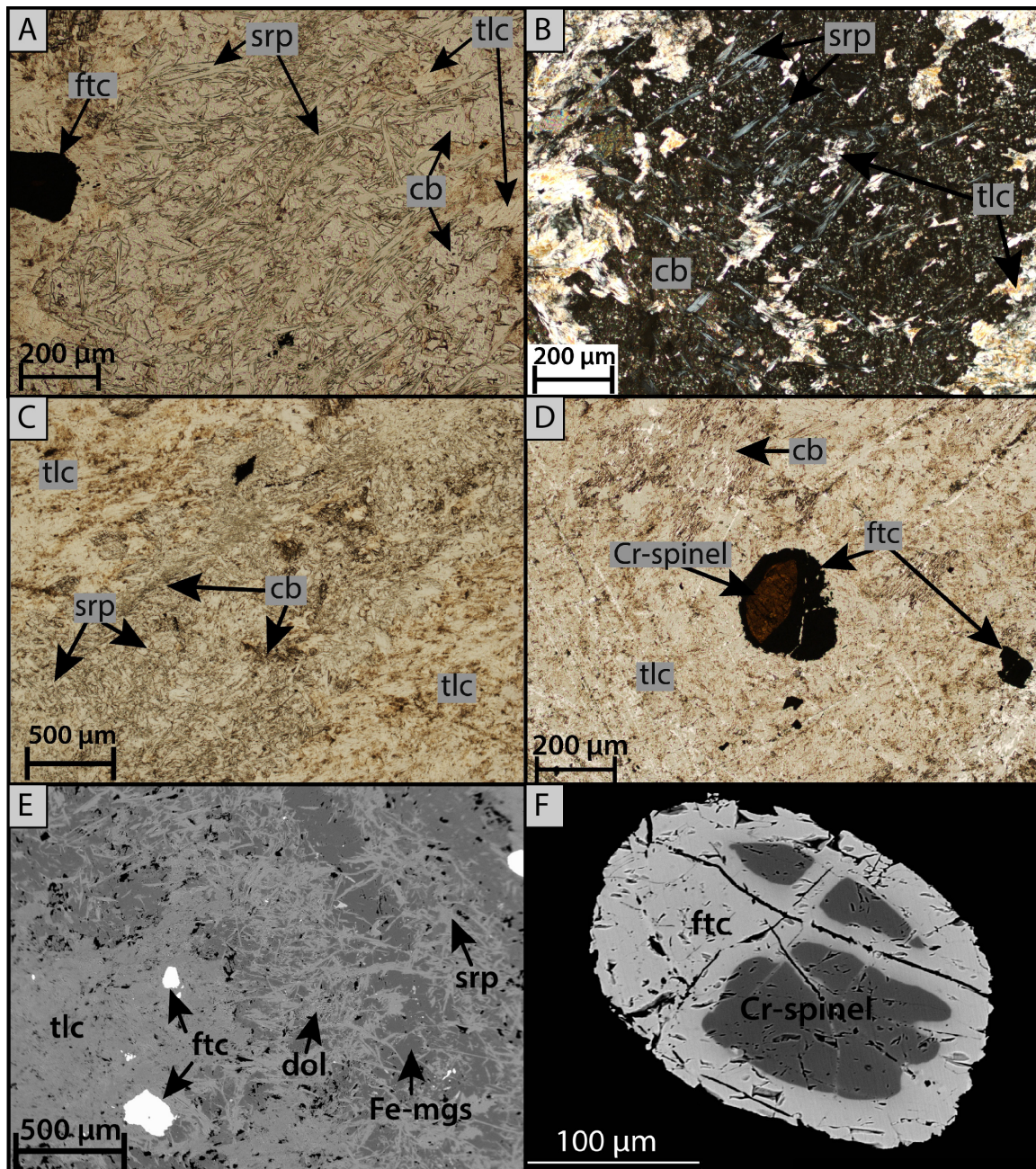


Fig 24: Photomicrographs and BSE images of talc-carbonate sample LE-13-04. A) Relics of serpentine (srp) enclosed within a carbonate grain (cb) in a fine-grained talc (tlc) matrix observed in PPL. B) Serpentine enclosed within a carbonate grain in cross polarized light (XPL). C) Vein of carbonate cutting through the fine-grained talc-matrix. D) Optically visible zoning of a Cr-spinel. Ferritchromite (ftc) forms rims around the primary Cr-spinel. E) BSE image showing the relationship between iron-rich magnesite (Fe-mgs), serpentine and talc. F) BSE image showing primary Cr-spinel rimmed with ferritchromite.

5.1.5 *Talc-carbonate Group Two*

Talc-carbonate group two (TCG2) is represented by sample LE-13-03, which consists of talc (~50%), carbonate (~45%), spinel and chlorite. Talc forms the a fine-grained matrix together with carbonate ranging in size from < 0.1 mm to 0.3 mm. Carbonate also occurs in veins (Fig. 25 E).

5.1.5.1 *Talc*

Talc from TCG2 has a similar chemistry as the talc from TCG1, with a Mg# of 0.94 and low concentrations of CaO, NiO and MnO (≤ 0.05 wt.%).

5.1.5.2 *Carbonate*

Dolomite in sample LE-13-03 has a Mg# of 0.90. The dolomite in TCG2 is characterized by Ca content of 1.02 to 1.04 a.p.f.u and a Fe content of 0.09 a.p.f.u.

5.1.5.3 *Chlorite*

Chlorite has Mg# between 0.85 and 0.86 and a higher aluminium content (~5.6 to 5.8 a.p.f.u) compared to the chlorite from TCG1. Cr₂O₃ content is between 1.58 to 1.93 wt.% while the concentration of CaO, NiO and MnO is low (≤ 0.10 wt.%).

5.2 WHOLE-ROCK GEOCHEMISTRY

Whole-rock compositions of the analyzed rocks are shown in appendix Tab.3. Also shown are the results recalculated on a volatile free basis, which allows the comparison of their chemistry with fresh peridotite samples. Whole-rock analyses of ultramafic rocks from Leka by Furnes et al. (1991); Maalø e (2005); Iyer et al. (2008a) and Plümer et al. (2012) are shown in the ternary SiO₂ - MgO - CaO system (Fig. 26 A). The whole-rock chemistry of the serpentinite and the talc-carbonate rocks from this study are shown in the same system in Fig. 26 B.

5.2.1 *Partly Altered Peridotites*

Whole-rock analyses show that there are small chemical changes between sample LE-12-01 from the mantle tectonite and sample LE-13-05 from the cumulate section (Tab. 3). The partly altered peridotite sample LE-12-01 from the mantle tectonite is relatively rich in MgO (44.7 wt.%) and SiO₂ (~44 wt.%) compared to average values of peridotites in the mantle tectonite obtained by Furnes et al. (1991). However, the values are lower than those obtained by Iyer et al. (2008a) and Plümer et al. (2012). A LOI of 11.8 wt.% and a CO₂ concentration of 0.38 wt.% was obtained for sample LE-12-01.

Sample LE-13-05 from the cumulate section has a MgO concentration of 45.9 wt.% which, according to Maalø e (2005), is a transition between peridotite (MgO < ~45 wt.%) and pure dunite (MgO > 48.5 wt.%). A LOI of 11.8 wt.% and a CO₂ concentration of 0.12 wt.% was measured for sample LE-13-05.

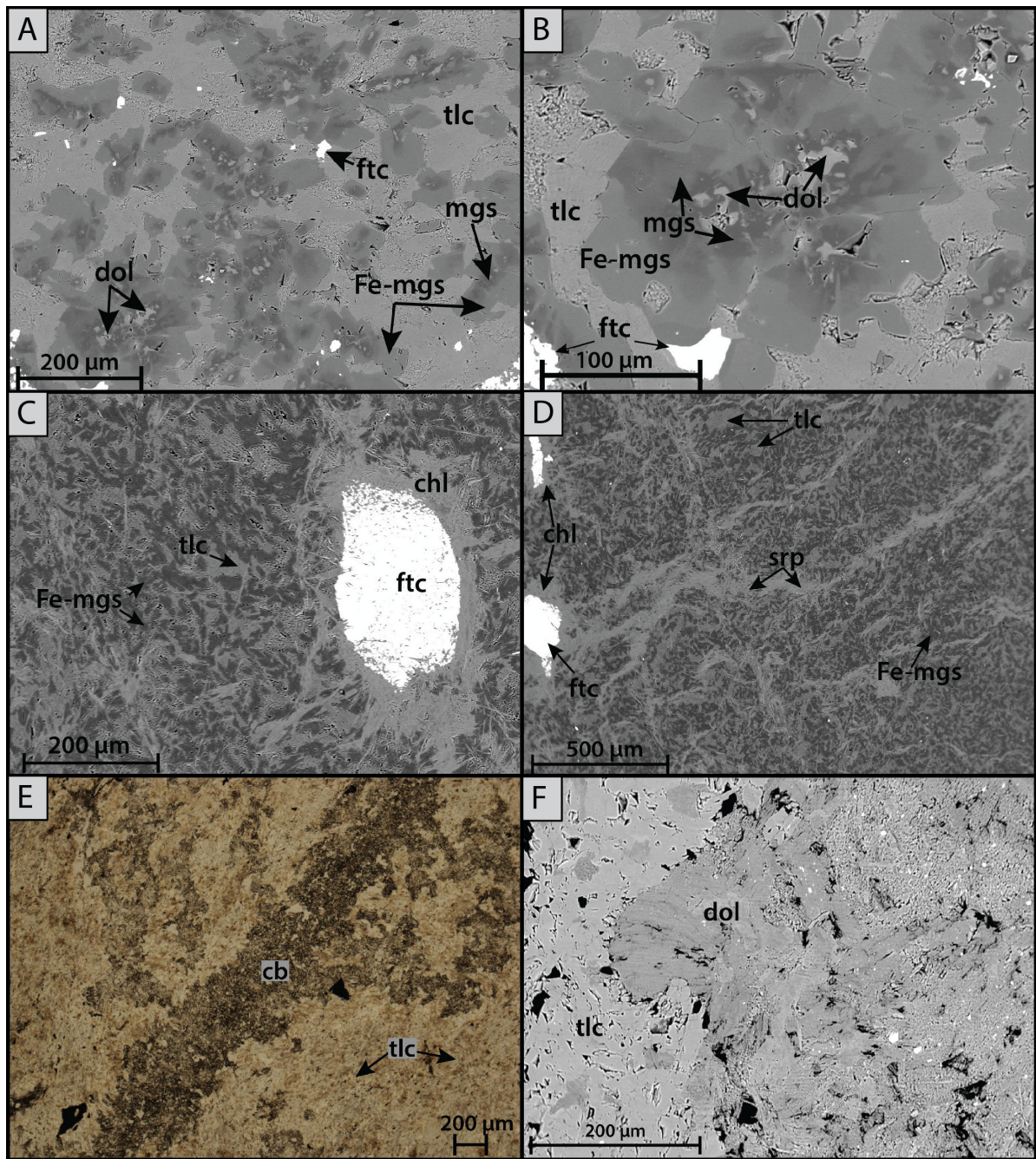


Fig 25: BSE images A) and B) from sample LE-11-01 show the compositional zoning pattern observed in carbonates, with dolomite (dol) forming cores of magnesite (mgs) rimmed by iron-rich magnesite (Fe-mgs). Talc (tlc) commonly forms sub-hedral, bladed crystals. Ferritchromite (ftc) occurs as 0.05 – 0.1 mm large grains and often shows sharp contacts with crystals of carbonate. BSE images C) and D) from sample LE-12-02 show the fine-grained matrix with talc and iron-rich magnesite occurring in approximately similar proportions. Grains of ferritchromite (ftc) are commonly replaced by chlorite (chl) in this sample (see also Fig. 23). A very fine-grained vein of serpentine (srp) cuts through the matrix. E) and F) Talc and dolomite (dol) forming the matrix and a vein of carbonate (cb) in sample LE-13-03 from TCG2.

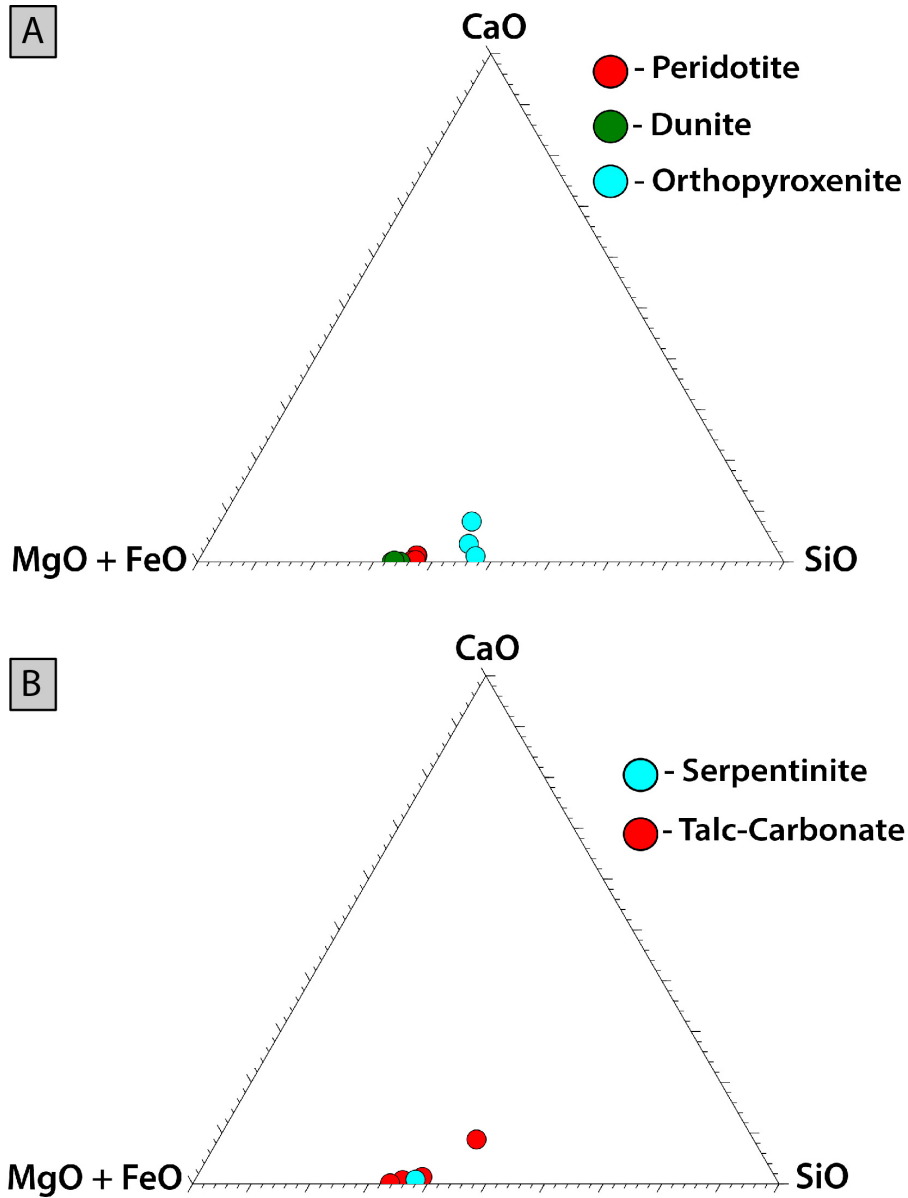


Fig 26: A) Ternary plot in the $\text{SiO}_2 - \text{MgO} + \text{FeO} - \text{CaO}$ system, depicting the ultramafic rock compositions from this thesis and from the literature (molar proportions calculated from Furnes et al., 1991; Maaløe, 2005; Iyer et al., 2008a and Plümper et al., 2012). B) Ternary plot of the compositions of the rocks from the alteration zones in the $\text{SiO}_2 - \text{MgO} + \text{FeO} - \text{CaO}$ system (molar proportions calculated from Tab.3). The diagram shows that the composition of the altered rocks is similar to that of the partly altered peridotites.

5.2.2 Serpentinite

The analyzed serpentinite has a Mg# of 0.91 which is similar to that of the partly altered peridotites. The concentrations of both MgO and SiO₂ are 44,9 wt.%. CaO and Al₂O₃ are both close to 1 wt.%. The serpentinite has a LOI of 15.99 wt.% and a measured CO₂- concentration of 2.12 wt.%. The concentration of FeO and Fe₂O₃ is 5.9 and 2.2 wt.%, respectively.

5.2.3 Talc-Carbonate Rocks

Talc carbonate rocks of the group one is characterized by SiO₂ and MgO values of ~40 – 45 wt.% and ~41 – 46 wt.%, respectively, similar to the partly altered peridotites. FeO and Fe₂O₃ values range between 7.4 to 9.9 wt.% and 1.9 to 3.8 wt.%, respectively. LOI in the TCG1 is high, ranging from 20.3 to 25.4 wt.% and CO₂ content from ~3.5 to 6.1 wt.%.

Talc-carbonate rocks of the group two have similar whole-rock composition as the orthopyroxenite dykes, with relatively higher concentration of SiO₂ and CaO (49.7 wt.% and 9.2 wt.%, respectively), and lower concentration of MgO (31.8 wt.%) and FeO (4.9 wt.%) with respect to the TCG1. Values for LOI are lower (15.6 wt.%) than in the TCG1. However, CO₂- values are much higher with 10.9 wt.%.

Table 3: Whole-rock composition of the partly altered peridotites, serpentinite and talc-carbonate measured with X-ray fluorescence.

Rock Type	Partly Altered Peridotite		Serpentinite	Talc-carbonate 1			Talc-carbonate 2
Sample	LE-12-01	LE-13-05	LE-11-02	LE-11-01	LE-12-02	LE-13-04	LE-13-03
wt%							
SiO ₂	38,72	38,22	37,47	31,61	29,88	35,64	41,60
Al ₂ O ₃	0,78	0,51	0,87	0,83	0,63	0,77	1,60
Fe ₂ O ₃	5,23	7,25	1,84	1,42	1,89	3,01	1,81
FeO*	2,70	4,08	4,95	5,78	7,39	5,90	4,15
MgO	39,40	42,48	37,48	34,22	34,40	32,51	26,68
CaO	1,24	0,03	0,78	0,64	0,10	1,18	7,72
TiO ₂	0,02	0,03	0,03	0,02	0,01	0,02	0,04
LOI	11,80	6,25	15,99	25,01	25,41	20,30	15,64
CO ₂ *	0,38	0,12	2,12	3,49	6,14	3,97	10,92
Compositional data, recalculated on volatile-free basis							
SiO ₂	43,95	41,28	44,93	42,42	40,21	45,10	49,76
Al ₂ O ₃	0,88	0,55	1,04	1,11	0,85	0,97	1,92
Fe ₂ O ₃	5,94	7,83	2,20	1,91	2,55	3,81	2,16
FeO	3,07	4,41	5,93	7,76	9,94	7,47	4,96
MgO	44,73	45,88	44,94	45,93	46,29	41,14	31,91
CaO	1,41	0,03	0,94	0,86	0,14	1,49	9,23
TiO ₂	0,02	0,03	0,03	0,02	0,02	0,02	0,05
Mg#	0,90	0,88	0,91	0,90	0,87	0,87	0,89

*Determined separately at Acme Labs. Fe₂O₃ was recalculated based on this analysis.

5.3 STABLE ISOTOPES

Oxygen and carbon isotopic compositions have been determined for dolomite from the coarse-grained carbonate lens within the talc-carbonate rock. The obtained values of $\delta^{18}\text{O}$ are shown in Tab. 4 and range from 10.8 to 11.3‰. Values for $\delta^{13}\text{C}$ are low and fall within the range of mantle derived carbon ($\delta^{13}\text{C} \sim 5.0\text{‰}$; Deines, 2002; Hoefs, 2009).

Table 4: Oxygen isotope data

Mineral	Carbonate $\delta^{18}\text{O}$ (SMOW)	Carbonate $\delta^{13}\text{C}$ (VPDB)	Temperature calculated (C°)*	Host rock lithology	Sample
Dol	11,24	-5,47	228	Carbonate Lens	BE10-1
Dol	11,34	-5,25	226	Carbonate Lens	BE10-3
Dol	11,18	-5,40	229	Carbonate Lens	BE10-5
Dol	11,05	-4,79	232	Carbonate Lens	BE10-7
Dol	11,13	-4,61	230	Carbonate Lens	BE10-9
Dol	10,87	-5,20	233	Carbonate Lens	BE10-11
Dol	10,98	-5,24	234	Carbonate Lens	BE10-18

*Calculated from the fractionation factor $1000 \ln \alpha_{\text{dolomite-water}} = 2.76 * 10^6 T^{-2} + 0.26$ from Vasconcelos et al. (2005).

5.4 STRONTIUM ISOTOPES

The partly altered peridotites show very low concentrations of strontium (≤ 0.26 ppm) which may reflect the low strontium content observed in ultramafic rocks from ophiolites. Alternatively, strontium could have been removed by the infiltrating fluids. However, recent investigations have shown that oceanic serpentinization causes an enrichment of trace elements like strontium in peridotites (Scambelluri et al., 2004; Paulick et al., 2006; Vils et al., 2008; Andreani et al., 2007; Debret et al., 2013), indicating that the rocks were initially depleted in strontium.

The serpentinite shows strontium concentrations of ~ 1 ppm. The rocks from TCG1 show variable, but low, concentrations of strontium in the range 0.11 – 2.69 ppm. The highest strontium concentrations were obtained for samples LE-13-03 from TCG2, and sample LECB, which represents the carbonate lens, with 12 ppm and 92 ppm, respectively. Initial $^{87}\text{Sr}/^{86}\text{Sr}$ values calculated at 400 Ma for samples LE-13-03 (0.7029), LE-13-04 (0.7045) and LECB (0.7063) indicate that the strontium originated from partial melting of the mantle and has not interacted with more evolved reservoirs (Faure, 2001; Winter, 2010).

Table 5: Strontium isotope data.

Sample no	Rock Type	[Rb] (ppm)	[Sr] (ppm)	$^{87}\text{Rb}/^{86}\text{Sr}$	$^{87}\text{Sr}/^{86}\text{Sr}$ at 400 Ma	$\pm 2\sigma_m$
LE-12-01	Partly altered peridotite (tectonite)	0,74	0,26	8,23	0,659253	0,000014
LE-13-05	Partly altered peridotite (cumulate)	0,78	0,11	20,53	0,595780	0,000021
LE-11-02	Serpentinite	0,72	1,41	1,48	0,698879	0,000009
LE-11-01	Talc-carbonate group 1	0,53	1,02	1,50	0,699639	0,000012
LE-12-02	Talc-carbonate group 1	0,87	0,11	22,90	0,584769	0,000032
LE-13-04	Talc-carbonate group 1	0,53	2,69	0,13	0,704749	0,000007
LE-13-03	Talc-carbonate group 2	0,55	12,15	0,57	0,703794	0,000009
LECB	Carbonate Lens	0,08	92,27	0,003	0,706314	0,000008

METAMORPHIC EVOLUTION

6.1 INTRODUCTION AND BACKGROUND

Because of the lack of geothermometers for low-grade metamorphism of ultramafic rocks it is difficult to obtain precise pressure and temperature conditions of metamorphism (e.g., Essene, 1989; Bucher and Grapes, 2011). In contrast to mafic rocks which show a wide variety of parageneses with changing metamorphic conditions, ultramafic rocks generally display large stability fields for single assemblages. Forward modeling using the thermodynamic software *Perple_X* (Connolly, 2005, 2009) has been utilized to assess the metamorphic evolution of the studied alteration zones. The calculations were done with the internally consistent database of thermodynamic properties for mineral endmembers published by Holland and Powell, 1998 (2002 upgrade) and mixing models for carbonates from Franzolin et al. (2010) and clinopyroxene from Holland and Powell (1996). Olivine, antigorite and talc were treated as ideal iron-magnesium solutions with site occupancies from Holland and Powell (1998). Mineral assemblages, microstructural relationships and mineral compositions are interpreted to represent phase equilibrium in the studied samples.

The main factors controlling the mineral assemblages are bulk composition, partial pressure of CO₂ (X_{CO_2}), temperature (T) and pressure (P). The calculated modal volumes of minerals and their composition from all the rock types correlate reasonably well with those measured by the microprobe and observed in thin sections. Some discrepancy exists, however, between the measured and the modeled carbonate composition (Fig. 33).

6.1.1 *General Assumptions*

The LOC has undergone low-grade regional metamorphism at the upper greenschist to lower amphibolite facies during the Caledonian orogenesis, but precise pressure estimates are lacking (Prestvik, 1972, 1980; Bucher, 1988; Bucher-Nurminen, 1991; Furnes et al., 1988). Regional studies suggest that the LOC is a part of the Helgeland Nappe Complex belonging to the Uppermost Allochthon, which is inferred to be the highest stratigraphical unit in the Scandinavian Caledonides (Bucher-Nurminen, 1991; Titus et al., 2002; Nordgulen et al., 2011; McArthur et al., 2013). Bucher-Nurminen (1991) suggested that the antigorite overprint observed in the ultramafic rocks on Leka is a consequence of the Caledonian metamorphism, which produced a regional metamorphic pattern in the ultramafic rocks in the central Norwegian Caledonides. The metamorphic grade increases from Leka in the southeast, to the Svartisen nappe complex in the northwest with estimated pressures of ~5 kbar for the rocks along the Helgeland coast, and pressures of ~1 to 3 kbar for the LOC. Based on this information, phase diagrams have been calculated for pressures of 1 kbar and 3 kbar to account for uncertainties in the pressure estimates.

There are small amounts of aluminum present in all of the studied rocks (Tab. 3). Aluminum in the partly serpentinized peridotites is primarily stored in the spinel and clinopyroxene, and minor amounts were measured in serpentine minerals (chapter 5). In the serpentinite there are negligible amounts of aluminum in the main alteration phases (i.e., serpentine and carbonate) while the talc-carbonate rocks locally have aluminum in the spinel and chlorite. The aluminum in the carbonate-bearing samples

does not appear to participate in any reactions producing serpentine or talc (Fig. 23). Instead, the formation of chlorite is restricted to the presence of Al-bearing spinel (Fig. 23; Evans, 1977). On the basis of this spatially localized occurrence of Al-rich minerals, aluminum is excluded from the system compositions used for the calculations. Recent experiments with Tschermak's substitution in serpentine, however, reveals the possibility of utilizing aluminum content in serpentine as a geothermometer in the future (Padrón-Navarta et al., 2013).

The absence of relic primary phases in the alteration zones (chapter 5) suggests that the saturated fluid conditions can be used as an assumption for the modeling of the evolution of these rocks.

6.2 THERMODYNAMIC MODELING OF PARTIAL ALTERATION OF PERIDOTITE

The mineral assemblage occurring in the investigated partly altered peridotite is Ol-Cpx-Srp-Mag-Brc. A representative T-H₂O_{mol} sections for the partly altered peridotite sample LE-13-05 at 1 kbar and 3 kbar are shown in Fig. 27. The sections are calculated in the SiO₂ - MgO - FeO - Fe₂O₃ - CaO - H₂O system with variable H₂O content along the horizontal axis of the diagram and the following molar bulk-rock composition - SiO₂ : 0.689, MgO : 1.142, FeO : 0.057, Fe₂O₃ : 0.045, CaO : 0.025 and H₂O increasing from 0 to 1 mol. The red dotted line represents the stability line for H₂O, with the stability of H₂O to the right of the line. This also marks the transition to a fully hydrated assemblage in the partly altered peridotites at temperatures < 400°C with the complete removal of olivine (Fig. 28). With increasing H₂O_{mol} the serpentine and brucite content increase on the account of olivine (Fig. 28).

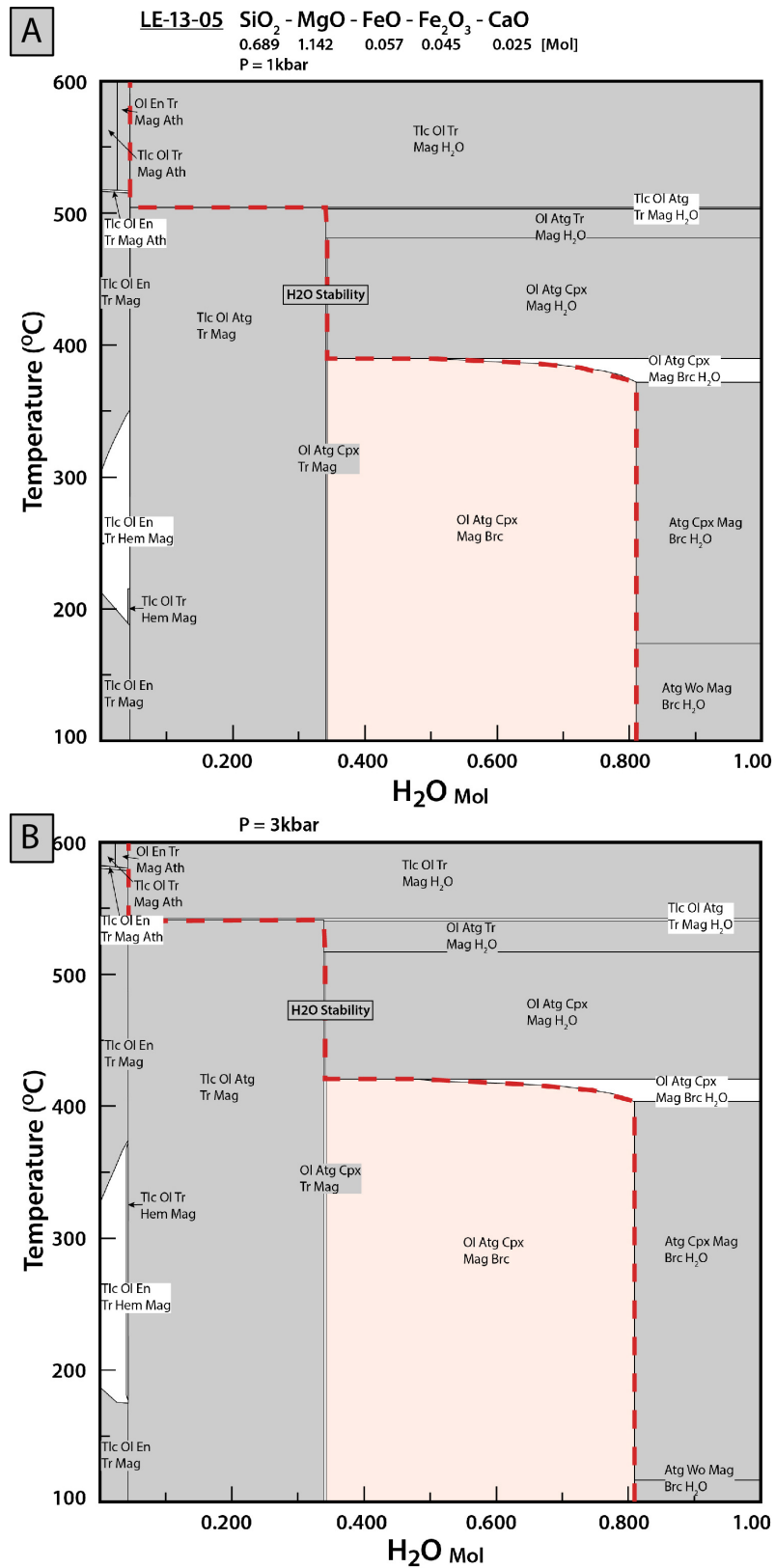


Fig. 27: T-H₂O_{Mol} section for partly altered peridotite sample LE-13-05 calculated in the SiO₂ - MgO - FeO - Fe₂O₃ - CaO system with the measured whole rock composition. The colored 5-phase field corresponds to the Ol-Atg-Cpx-Mag-Brc in the partly altered peridotites. The red dotted line represents the stability line for H₂O, with the stability of H₂O to the right of the line. A) Diagram at 1kbar. B) Diagram at 3 kbar.

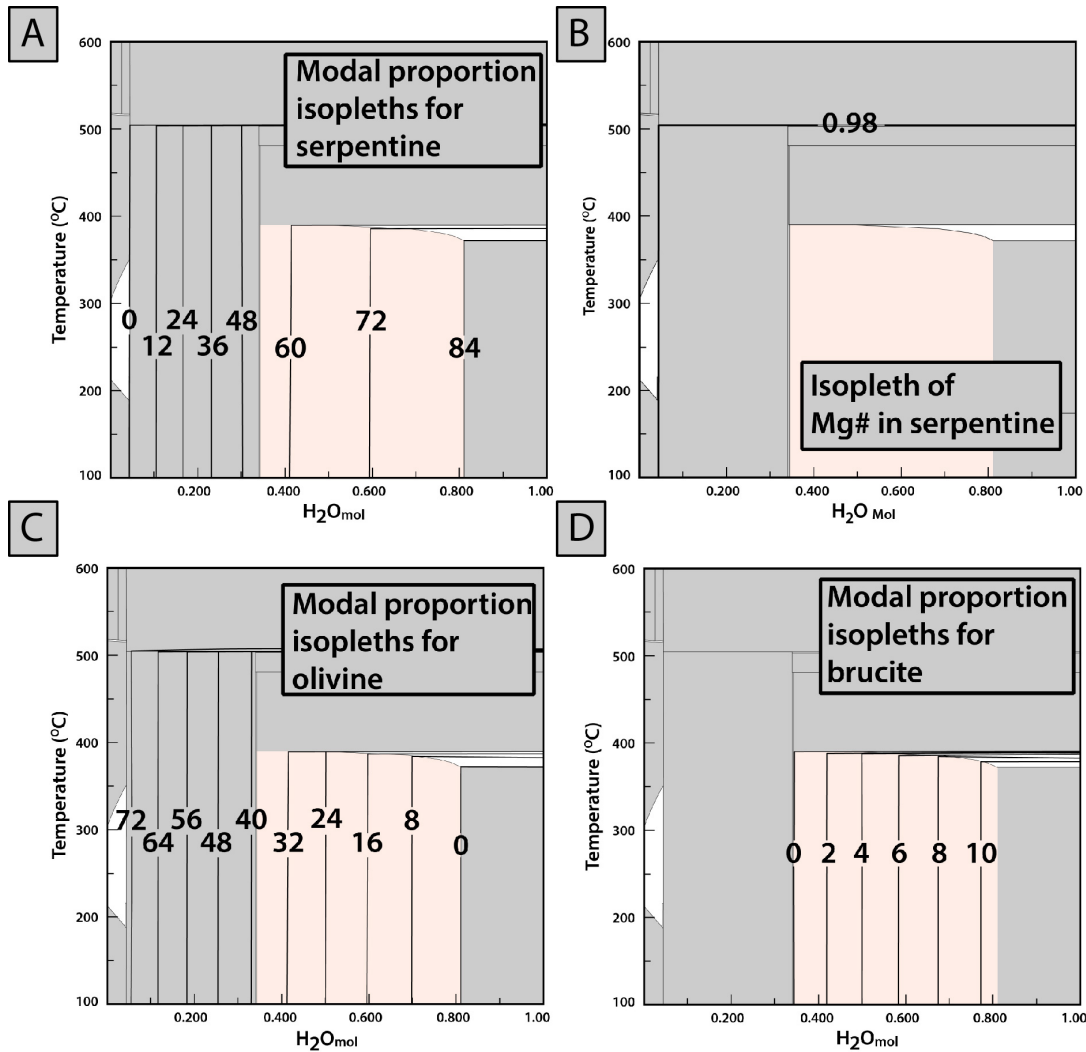


Fig. 28: T- H_2O_{Mol} section calculated for sample LE-13-05 with the whole rock compositions from Fig. 27 at 1 kbar. The colored stability field corresponds to the Ol-Atg-Cpx-Mag-Brc stability field in Fig. 27. Modal proportions of serpentine, olivine and brucite is shown in Fig A, B and C. Isopleth for Mg# in serpentine is shown in Fig B.

6.3 THERMODYNAMIC MODELING OF THE SERPENTINITE ASSEMBLAGE

Temperature and X_{CO_2} conditions for the stability of the serpentinite assemblage Srp-Mgs-Mag-Dol were estimated from the T- X_{CO_2} sections constructed for the sample LE-11-02. The T- X_{CO_2} sections were calculated in the $SiO_2 - MgO - FeO - Fe_2O_3 - CaO - H_2O - CO_2$ system with saturated $H_2O + CO_2$ fluid and the following molar bulk composition $SiO_2 : 0.747, MgO : 1.114, FeO : 0.069, Fe_2O_3 : 0.011$ and $CaO : 0.017$.

The calculated T- X_{CO_2} sections indicate that the stability of the Srp-Mgs bearing assemblage at 1 kbar is restricted to temperatures below $450^\circ C$ and X_{CO_2} compositions of < 0.24 (Fig. 29). At the pressure of 3 kbar, the Srp-Mgs-Mag-Dol stability field shrinks and the stability is limited to temperatures $< 500^\circ C$ and $X_{CO_2} \leq 0.08$ (Fig. 30). The colored 4-phase fields correspond to the observed mineral assemblage of the serpentinite.

6.4 THERMODYNAMIC MODELING OF TALC-CARBONATE GROUP ONE

Talc-carbonate group one is represented by three samples: LE-11-01, LE-12-02 and LE-13-03, and consists of the assemblage Tlc-Mgs-Mag-Dol. As the chemical composition of all the sampled rocks from the TCG1 are similar (Tab. 3), representative phase diagrams are presented for the sample LE-11-01. Calculated T- X_{CO_2} sections for sample LE-11-01 based on the following molar bulk-rock composition SiO_2 : 0.705 , MgO : 1.137, FeO : 0.080, Fe_2O_3 : 0.009 and CaO : 0.015 indicate that the stability of the Tlc-Mgs-Mag-Dol assemblage is restricted to temperatures of $< 460^\circ C$ and X_{CO_2} of ≥ 0.03 at 1 kbar (Fig. 31). At the pressure of 3 kbar, the stability field is shifted to higher temperatures corresponding to $< 550^\circ C$ and X_{CO_2} of > 0.02 (Fig. 32). The colored 4-phase fields corresponds to the observed mineral assemblage of the talc-carbonate group one. Isoleths of Mg# in talc and serpentine together with isopleths of $Mg/(Mg + Fe + Ca)$ of magnesite is shown in Fig. 33 A, C and E. Modal proportion isopleths for talc, magnesite and serpentine are shown in Fig. 33 B, D and F.

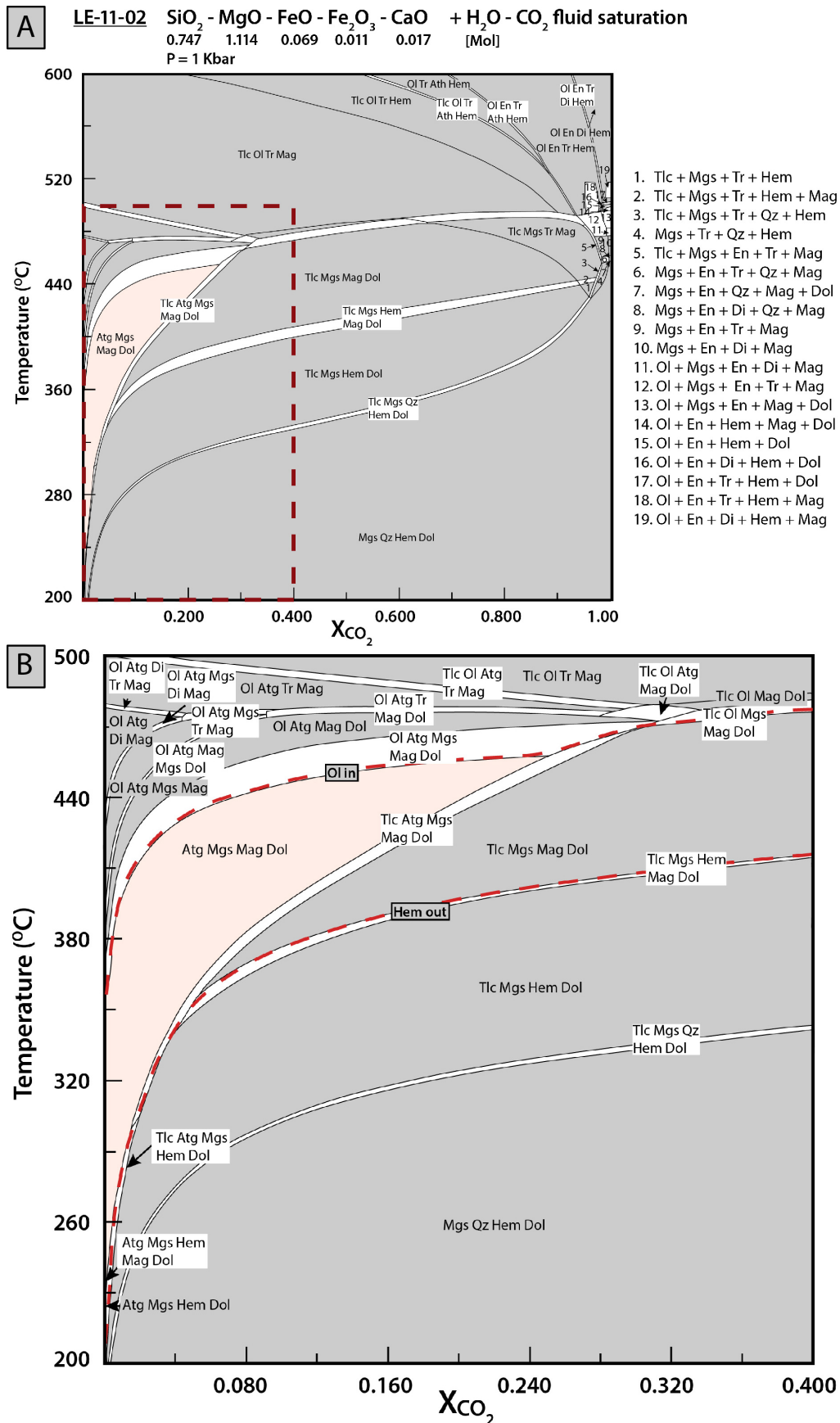


Fig. 29: A) T- X_{CO_2} section for serpentinite sample LE-11-02 calculated in the $\text{SiO}_2 - \text{MgO} - \text{FeO} - \text{Fe}_2\text{O}_3 - \text{CaO} - \text{H}_2\text{O} - \text{CO}_2$ system with the measured whole rock composition at 1 kbar. The colored 4-phase field corresponds to the observed Atg-Mgs-Mag-Dol assemblage in the serpentinite. Mineral assemblages in the blank fields are labelled in Fig B. B) Enlarged area marked by the red dotted square in Fig A.

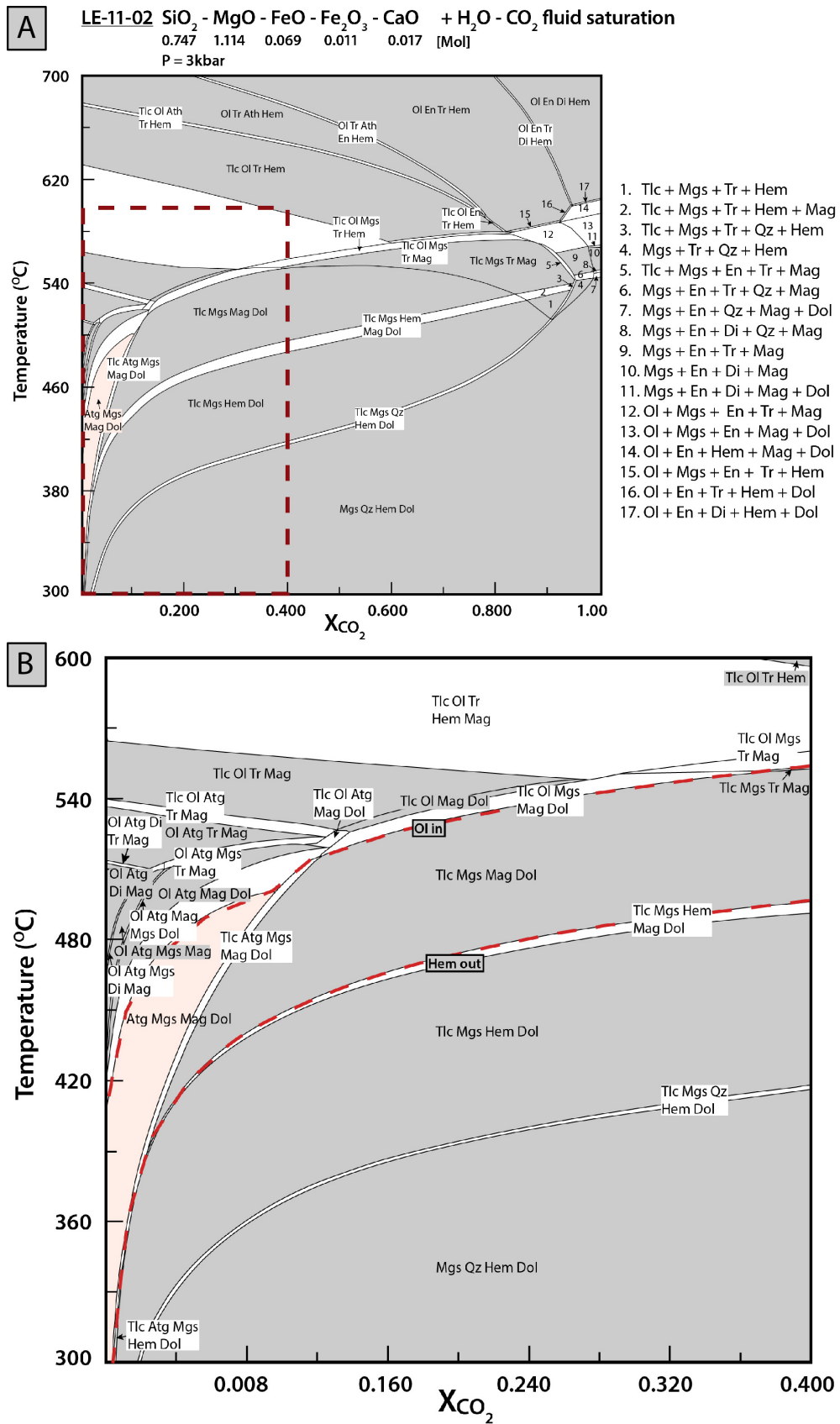


Fig. 30: A) T - X_{CO_2} section for serpentinite sample LE-11-02 calculated in the SiO_2 - MgO - FeO - Fe_2O_3 - CaO - H_2O - CO_2 system with the measured whole rock composition at 3 kbar. Mineral assemblages in the blank fields are labeled in Fig B. Estimated T - X_{CO_2} conditions are indicated by the colored Atg-Mgs-Mag-Dol field. B) Enlarged area marked by the red dotted square in Fig A.

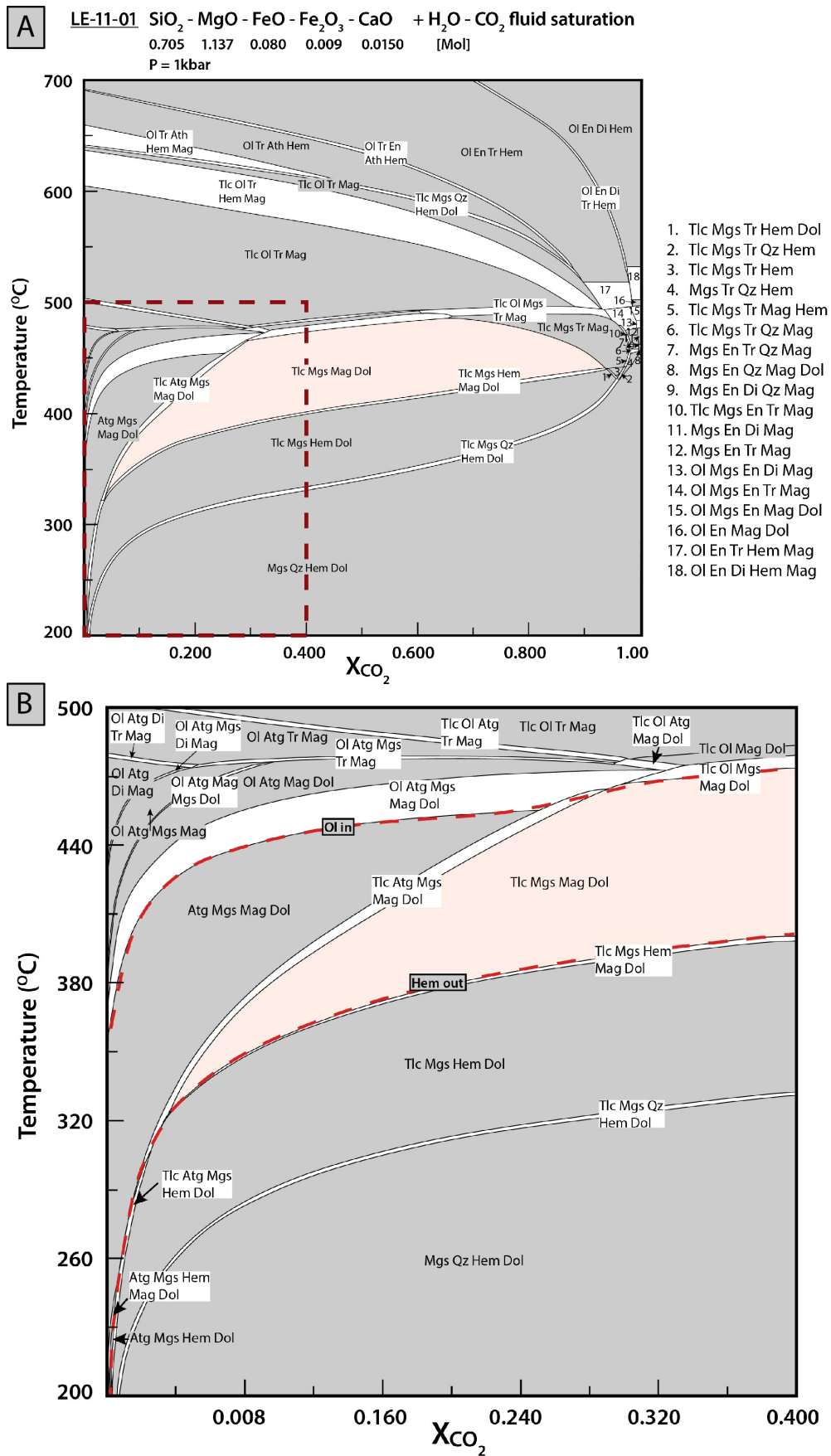
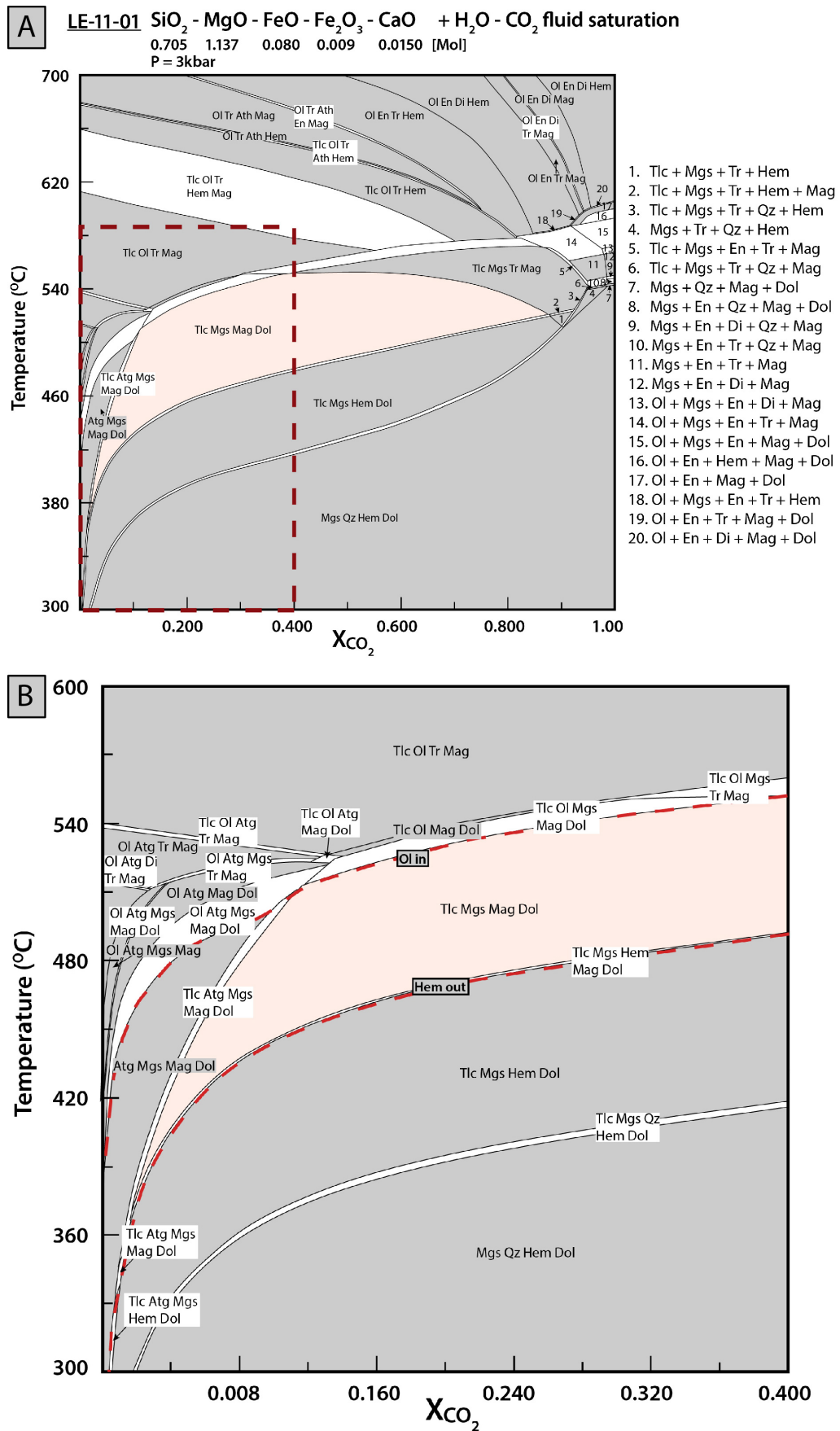


Fig. 31: T- X_{CO_2} section for TCG1 sample LE-11-01 calculated in the $\text{SiO}_2 - \text{MgO} - \text{FeO} - \text{Fe}_2\text{O}_3 - \text{CaO} - \text{H}_2\text{O} - \text{CO}_2$ system at a pressure of 1 kbar with the measured whole rock composition. The colored 4-phase field correspond to the observed Tlc-Mgs-Mag-Dol assemblage in the talc-carbonate. Mineral assemblages in the blank fields are labeled in Fig B. B) Enlarged area marked by the red dotted square in Fig A.



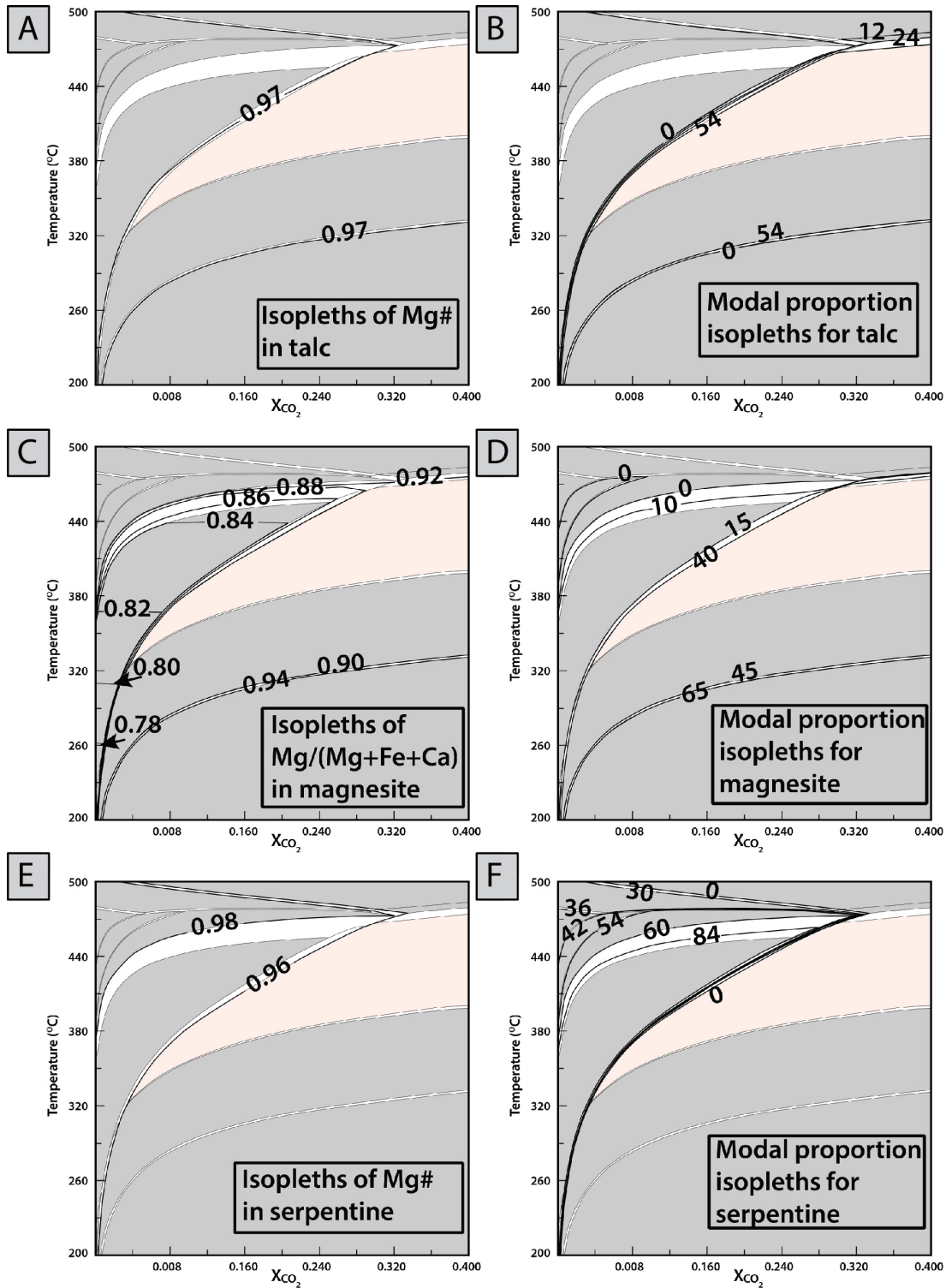


Fig. 33: T- X_{CO_2} section calculated for sample LE-11-01, with whole-rock composition from Fig.31 at 1 kbar. The colored field corresponds to the Tlc-Mgs-Mag-Dol stability field from Fig.31. Isopleths of Mg# in talc and serpentine and Mg/(Mg + Fe + Ca) for magnesite is shown in A, C and E. The modal proportions of each mentioned mineral is shown in Fig B, D and F. The Mg# in talc and serpentine correlates well with the ones measured. Some discrepancy exists between the measured and modeled magnesite composition. Modal proportions correlate well with the ones observed in this section.

INTERPRETATION AND DISCUSSION

7.1 GEOCHEMISTRY OF THE ALTERATION

There are small chemical differences among the partly altered peridotites and the completely serpentinized and carbonated rocks after recalculation to a volatile-free basis (Fig. 26). It is suggested that these small differences can be attributed to local variations in SiO₂, MgO, FeO and CaO content due to 1) varying proportions of primary olivine and clinopyroxene and 2) mobility of elements during serpentinization. These results support several field studies suggesting that the talc-carbonate alteration is mainly isochemical (Chidester, 1962; Naldrett, 1966; Eckstrand, 1975; Coats and Buchan, 1979; Donaldson, 1981; Hansen et al., 2005; Shervais et al., 2005; Beinlich et al., 2012). Following the recommendations of the International Union of Geological Sciences (IUGS), the rocks are not classified as metasomatic rocks, but rather as a product of isochemical metamorphism where the partial pressure of H₂O and CO₂ in the reacting fluids, together with the original rock composition have been the controlling chemical factors during the alteration (Zharikov et al., 2007).

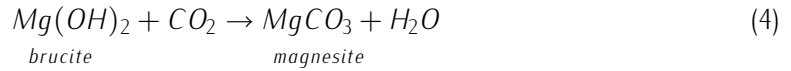
Field relationships demonstrate the importance of zones with high permeability for complete alteration of the ultramafic rocks at Leka. Complete serpentinization and carbonation are restricted to macroscopically visible fracture zones in sharp contact with the surrounding partly altered peridotites (Fig. 11). The most voluminous (~12 meters thick) alteration zone occurs along the lithological contact between the partly altered peridotites from the mantle tectonite and the partly altered peridotites from the cumulate section.

The alteration products, talc, serpentine and dolomite usually have a higher Mg# than the relic primary minerals olivine and clinopyroxene, a feature that has been extensively described from serpentinized and carbonated peridotites elsewhere (Evans, 1977; Frost, 1985; Janecky and Seyfried, 1986; Früh-Green, 1996; Mével and Stamoudi, 1996; Früh-Green et al., 2004; Frost and Beard, 2007; Evans, 2008; Klein et al., 2009; McCollom and Bach, 2009; Kelemen et al., 2011; Klein et al., 2013). It is proposed that excess iron has been fractionated into magnetite and iron-rich magnesite during alteration (Fig. 33). All the minerals show limited variations in the chemistry (Fig. 16). Serpentine minerals show the most variable Fe²⁺Mg₋₁ substitution, with Mg# ranging from 0.88 to 0.98. It is possible that the variable chemistry of the serpentine minerals is related to variable chemistry in the precursor minerals (Evans, 2008; Evans et al., 2012).

In the alteration zones, iron in primary spinel has been oxidized to form ferritchromite and magnetite (Fig. 19), leading to contrasting oxidation states between the partly altered peridotites and the alteration zones. This indicates that the oxygen fugacity has been controlled by the altering fluids, and that the fluids responsible for the alteration created oxidizing conditions (high fO₂). This correlates well with the redox model proposed by Eckstrand (1975). Dissociation of water during serpentinization has been proposed as a way to produce oxygen to oxidate Fe²⁺ in silicates to Fe³⁺ (O'Hanley, 1996).

7.2 PARTLY ALTERED PERIDOTITES

The partly altered peridotites consist of the mineral assemblage Ol-Cpx-Srp-Mag-Brc. Bladed crystals of serpentine are seen to replace olivine crystals along fractures (Fig. 20). Primary Cr-spinel is seen



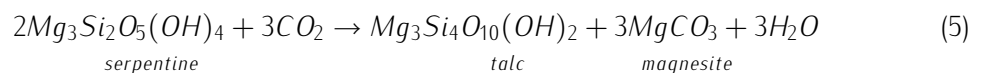
These reactions have not been observed in thin sections because they have run to completion, which is evident from the absence of brucite, relic olivine and pyroxene. The phase diagram calculations show that the stability of the observed 4-phase mineral assemblage of the serpentinite is bound by 5-phase fields (Fig. 29). The serpentinite assemblage at 1 kbar is thus limited to temperatures below 460°C and X_{CO_2} values of < 0.28 , while for the pressure of 3 kbar the temperature limit is < 510 °C and X_{CO_2} values of ≤ 0.14 . Higher temperature phase fields are characterized by the gradual replacement of serpentine by olivine until the complete removal of serpentine at $\sim 490^\circ\text{C}$ and $X_{\text{CO}_2} = 0.1$ at 1 kbar (Fig. 29 and Fig. 33). Tremolite is stabilized at $\sim 470^\circ\text{C}$. Stability fields at higher X_{CO_2} are marked by the presence of talc and/or hematite. At lower temperatures, quartz becomes stable with Mgs-Hem-Dol.

7.4 CONDITIONS DURING TALC-CARBONATE ALTERATION

Field evidence and microscopic observations indicate static conditions during carbonation of the completely serpentinitized rocks. Formation of the observed Tlc-Mgs-Mag-Dol assemblage can be explained by the breakdown of the serpentine minerals in the previously formed serpentinite. The observed zoning in the carbonates (a core of dolomite enclosed in magnesite rimmed with iron-rich magnesite; Fig. 25) can be explained by the breakdown of minerals during alteration and fractionation of iron and calcium. During carbonation and formation of the talc-carbonate mineral assemblage from serpentinite, serpentine minerals are rapidly replaced while the breakdown of magnetite/ferritchromite is slower (c.f., Karlsen et al., 2000; Hansen et al., 2005). Iron released from olivine, clinopyroxene and serpentine can enter the magnesite and leads to the observed zoning with iron-rich rims. Another possibility is that the magnesite represents remnants from reaction 3.

A possible source for the calcium required to form dolomite is clinopyroxene, which was observed in the partly altered peridotite (Fig. 18). It is likely that the clinopyroxene broke down faster than olivine and supplied the additional calcium to stabilize dolomite as the early carbonate phase (e.g., Kelemen et al., 2011). When all the clinopyroxene has been consumed, no more calcium is available for further growth of dolomite and magnesite is stabilized instead. A higher abundance of dolomite is indeed observed in samples which presumably consisted of a higher proportion of clinopyroxene (Fig. 25). Alternatively, the calcium could have been externally introduced to the system by the altering fluids (e.g., hydrothermal alteration of associated basalts and/or gabbros), or the dolomite could have been already present in the partly altered peridotites (Fig. 18) prior to the alteration. It has been shown that an influx of Ca-CO₂-enriched solutions to partly altered peridotites can lead to the depletion of the magnesium content, and favor the precipitation of calcite as the major carbonate mineral (Hövelmann et al., 2011). As calcite is not observed within the alteration zones, it is suggested that the infiltrating fluids have been poor in calcium and that the calcium most likely has been derived from clinopyroxene or dolomite from the partly altered peridotite.

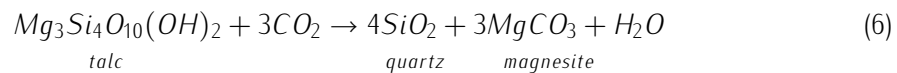
The reaction:



is responsible for the growth of talc at the expense of serpentine and occurs already at low CO₂ concentrations (Spear, 1995; O'Hanley, 1996; Bucher and Grapes, 2011). The assemblage Tlc-Mgs-Mag-Dol is stable within a narrow range of temperature and a wide range of X_{CO_2} concentrations, and is limited by the stability of olivine at higher temperatures and the stability of hematite and quartz at lower temperatures (Fig. 31 and Fig. 32). The stability of tremolite and enstatite is met at higher X_{CO_2} ,

while lower X_{CO_2} allows for the stabilization of serpentine. The absence of olivine, enstatite and anthophyllite indicates formation temperatures below 460°C with $X_{CO_2} \geq 0.03$ at 1 kbar, and < 550°C at 3 kbar. These temperatures are somewhat higher than those suggested at Leka for the Atg + Brc assemblage formed during Caledonian metamorphism (< 400°C; Prestvik, 1980; Bucher, 1988; Furnes et al., 1988; Iyer et al., 2008a). This opens up for the possibility that fluids with higher temperatures could have been flowing through permeable layers creating a thermal anomaly between the carbonated rocks and the partly altered peridotites. Thermal anomalies due to focused fluid flow have previously been described for rocks in central New Hampshire, USA (Chamberlain and Rumble, 1989; Thompson and Connolly, 1992).

The presence of undeformed talc veins, locally associated with carbonate, within the carbonated bodies possibly represent a stage during the alteration in which fluids infiltrating smaller shear- or fracture zones precipitated carbonate minerals, reducing the CO_2 concentration of the fluid phase and thereby allowing the precipitation of talc. Alternatively, silica could have been locally concentrated in the fractures with lower concentrations of CO_2 . Formation of magnesite and dolomite reduces the Mg/Si ratio of the remaining silicates in the rock (O'Hanley, 1996). This means that talc + magnesite, represents a lower extent of carbonation than quartz + magnesite, which is evident from the phase diagrams, where talc is replaced by quartz with increasing CO_2 / H_2O -ratios (e.g., Frost, 1985; O'Hanley, 1996). It is thus likely that the carbonation ceased shortly after all the serpentine minerals were consumed. Further carbonation at decreasing temperatures would likely have initiated the formation of a quartz-magnesite rich assemblage commonly named listwanite (Fig. 33; Ash and Arksey, 1990; Hansen et al., 2005; Robinson et al., 2005; Klein and Garrido, 2011) by the breakdown of talc, in the reaction:



The presence of serpentinite flanking the talc-carbonate rocks in the alteration zones (Fig. 11), either means that the influx of fluids suddenly ceased, or that further conversion was prevented by other means. Several experimental studies have shown that the precipitation of carbonates, or silica-rich layers leads to clogging of the system by acting as diffusion barriers (Park and Fan, 2004; Schulze et al., 2004; Boschi et al., 2009). The exact cause that prevented complete talc-carbonate alteration of the serpentinites has not been identified.

7.5 POSSIBLE FLUID SOURCES

Oxygen isotope analysis shows that the fluids responsible for the talc-carbonate alteration have been isotopically heavy ($\delta_{SMOW}^{18}O \sim 10.8 - 11.3\%$) and resemble those of metamorphic waters. $\delta^{13}C$ values of ~ -5 indicate a mantle origin for the carbon source (Deines, 1992, 2002; Hoefs, 2009). Initial $^{87}Sr / ^{86}Sr$ values of 0.7037 - 0.7063 in talc-carbonate rocks indicate that the strontium originated from partial melting of the mantle and have not interacted with more evolved reservoirs (Rollinson, 1993; Faure, 2001; Winter, 2010 and references therein). Sheppard, 1980 (in O'Hanley, 1996) found similar $\delta^{18}O$ values for serpentinitized ultramafic rocks, and concluded that the isotopic signature represent a mixing between seawater and metamorphic waters derived from the dehydration reactions of previously hydrated oceanic crust. However, the low concentrations of strontium in the rocks and the fact that seawater enriches rocks in strontium (Scambelluri et al., 2004; Paulick et al., 2006; Vils et al., 2008; Andreani et al., 2007; Debret et al., 2013), suggest that seawater has not been the main fluid source. Based on the combined isotope analysis and the regional geology, it is suggested that most of the altering fluids were derived from the devolatilization reactions of hydrous ultramafic rocks occurring in the deeper parts of the ophiolite complex.

The carbon source is not obvious. Prograde metamorphism of rocks with carbon-bearing minerals leads to breakdown of the minerals and the generation of binary H₂O – CO₂ fluids (e.g., Elmer et al., 2006). Dolomite overgrown by serpentine, as observed in the partly altered peridotite from the mantle section suggests the presence of carbonate minerals prior to the first serpentinization event (Fig. 18). The stability of carbonate minerals in peridotite assemblages in the mantle environment has been established experimentally (e.g., Eggler, 1978; Wyllie, 1978). There is, indeed, ample evidence for the presence of carbon in the mantle (Wyllie, 1977; Luth, 1999; Deines, 2002; Früh-Green et al., 2004; Dasgupta et al., 2009; Dasgupta and Hirschmann, 2010; Kelemen et al., 2011; Manning, 2013) with estimates ranging from 20 ppm to 300 ppm (Javoy and Pineau, 1991; Trull et al., 1993; Zhang and Zindler, 1993; Dasgupta et al., 2009) and an estimated carbon flux of $\sim 10^{12}$ mol/year at mid-ocean ridges (Saal et al., 2002; Shaw et al., 2010). Several authors have documented carbonate alteration involving mantle-derived carbon (Bogoch et al., 1986; Stern and Gwinn, 1990; Auclair et al., 1993; Dahlgren et al., 1993; Oliver et al., 1993; Wickham et al., 1994).

Mantle derived rocks have been shown to contain native carbon in the form of diamonds and graphite (c.f., Crespo et al., 2006; Dasgupta and Hirschmann, 2010). Graphite has also been reported from a range of different mantle-derived rocks such as peridotites, gabbros and basalts (Hollister, 1980; Ballhaus and Stumpfl, 1985; Mathez, 1987; Pineau et al., 1987; Luque et al., 1992; Barrenechea et al., 1997; Deines, 2002; Crespo et al., 2006). Sato and Valenza (1980) suggested that graphite is a common igneous mineral in many deep-seated basaltic intrusions that may have been largely overlooked. Investigations on olivine from kimberlites have shown that olivine with composition Fo₉₀ can be composed of graphite accounting for as much as 6 wt.% of olivine grains, and 9% in serpentine grains (although it is not likely that all the graphite from the serpentine pseudomorphs originates from the original olivine; Freund et al., 1980; Pasteris, 1981). Carbon solubility in olivine is, however, disputed, and a recent article by Keppler et al. (2003) suggests, based on experiments with carbonatite melts, that carbon solubility in olivine is low (in the order of 0.1 to 1 ppm by weight). Further research should be done in order to explain the carbon source for the carbonation of the partly altered peridotites on Leka.

7.6 EVOLUTION OF THE ALTERATION

The ultramafic rocks of the Leka Ophiolite Complex have been through a series of deformation and metamorphic events since their formation at a spreading ridge in a supra-subduction and back-arc setting (Furnes et al., 1988). It has been shown that the processes responsible for the formation of serpentinites and talc-carbonate rocks occur in a wide variety of tectonic settings. Numerous observations and samples of carbonated peridotites come from oceanic core-complexes, oceanic fracture zones, altered ophiolites and sub-seafloor hydrothermal vent systems (Früh-Green et al., 2003; Hopkinson et al., 2004; Boschi et al., 2006; Eickmann et al., 2009a,b; Kelemen et al., 2011; Picazo et al., 2012), clearly demonstrating that carbonation occurs during the ocean-floor stage. In addition, the formation of talc-carbonate rocks and listwanites is often related to the carbonation of ultramafic rocks in collisional settings, where tectonic processes generate fault zones that can act as pathways for altering and mineralizing fluids (e.g., Ash and Arksey, 1990; Jamtveit et al., 2000; Manning, 2013). There are thus three settings which seem likely for the carbonation of partly altered peridotites on Leka: 1) Carbonation at the ocean floor 2) Carbonation during the Caledonian Orogeny or 3) Carbonation during the later post-orogenic stage. Investigations of the mineral assemblages and modeling of their stability suggest that the observed alteration differs from the serpentinization and rodingitization described on Leka by Iyer et al. (2008a) and Austrheim and Prestvik (2008) who attributed the alteration to the ocean-floor stage. Emplacement of the ophiolite complex in Ordovician to Early Silurian led to folding of the ultramafic rocks and the unconformable overlying sedimentary

sequence and the rocks were metamorphosed to the upper greenschist– lower amphibolite facies (Furnes et al., 1988; Titus et al., 2002). If the talc–carbonate formation preceded the emplacement of the ophiolite complex, the rocks in the alteration zones should have developed a similar degree of ductile deformation as the adjacent rocks and the overlying sedimentary sequence. The lack of deformation observed in the alteration zones therefore, suggests that the alteration occurred after the emplacement of the ophiolite complex on top of the continental crust.

The post-orogenic extension in the Devonian led to backsliding of nappe sheets along the Møre–Trøndelag fault zone (Seranne, 1992; Gabrielsen et al., 1999; Braathen et al., 2000). Titus et al. (2002) have suggested that a strike–slip motion in a late phase of the extension led to the formation of a pull–apart structure in which the LOC block is situated, and that the bottom of the LOC block is situated ~6 km beneath the surface. Geothermal gradients suggested for the three largest Devonian basins of western Norway, the Hornhelen/Kvamshesten (~27°C/km) and the Solund basin (23°C/km; Svensen et al., 2001) correspond to the modern geothermal gradients for western Norway (~25°C; Pascal et al., 2007; Slagstad et al., 2009). Souche et al. (2012) found an even higher geothermal gradient (~30°C) for the Kvamshesten basin. It is thus likely that the down-dropping of the Leka block, which is now surrounded by rocks from lower structural positions within the nappe stack, led to heating of the rocks occurring in the deeper parts of the ophiolite.

To assess the evolution from the partly altered peridotites to the completely serpentinized and carbonate rocks, a P–T section is presented (Fig. 34). It is assumed that the temperature conditions estimated for the talc–carbonate formation represents the minimum–temperature for the formation of fluids at depth. It has not been possible to do any estimates on cooling of the fluids during ascent. As mentioned previously, there are no good estimates of the pressure conditions (and corresponding depth) at which the carbonation of the partly altered peridotites occurred. For this reason the scenario for the formation of the alteration zones is presented for two values of pressure. In scenario one, the talc–carbonate rocks formed at a pressure of 1 kbar, corresponding to a depth of ~3.3 km and the bottom of the LOC block is thus located at a depth of ~9 km (Fig. 34). Assuming that the rocks at the bottom of the LOC block are similar to the investigated partly hydrated peridotites, the modeling suggests that the minimum temperatures for the altering fluids is high enough to initiate the dehydration of the rocks by the breakdown of serpentine and brucite at this depth (Fig. 34). The geothermal gradient required to produce these temperatures at those depths is ~45 – 55°C/km. In scenario two, the talc–carbonate rocks formed at a pressure of 3 kbar, corresponding to a depth of ~9.9 km and the bottom of the LOC block thus should have been located at a depth of ~15.9 km. The estimated temperature conditions (Fig. 34) at this depth are sufficient to trigger dehydration reactions in the partly altered peridotites. The geothermal gradient required for these conditions is ~27 – 35°C/km. As all the peridotites are serpentinized to variable degrees (10 – 90%; chapter 5; Furnes et al., 1988; Albrektsen, 1990; Iyer et al., 2008a), Fig. 34 shows that there is a potential to trigger dehydration reactions at the bottom of the LOC block that will produce a considerable amount of the free fluid phase. Production of H₂O results from the breakdown of the hydrous minerals serpentine and brucite to form less hydrous minerals at ~420°C (at 3 kbar) and ~440°C (at 5 kbar; Fig. 34).

Data for the thermal evolution of the Devonian basins (Svensen et al., 2001; Pascal et al., 2007; Slagstad et al., 2009; Souche et al., 2012) suggests that the geothermal gradient of ~45 – 55°C/km required for scenario one is higher than expected for the present regional setting. Such high geothermal gradients are generally observed in island arcs, ocean ridges, contact aureoles and areas with thick crust (70 km) related to collisional belts like the present day Himalaya (Spear, 1995). It is, however, noted that high geothermal gradients also occur in areas with tectonically thinned crust in extensional regimes (such as the Basin and Range province of western USA). It has been shown that high geothermal gradients can occur close to detachment faults (Mulch et al., 2006; Cottle et al., 2011; Gottardi et al., 2011; Souche et al., 2014). The LOC is currently located in proximity of the Kollstraumen

Detachment Zone, which separates the Helgeland Nappe Complex from the basement gneisses (Fig. 4; Braathen et al., 2000; Heldal, 2001; Titus et al., 2002). This opens up the possibility that high geothermal gradients may have occurred during the post-orogenic extension in the Devonian, although there are no data to support this.

The second scenario requires a geothermal gradient of $\sim 27 - 35^\circ\text{C}/\text{km}$ at a depth of ~ 15.9 km. As similar geothermal gradients have been proposed for the three largest Devonian basins in western Norway this scenario is more readily explained. In this scenario, the pressure conditions of 3 kbar for the carbonation of the partly altered peridotites implies that ~ 10 km of overburden must have been eroded to reach the present day erosion level.

The mineralogy in the alteration zones suggests either an increase in X_{CO_2} or cooling of the fluids in a late stage of their evolution (Fig. 35 and Fig. 36). This leads to the change in mineralogy and the incomplete conversion of the serpentine-carbonate bearing rock into the talc-carbonate assemblage. There is no unequivocal evidence for which of these two possibilities is responsible for the evolution, but the increase in X_{CO_2} of the fluid phase needs to be accounted for. From the previous discussion, it is clear that the source for the carbon has not been adequately constrained. It is therefore difficult to explain how the enrichment of CO_2 occurred. Based on the current data, a decrease in temperature is the preferred explanation. A model for the evolution of the alteration is presented in Fig. 37.

Both the proposed scenarios can explain high temperature conditions at the bottom of the LOC block, and in both scenarios the expected temperatures are high enough to trigger dehydration reactions of hydrous rocks occurring in the deeper parts of the ophiolite complex. The released fluids moved up through the permeable fracture zones and reacted with the rocks at shallower depths. Although it is likely that the fluid conduits formed in an earlier tectonic stage (c.f., Titus et al., 2002), differences between lithostatic and fluid pressure, or high gradients in the fluid pressure could have enhanced the permeability by hydrofracturing (Dutrow and Norton, 1995; Spear, 1995; Kostenko et al., 2002; Fossen, 2011). The presence of modern day geothermal systems associated with pull-apart structures in Sumatran (western Indonesia Hickman et al., 2004; Muraoka and Takahashi, 2010) and Coso Geothermal Field (California; Monastero et al., 2005; Pluhar et al., 2006), in addition to high geothermal gradients observed in the Bohai Basin (northern China; Hu et al., 2001), testify that geothermal alteration within a pull-apart basin setting is a possible scenario.

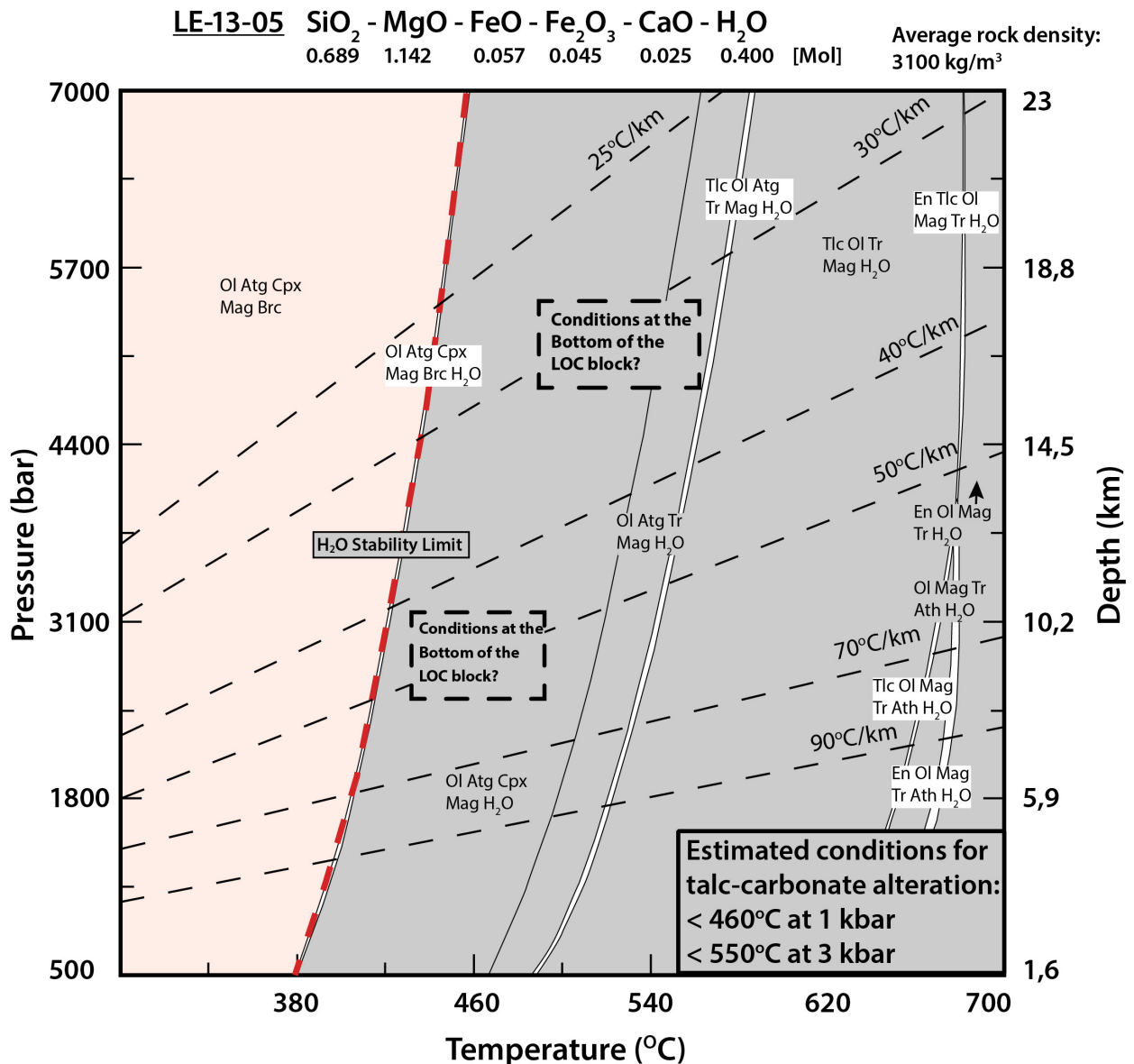


Fig. 34: P-T section for a partly altered peridotite from the cumulate section calculated in the $\text{SiO}_2 - \text{MgO} - \text{FeO} - \text{Fe}_2\text{O}_3 - \text{CaO} - \text{H}_2\text{O}$ system for the analyzed whole rock compositions, assuming that all the measured LOI represents H_2O . Depth is calculated assuming a density of 3100 kg/m³ in accordance with measured densities of the rocks on Leka (Sindre and Pedersen, 1990; Titus et al., 2002). The colored 5-phase field Ol-Atg-Cpx-Mag-Brc corresponds to the mineral assemblage observed in the partly altered peridotites from the cumulate section. The red dotted line represents the stability limit for H_2O . Minimum temperature conditions expected at the bottom of the LOC block, corresponding to the temperature of formation of the talc-carbonate assemblage, are represented by the dotted boxes. In scenario one, the talc-carbonate alteration occurred at a pressure of 1 kbar (corresponding to a depth of 3.3 km) and temperature $< 460^\circ\text{C}$. Adding 6 km (the approximately thickness of the LOC block) to the depth of 3.3 km results in the expected geothermal gradient required to get the temperatures at those pressures. In this scenario a geothermal gradient corresponding to $\sim 50^\circ\text{C}$ is required. In scenario two, the talc-carbonate rocks form at temperatures below 550°C at a pressure of 3 kbar (corresponding to a depth of 9.9 km). Adding 6 km of thickness puts the bottom of the Leka block to ~ 16 km. To achieve these temperatures at this depth requires a geothermal gradient of 27 - 35°C .

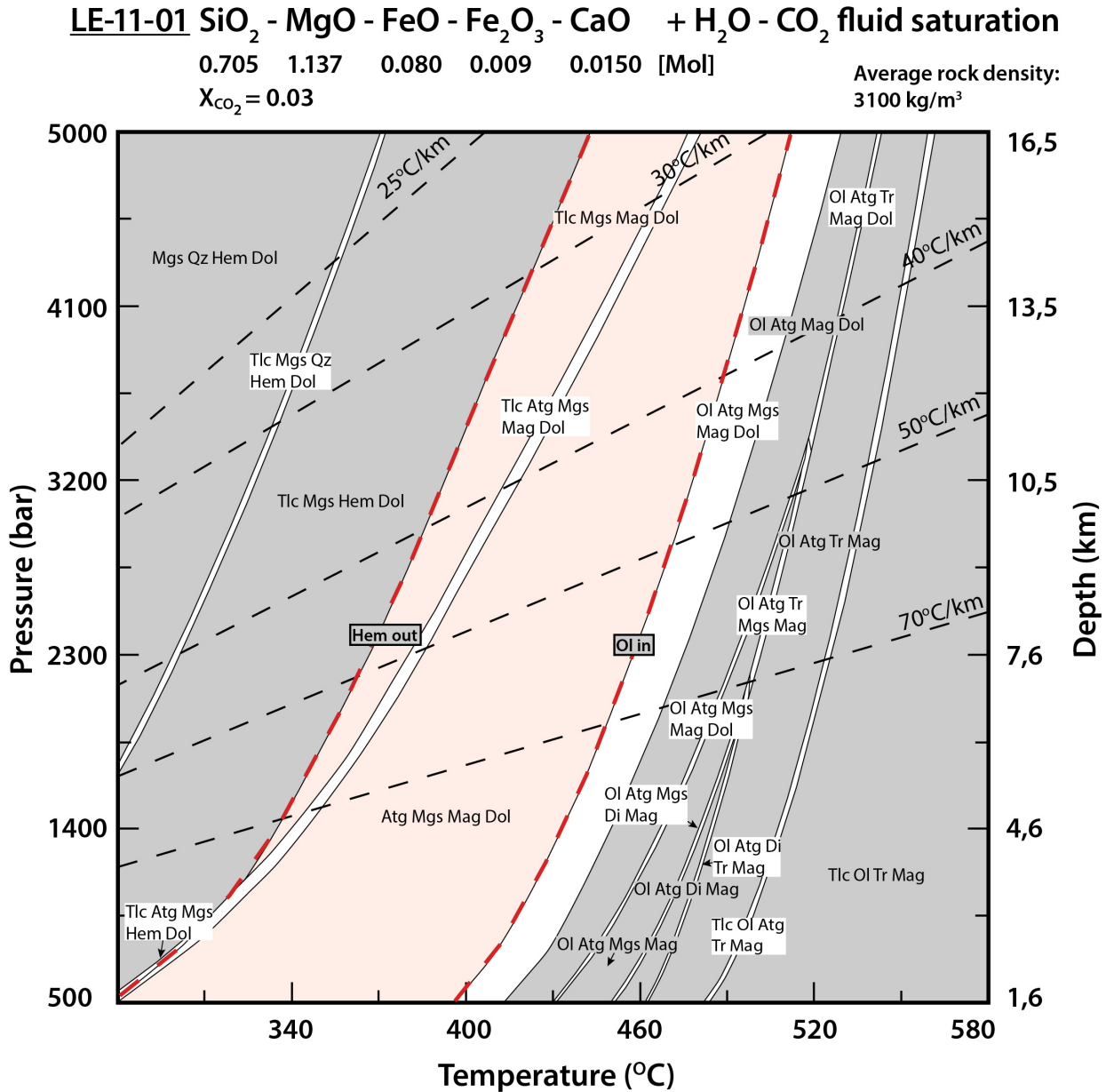


Fig. 35: P-T section for talc-carbonate sample LE-11-01 at $X_{\text{CO}_2} = 0.03$, calculated in the $\text{SiO}_2 - \text{MgO} - \text{FeO} - \text{Fe}_2\text{O}_3 - \text{CaO} - \text{H}_2\text{O} - \text{CO}_2$ system with the obtained whole rock compositions. The two colored 4-phase fields separated by a narrow 5-phase field corresponds to the observed mineral assemblages for serpentinite (at the high temperature side) and talc-carbonate (at the low temperature side).

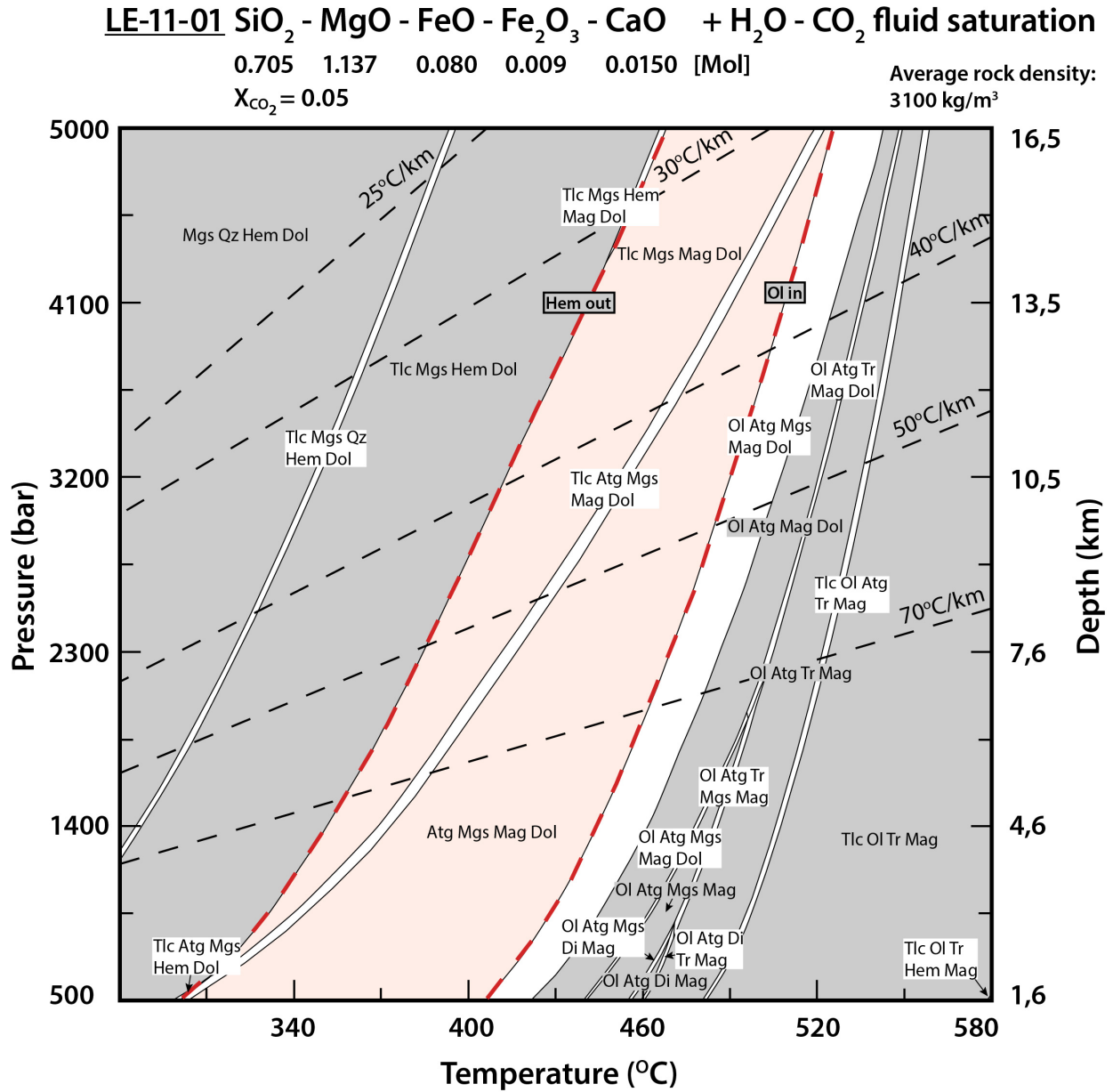


Fig. 36: P-T section for talc-carbonate sample LE-11-01 at $X_{\text{CO}_2} = 0.05$, calculated in the $\text{SiO}_2 - \text{MgO} - \text{FeO} - \text{Fe}_2\text{O}_3 - \text{CaO} - \text{H}_2\text{O} - \text{CO}_2$ system with the obtained whole rock compositions. The two colored 4-phase fields separated by a narrow 5-phase field corresponds to the observed mineral assemblages for serpentinite (at the high temperature side) and talc-carbonate (at the low temperature side).

CONCLUSIONS

The results obtained in this study provide constraints on the temperature and fluid composition of complete serpentinization and carbonation of partly altered peridotites located in the Skråa block of the Leka Ophiolite Complex. Field relationships together with stable and radiogenic isotopic evidence provide insight into fluid sources and the succession of processes leading to alteration.

- The partly altered peridotites are successively transformed into serpentinite and finally talc-carbonate rock. Sharp reaction zones between the alteration sequences and the peridotites can be followed for tens of meters. The presence of the zoned and laterally continuous alterations suggests that permeable zones were the main fluid conduits for the CO₂ bearing fluids.
- Alteration of the country rock peridotites by replacement of olivine + clinopyroxene by serpentine + brucite occurred at temperatures below 400°C involving pure H₂O fluids. Whole-rock analysis together with thermodynamic modeling suggests that the rocks did not reach a fully hydrated state.
- Complete serpentinization and carbonation was essentially isochemical with respect to the major elements, and only accompanied by the addition of the volatiles H₂O and CO₂.
- Complete serpentinization to the mineral assemblage Srp-Mgs-Mag-Dol occurred at temperatures < 510°C and low X_{CO₂} concentrations obscuring the original peridotite textures.
- Cooling of the fluids or an increase in the X_{CO₂} of the fluid phase resulted in the replacement of serpentine minerals and formation of the Tlc-Mgs-Mag-Dol mineral assemblage. The transformation took place at temperatures < 550°C during static conditions.
- The combination of radiogenic and stable isotopes indicates that the fluids responsible for the alteration are derived from metamorphic devolatilization reactions of hydrous peridotites occurring in the deeper parts of the ophiolite complex.
- It is suggested that the dehydration reactions post-date the ophiolite obduction. The dehydration probably occurred as a result of the down-dropping of the Leka block during the Devonian extensional event. Temperatures of ~460 – 550°C for the talc-carbonate alteration represents the minimum temperature at the bottom of the LOC block. These high temperatures can trigger dehydration reactions in partly altered peridotites occurring in the deeper parts of the ophiolite complex. In which fluids can have been propagated upwards in fractures and reacted with the rocks at shallower levels.

BIBLIOGRAPHY

- Albrektsen, B., Furnes, H., Pedersen, R., Jan. 1991. Formation of dunites in mantle tectonites, Leka Ophiolite complex, Norway. *Journal of Geodynamics* 13 (2-4), 205–220.
- Albrektsen, B. A., 1990. Geologiske relasjoner og petrogenetisk utvikling i Lauvhatten mantelperidotitt, Leka ofiolittkompleks.
- Andersen, T. B., Jamtveit, B. r., Oct. 1990. Uplift of deep crust during orogenic extensional collapse: A model based on field studies in the Sogn-Sunnfjord Region of western Norway. *Tectonics* 9 (5), 1097–1111.)
- Andreani, M., Mével, C., Boullier, A.-M., Escartín, J., Feb. 2007. Dynamic control on serpentine crystallization in veins: Constraints on hydration processes in oceanic peridotites. *Geochemistry, Geophysics, Geosystems* 8 (2), 1–24.
- Arai, S., Apr. 1994. Characterization of spinel peridotites by olivine-spinel compositional relationships: Review and interpretation. *Chemical Geology* 113 (3-4), 191–204.)
- Ash, C. H., Arksey, R. L., 1990. The listwanite-lode gold association in British Columbia. Ministry of Energy, Mines & petroleum Resources, 359–364.
- Auclair, M., Gauthier, M., Trottier, J., Jebrak, M., Chartrand, F., Feb. 1993. Mineralogy, geochemistry, and paragenesis of the Eastern Metals serpentinite-associated Ni-Cu-Zn deposit, Quebec Appalachians. *Economic Geology* 88 (1), 123–138.)
- Austrheim, H., Prestvik, T., Aug. 2008. Rodingitization and hydration of the oceanic lithosphere as developed in the Leka ophiolite, north-central Norway. *Lithos* 104 (1-4), 177–198.
- Ballhaus, C. G., Stumpfl, E. F., Jun. 1985. Occurrence and petrological significance of graphite in the Upper Critical Zone, western Bushveld Complex, South Africa. *Earth and Planetary Science Letters* 74 (1), 58–68.)
- Barnes, C. G., Frost, C. D., Yoshinobu, A. S., McArthur, K., Barnes, M. A., Allen, C. M., Nordgulen, O. y., Prestvik, T., Dec. 2007. Timing of sedimentation, metamorphism, and plutonism in the Helgeland Nappe Complex, north-central Norwegian Caledonides. *Geosphere* 3 (6), 683.
- Barnes, I., O'Neill, J. R., Rapp, J. B., White, D. E., May 1973. Silica-Carbonate Alteration of Serpentine; Wall Rock Alteration in Mercury Deposits of the California Coast Ranges. *Economic Geology* 68 (3), 388–398.)
- Barrenechea, J., Luque, F., Rodas, M., Pasteris, J., 1997. Vein-type graphite in Jurassic volcanic rocks of the external zone of the Betic Cordillera, southern Spain. *The Canadian Mineralogist* 35, 1379 – 1390.)
- Bedard, J. H., Escayola, M., Mar. 2010. The Advocate ophiolite mantle, Baie Verte, Newfoundland: regional correlations and evidence for metasomatism. Geological Survey of Canada, Earth Sciences Sector, Contribution 20090211. *Canadian Journal of Earth Sciences* 47 (3), 237–253.)
- Beinlich, A., Plümper, O., Hövelmann, J., Austrheim, H. k., Jamtveit, B. r., Dec. 2012. Massive serpentinite carbonation at Linnajavri, N-Norway. *Terra Nova* 24 (6), 446–455.
- Bogoch, R., Magaritz, M., Michard, A., Oct. 1986. Dolomite of possible mantle origin, southeast Sinai. *Chemical Geology* 56 (3-4), 281–288.)

- Bohlke, J., Apr. 1989. Comparison of metasomatic reactions between a common CO₂-rich vein fluid and diverse wall rocks; intensive variables, mass transfers, and Au mineralization at Alleghany, California. *Economic Geology* 84 (2), 291–327.
- Boschi, C., Dini, A., Dallai, L., Ruggieri, G., Gianelli, G., 2009. Enhanced CO₂-mineral sequestration by cyclic hydraulic fracturing and Si-rich fluid infiltration into serpentinites at Malentrata (Tuscany, Italy). *Chemical Geology* 265, 209–226.)
- Boschi, C., Früh-Green, G., Escartín, J., 2006. Occurrence and significance of serpentinite-hosted, talc- and amphibole-rich fault rocks in modern oceanic settings and ophiolite complexes: An overview. *Ophioliti* 31 (2), 129 – 140.)
- Braathen, A., Nordgulen, O. y., Osmundsen, P.-T., Andersen, T. B., Solli, A., Roberts, D., Nordgulen, O., Jul. 2000. Devonian, orogen-parallel, opposed extension in the Central Norwegian Caledonides. *Geology* 28 (7), 615.
- Bucher, K., Grapes, R., 2011. *Petrogenesis of Metamorphic Rocks*, 8th Edition. Springer Berlin Heidelberg, Berlin, Heidelberg.
- Bucher, N. K., 1988. Metamorphism of ultramafic rocks in the Central Scandinavian Caledonides. *Norsk Geologisk Undersøkelse Special Publication* 3, 86–95.
- Bucher-Nurminen, K., May 1991. Mantle fragments in the Scandinavian caledonides. *Tectonophysics* 190 (2–4), 173–192.)
- Chamberlain, C. P., Rumble, D., Jan. 1989. The influence of fluids on the thermal history of a metamorphic terrain: New Hampshire, USA. *Geological Society, London, Special Publications* 43 (1), 203–213.)
- Chidester, A. H., 1962. *Petrology and geochemistry of selected talc-bearing ultramafic rocks and adjacent country rocks in north-central Vermont*. US Government Printing Office.)
- Coats, C. J. A., Buchan, R., 1979. Petrology of serpentinitized metamorphic olivine, Bird River sill, Manitoba. *The Canadian Mineralogist* 17, 847–855.)
- Connolly, J., Jul. 2005. Computation of phase equilibria by linear programming: A tool for geodynamic modeling and its application to subduction zone decarbonation. *Earth and Planetary Science Letters* 236 (1–2), 524–541.)
- Connolly, J. A. D., Oct. 2009. The geodynamic equation of state: What and how. *Geochemistry, Geophysics, Geosystems* 10 (10).)
- Connolly, J. A. D., Jun. 2010. The Mechanics of Metamorphic Fluid Expulsion. *Elements* 6 (3), 165–172.)
- Corfu, F., Roberts, R., Torsvik, T., Ashwal, L., Ramsay, D., Feb. 2007. Peri-Gondwanan elements in the Caledonian Nappes of Finnmark, Northern Norway: Implications for the paleogeographic framework of the Scandinavian Caledonides. *American Journal of Science* 307 (2), 434–458.)
- Cottle, J. M., Waters, D. J., Riley, D., Beyssac, O., Jessup, M. J., Jun. 2011. Metamorphic history of the South Tibetan Detachment System, Mt. Everest region, revealed by RSCM thermometry and phase equilibria modelling. *Journal of Metamorphic Geology* 29 (5), 561–582.)
- Crespo, E., Luque, F., Rodas, M., Wada, H., Gervilla, F., Apr. 2006. Graphite-sulfide deposits in Ronda and Beni Bousera peridotites (Spain and Morocco) and the origin of carbon in mantle-derived rocks. *Gondwana Research* 9 (3), 279–290.)
- Dahlgren, S., Bogoch, R., Magaritz, M., Michard, A., Mar. 1993. Hydrothermal dolomite marbles associated with charnockitic magmatism in the Proterozoic Bamble Shear Belt, south Norway. *Contributions to Mineralogy and Petrology* 113 (3), 394–409.)

- Dasgupta, R., Dixon, J. E., Hirschmann, M. M., 2009. The H/C ratios of Earth's near-surface and deep reservoirs, and consequences for deep Earth volatile cycles. *Chemical Geology* 262 (1), 4–16.)
- Dasgupta, R., Hirschmann, M. M., Sep. 2010. The deep carbon cycle and melting in Earth's interior. *Earth and Planetary Science Letters* 298 (1–2), 1–13.)
- Debret, B., Andreani, M., Godard, M., Nicollet, C., Schwartz, S., Lafay, R., Oct. 2013. Trace element behavior during serpentization/de-serpentization of an eclogitized oceanic lithosphere: A LA-ICPMS study of the Lanzo ultramafic massif (Western Alps). *Chemical Geology* 357, 117–133.
- Deines, P., 1992. Mantle carbon: concentration, mode of occurrence, and isotopic composition. In: *Early Organic Evolution*. Springer Berlin Heidelberg, pp. 136 – 146.)
- Deines, P., Oct. 2002. The carbon isotope geochemistry of mantle xenoliths. *Earth-Science Reviews* 58 (3–4), 247–278.
- Deniel, C., Pin, C., Jan. 2001. Single-stage method for the simultaneous isolation of lead and strontium from silicate samples for isotopic measurements. *Analytica Chimica Acta* 426 (1), 95–103.)
- Dilek, Y., Moores, E. M., Furnes, H., 1998. Structure of modern oceanic crust and ophiolites and implications for faulting and magmatism at oceanic spreading centers. *Geophysical Monograph Series* 106, 219–265.)
- Dobrzhinetskaya, L. F., Eide, E. A., Larsen, R. B., Sturt, B. A., Trø nnes, R. G., Smith, D. C., Taylor, W. R., Posukhova, T. V., 1995. Microdiamond in high-grade metamorphic rocks of the Western Gneiss region, Norway. *Geology* 23 (7), 597.)
- Donaldson, M. J., Oct. 1981. Redistribution of ore elements during serpentization and talc-carbonate alteration of some Archean dunites, Western Australia. *Economic Geology* 76 (6), 1698–1713.)
- Dunning, G., Krogh, T., Nov. 1985. Geochronology of ophiolites of the Newfoundland Appalachians. *Canadian Journal of Earth Sciences* 22 (11), 1659–1670.)
- Dunning, G. R., Pedersen, R., Jan. 1988. U/Pb ages of ophiolites and arc-related plutons of the Norwegian Caledonides: implications for the development of Iapetus. *Contributions to Mineralogy and Petrology* 98 (1), 13–23.
- Dutrow, B., Norton, D., Nov. 1995. Evolution of fluid pressure and fracture propagation during contact metamorphism. *Journal of Metamorphic Geology* 13 (6), 677–686.)
- Eckstrand, O., Feb. 1975. The Dumont serpentinite; a model for control of nickeliferous opaque mineral assemblages by alteration reactions in ultramafic rocks. *Economic Geology* 70 (1), 183–201.)
- Eggler, D. H., Mar. 1978. The effect of CO₂ upon partial melting of peridotite in the system Na₂O-CaO-Al₂O₃-MgO-SiO₂-CO₂ to 35 kb, with an analysis of melting in a peridotite-H₂O-CO₂ system. *American Journal of Science* 278 (3), 305–343.)
- Eickmann, B., Bach, W., Peckmann, J., May 2009a. Authigenesis of Carbonate Minerals in Modern and Devonian Ocean-Floor Hard Rocks. *The Journal of Geology* 117 (3), 307–323.)
- Eickmann, B., Bach, W., Rosner, M., Peckmann, J., Oct. 2009b. Geochemical constraints on the modes of carbonate precipitation in peridotites from the Logatchev Hydrothermal Vent Field and Gakkell Ridge. *Chemical Geology* 268 (1–2), 97–106.)
- Eide, E., Haabesland, N., Osmundsen, P., Andersen, T., Roberts, D., Kendrick, M., 2005. Modern techniques and Old Red problems – determining the age of continental sedimentary deposits with ⁴⁰Ar/³⁹Ar provenance analysis in west-central Norway. *Norwegian Journal of Geology*, 133–149.)

- Elmer, F. L., White, R. W., Powell, R., Aug. 2006. Devolatilization of metabasic rocks during greenschist–amphibolite facies metamorphism. *Journal of Metamorphic Geology* 24 (6), 497–513.)
- Escayola, M. P., Proenza, J. A., van Staal, C., Rogers, N., Skulski, T., 2009. The Point Rouse listvenites, Baie Verte, Newfoundland: altered ultramafic rocks with potential for gold mineralization. Current research. Newfoundland and Labrador Department of Natural Resources, Geological Survey, Report, 1–9.)
- Essene, E. J., Jan. 1989. The current status of thermobarometry in metamorphic rocks. *Geological Society, London, Special Publications* 43 (1), 1–44.)
- Evans, B., May 1977. Metamorphism of Alpine Peridotite and Serpentinite. *Annual Review of Earth and Planetary Sciences* 5 (1), 397–447.
- Evans, B. W., Sep. 2008. Control of the Products of Serpentinization by the Fe₂+Mg-1 Exchange Potential of Olivine and Orthopyroxene. *Journal of Petrology* 49 (10), 1873–1887.)
- Evans, B. W., Dyar, M. D., Kuehner, S. M., Jan. 2012. Implications of ferrous and ferric iron in antigorite. *American Mineralogist* 97 (1), 184–196.)
- Evans, B. W., Trommsdorff, V., Mar. 1974. Stability of enstatite + talc, and CO₂-metasomatism of metaperidotite, Val d'Efra, Lepontine Alps. *American Journal of Science* 274 (3), 274–296.)
- Evans, K., Powell, R., Frost, B., May 2013. Using equilibrium thermodynamics in the study of metasomatic alteration, illustrated by an application to serpentinites. *Lithos* 168–169, 67–84.)
- Faure, G., 2001. *Origin of Igneous Rocks: The Isotopic Evidence*. Springer Berlin Heidelberg, Berlin, Heidelberg.
- Flekkøy, E. G., Malthesørensen, A., Jamtveit, B. r., 2002. Modeling hydrofracture. *Journal of Geophysical Research* 107 (B8), 2151.)
- Fletcher, R., Buss, H., Brantley, S. L., 2006. A spheroidal weathering model coupling porewater chemistry to soil thicknesses during steady-state denudation. *Earth and Planetary Science Letters* 244 (1), 444–457.)
- Fossen, H., Aug. 1992. The role of extensional tectonics in the Caledonides of south Norway. *Journal of Structural Geology* 14 (8–9), 1033–1046.
- Fossen, H., Apr. 2000. Extensional tectonics in the Caledonides: Synorogenic or postorogenic? *Tectonics* 19 (2), 213–224.
- Fossen, H., Jun. 2010. Extensional tectonics in the North Atlantic Caledonides: a regional view. *Geological Society, London, Special Publications* 335 (1), 767–793.)
- Fossen, H., 2011. *Structural Geology*. Cambridge University Press.
- Fossen, H., Dunlap, W. J., Jun. 1998. Timing and kinematics of Caledonian thrusting and extensional collapse, southern Norway: evidence from ⁴⁰Ar/³⁹Ar thermochronology. *Journal of Structural Geology* 20 (6), 765–781.)
- Fossen, H., Rykkelid, E., Aug. 1992. Postcollisional extension of the Caledonide orogen in Scandinavia: Structural expressions and tectonic significance. *Geology* 20 (8), 737–740.)
- Franzolin, E., Schmidt, M. W., Poli, S., Apr. 2010. Ternary Ca–Fe–Mg carbonates: subsolidus phase relations at 3.5 GPa and a thermodynamic solid solution model including order/disorder. *Contributions to Mineralogy and Petrology* 161 (2), 213–227.)

- Freund, F., Kathrein, H., Wengeler, H., Knobel, R., Reinen, H., Sep. 1980. Carbon in solid solution in forsterite – a key to the untractable nature of reduced carbon in terrestrial and cosmogenic rocks. *Geochimica et Cosmochimica Acta* 44 (9), 1319–1333.)
- Frost, B. R., Feb. 1985. On the Stability of Sulfides, Oxides, and Native Metals in Serpentinite. *Journal of Petrology* 26 (1), 31–63.
- Frost, B. R., Beard, J. S., Apr. 2007. On Silica Activity and Serpentinization. *Journal of Petrology* 48 (7), 1351–1368.)
- Früh-Green, G. L., 1996. Petrologic and stable isotope constraints on hydrothermal alteration and serpentinization of the EPR shallow mantle at Hess Deep (Site 895). *Proc. ODP Sci. Res* 147, 255 – 290.)
- Früh-Green, G. L., Connolly, J. A., Plas, A., Kelley, D. S., Grobéty, B., 2004. The Subseafloor Biosphere at Mid-Ocean Ridges. Vol. 144 of *Geophysical Monograph Series*. American Geophysical Union, Washington, D. C.
- Früh-Green, G. L., Kelley, D. S., Bernasconi, S. M., Karson, J. A., Ludwig, K. A., Butterfield, D. A., Boschi, C., Proskurowski, G., Jul. 2003. 30,000 years of hydrothermal activity at the lost city vent field. *Science (New York, N.Y.)* 301 (5632), 495–8.)
- Furnes, H., Pedersen, R., Hertogen, J., Albrektsen, B., Apr. 1991. Magma development of the Leka Ophiolite Complex, central Norwegian Caledonides. *Lithos* 27 (4), 259–277.
- Furnes, H., Pedersen, R. B., Stillman, C. J., Jun. 1988. The Leka Ophiolite Complex, central Norwegian Caledonides: field characteristics and geotectonic significance. *Journal of the Geological Society* 145 (3), 401–412.
- Fyon, J., Crocket, J., Schwarcz, H., Oct. 1983. Magnesite abundance as a guide to gold mineralization associated with ultramafic flows, Timmins area. *Journal of Geochemical Exploration* 18 (3), 245–266.)
- Gabrielsen, R., Odinsen, T., Grunnaleite, I., Aug. 1999. Structuring of the Northern Viking Graben and the Møre Basin; the influence of basement structural grain, and the particular role of the Møre-Trøndelag Fault Complex. *Marine and Petroleum Geology* 16 (5), 443–465.)
- Gee, D., Sturt, B., 1985. The Caledonide orogen: Scandinavia and related areas.)
- Giggenbach, W. F., Mar. 1981. Geothermal mineral equilibria. *Geochimica et Cosmochimica Acta* 45 (3), 393–410.)
- Gottardi, R., Teyssier, C., Mulch, A., Vennemann, T. W., Wells, M. L., Jul. 2011. Preservation of an extreme transient geotherm in the Raft River detachment shear zone. *Geology* 39 (8), 759–762.)
- Govindaraju, K., Jul. 1994. 1994 compilation of working values and sample description for 383 geostandards. *Geostandards and Geoanalytical Research* 18, 1–158.)
- Green, D. H., Jan. 1964. The Petrogenesis of the High-temperature Peridotite Intrusion in the Lizard Area, Cornwall. *Journal of Petrology* 5 (1), 134–188.)
- Greenwood, H., 1967. Mineral equilibria in the system MgO-SiO₂-H₂O-CO₂. *Researches in geochemistry*, 542–567.)
- Grenne, T., Ihlen, P., Vokes, F., Jul. 1999. Scandinavian Caledonide Metallogeny in a plate tectonic perspective. *Mineralium Deposita* 34 (5-6), 422–471.)
- Griffin, W. L., Austrheim, H., Brastad, K., Bryhni, I., Krill, A. G., Krogh, E. J., Mørk, M. B. E., Qvale, H., Tørrudbakken, B., 1985. High-pressure metamorphism in the Scandinavian Caledonides. *The Caledonide Orogen-Scandinavia and Related Areas*, 783–801.)

- Griffis, R., Feb. 1972. Genesis of a magnesite deposit, Deloro Twp., Ontario. *Economic Geology* 67 (1), 63–71.
- Groves, D. I., Barrett, F. M., Brotherton, R. H., 1983. Exploration significance of chrome-spinels in mineralized ultramafic rocks and nickel-copper ores. *Publications of the Geological Society of South Africa* 7 (Proceedings of the First International Congress on Applied Mineralogy.), 21–30.)
- Halls, C., Zhao, R., Jun. 1995. Listvenite and related rocks: perspectives on terminology and mineralogy with reference to an occurrence at Cregganbaun, Co. Mayo, Republic of Ireland. *Mineralium Deposita* 30 (3-4), 303–313.)
- Hansen, L. D., Dipple, G. M., Gordon, T. M., Kellett, D. a., Feb. 2005. Carbonated serpentinite (listwanite) at Atlin, British Columbia: A geological analogue to carbon dioxide sequestration. *The Canadian Mineralogist* 43 (1), 225–239.
- Harlov, D. E., Austrheim, H. k., 2013. *Metasomatism and the Chemical Transformation of Rock*. Lecture Notes in Earth System Sciences. Springer Berlin Heidelberg, Berlin, Heidelberg.)
- Heldal, T., 2001. Ordovician stratigraphy in the western Helgeland Nappe Complex in the Bronnoysund area, North-central Norway. *Norges Geologisk Undersøkelse*.
- Hickman, R., Dobson, P., Gerven, M., Sagala, B., Gunderson, R., Jul. 2004. Tectonic and stratigraphic evolution of the Sarulla graben geothermal area, North Sumatra, Indonesia. *Journal of Asian Earth Sciences* 23 (3), 435–448.)
- Hoefs, J., 2009. *Stable isotope geochemistry*. Springer-Verlag Berlin.
- Holland, T., Powell, R., 1996. Thermodynamics of order-disorder in minerals: II. Symmetric formalism applied to solid solutions. *American Mineralogist* 81, 1425–37.)
- Holland, T. J. B., Powell, R., Oct. 1998. An internally consistent thermodynamic data set for phases of petrological interest. *Journal of Metamorphic Geology* 16 (3), 309–343.)
- Hollister, V. F., Aug. 1980. Origin of graphite in the Duluth Complex. *Economic Geology* 75 (5), 764–766.)
- Hopkinson, L., Beard, J., Boulter, C., Mar. 2004. The hydrothermal plumbing of a serpentinite-hosted detachment: evidence from the West Iberia non-volcanic rifted continental margin. *Marine Geology* 204 (3-4), 301–315.)
- Hövelmann, J., Austrheim, H. k., Beinlich, A., Anne Munz, I., Nov. 2011. Experimental study of the carbonation of partially serpentinized and weathered peridotites. *Geochimica et Cosmochimica Acta* 75 (22), 6760–6779.
- Hu, S., O’Sullivan, P. B., Raza, A., Kohn, B. P., Nov. 2001. Thermal history and tectonic subsidence of the Bohai Basin, northern China: a Cenozoic rifted and local pull-apart basin. *Physics of the Earth and Planetary Interiors* 126 (3-4), 221–235.)
- Iyer, K., Austrheim, H., John, T., Jamtveit, B., Mar. 2008a. Serpentinization of the oceanic lithosphere and some geochemical consequences: Constraints from the Leka Ophiolite Complex, Norway. *Chemical Geology* 249 (1-2), 66–90.
- Iyer, K., Jamtveit, B., Mathiesen, J., Malthe-Sørensen, A., Feder, J., Mar. 2008b. Reaction-assisted hierarchical fracturing during serpentinization. *Earth and Planetary Science Letters* 267 (3-4), 503–516.
- Jamtveit, B., Austrheim, H., Jun. 2010. Metamorphism: The Role of Fluids. *Elements* 6 (3), 153–158.)
- Jamtveit, B., Austrheim, H., Malthe-Sørensen, A., Nov. 2000. Accelerated hydration of the Earth’s deep crust induced by stress perturbations. *Nature* 408 (6808), 75–8.

- Janecky, D., Seyfried, W., Jul. 1986. Hydrothermal serpentinization of peridotite within the oceanic crust: Experimental investigations of mineralogy and major element chemistry. *Geochimica et Cosmochimica Acta* 50 (7), 1357–1378.)
- Javoy, M., Pineau, F., Dec. 1991. The volatiles record of a 'popping' rock from the Mid-Atlantic Ridge at 14N: chemical and isotopic composition of gas trapped in the vesicles. *Earth and Planetary Science Letters* 107 (3-4), 598–611.)
- Jochum, K. P., Nohl, U., Herwig, K., Lammel, E., Stoll, B., Hofmann, A. W., Nov. 2005. GeoReM: A New Geochemical Database for Reference Materials and Isotopic Standards. *Geostandards and Geoanalytical Research* 29 (3), 333–338.)
- Johannes, W., 1967. Zur Bildung und Stabilität von Forsterit, Talk, Serpentin, Quarz und Magnesit im System MgO–SiO₂–H₂O–CO₂. *Contributions to Mineralogy and Petrology* 15 (3), 233–250.)
- Johannes, W., 1968. Experimental investigation of the reaction forsterite + H₂O – serpentine + brucite. *Contributions to Mineralogy and Petrology*.)
- Johannes, W., Nov. 1969. An experimental investigation of the system MgO–SiO₂–H₂O–CO₂. *American Journal of Science* 267 (9), 1083–1104.
- Karlsen, T. O. R. A., Rian, E., Olesen, O., 2000. Overview of talc resources in the Altermark talc province, northern Norway, and possible uses of the talc ore. *Norges Geologiske Undersøkelse* 436, 93–102.)
- Kelemen, P. B., Matter, J., Streit, E. E., Rudge, J. F., Curry, W. B., Blusztajn, J., May 2011. Rates and Mechanisms of Mineral Carbonation in Peridotite: Natural Processes and Recipes for Enhanced, in situ CO₂ Capture and Storage. *Annual Review of Earth and Planetary Sciences* 39 (1), 545–576.
- Kendrick, M. A., Eide, E. A., Roberts, D., Osmundsen, P., May 2004. The Middle to Late Devonian Hybakken detachment, central Norway: 40Ar–39Ar evidence for prolonged latepost-Scandian extension and uplift. *Geological Magazine* 141 (3), 329–344.)
- Keppler, H., Wiedenbeck, M., Shcheka, S. S., Jul. 2003. Carbon solubility in olivine and the mode of carbon storage in the Earth's mantle. *Nature* 424 (6947), 414–6.)
- Klein, F., Bach, W., Humphris, S. E., Kahl, W.-A., Jons, N., Moskowitz, B., Berquo, T. S., Dec. 2013. Magnetite in seafloor serpentinite – Some like it hot. *Geology* 42 (2), 135–138.)
- Klein, F., Bach, W., Jöns, N., McCollom, T., Moskowitz, B., Berquó, T., Nov. 2009. Iron partitioning and hydrogen generation during serpentinization of abyssal peridotites from 15N on the Mid-Atlantic Ridge. *Geochimica et Cosmochimica Acta* 73 (22), 6868–6893.)
- Klein, F., Garrido, C. J., 2010. On Serpentinization and Mineral Carbonation of Serpentinite. *American Geophysical Union*.
- Klein, F., Garrido, C. J., 2011. Thermodynamic constraints on mineral carbonation of serpentinized peridotite. *Lithos* 126, 147–160.
- Klein, F., McCollom, T. M., Oct. 2013. From serpentinization to carbonation: New insights from a CO₂ injection experiment. *Earth and Planetary Science Letters* 379, 137–145.
- Kostenko, O., Jamtveit, B., Austrheim, H., Pollok, K., Putnis, C., Aug. 2002. The mechanism of fluid infiltration in peridotites at Almklovdalen, western Norway. *Geofluids* 2 (3), 203–215.)
- Lindahl, I., Nilsson, L., 2008. Geology of the soapstone deposits of the Linnajavri area, Hamarøy, Nordland, north Norwegian Caledonides – Norway's largest reserves of soapstone. *Geology for Society, Geological Survey of Norway Special Publication* 11, 19–35.)

- Loney, R. A., Himmelberg, G. R., Coleman, R. G., Jun. 1971. Structure and Petrology of the Alpine-type Peridotite at Burro Mountain, California, U.S.A. *Journal of Petrology* 12 (2), 245–309.)
- Luque, F. J., Rodas, M., Galán, E., Jun. 1992. Graphite vein mineralization in the ultramafic rocks of southern Spain: Mineralogy and genetic relationships. *Mineralium Deposita* 27 (3), 226–233.)
- Luth, R., 1999. Carbon and carbonates in the mantle. *Mantle Petrology: Field Observations and High Pressure Experimentation*, 297 – 316.)
- Maaløe, S., Aug. 2005. The dunite bodies, websterite and orthopyroxenite dikes of the Leka ophiolite complex, Norway. *Mineralogy and Petrology* 85 (3–4), 163–204.
- Mackenzie, D. B., Mar. 1960. High-temperature alpine-type peridotite from Venezuela. *Geological Society of America Bulletin* 71 (3), 303.)
- Manning, C. E., Jul. 2013. Thermodynamic Modeling of Fluid-Rock Interaction at Mid-Crustal to Upper-Mantle Conditions. *Reviews in Mineralogy and Geochemistry* 76 (1), 135–164.)
- Mathez, E., Sep. 1987. Carbonaceous matter in mantle xenoliths: Composition and relevance to the isotopes. *Geochimica et Cosmochimica Acta* 51 (9), 2339–2347.)
- McArthur, K., 2007. Tectonic construction and sediment provenance of a far-travelled nappe, west-central Norway. Unpublished m.sc, University of Wyoming, Laramie.)
- McArthur, K. L., Frost, C. D., Barnes, C. G., Prestvik, T., Nordgulen, O., Sep. 2013. Tectonic reconstruction and sediment provenance of a far-travelled oceanic nappe, Helgeland Nappe Complex, west-central Norway. Geological Society, London, Special Publications.
- McCollom, T. M., Bach, W., Feb. 2009. Thermodynamic constraints on hydrogen generation during serpentinization of ultramafic rocks. *Geochimica et Cosmochimica Acta* 73 (3), 856–875.)
- Melezhik, V. A., Gorokhov, M., Fallick, A. E., Roberts, D., Kuznetsov, A. B., Zwaan, K. B., Pokrovsky, B. G., Oct. 2002. Isotopic stratigraphy suggests Neoproterozoic ages and Laurentian ancestry for high-grade marbles from the North-Central Norwegian Caledonides. *Geological Magazine* 139 (04), 375–393.)
- Mével, C., Stamoudi, C., 1996. Hydrothermal alteration of the upper-mantle section at Hess Deep. *Proc. ODP Sci. Res* 147, 293 – 309.)
- Monastero, F., Katzenstein, A., Miller, J., Unruh, J., Adams, M., Richards-Dinger, K., Nov. 2005. The Coso geothermal field: A nascent metamorphic core complex. *Geological Society of America Bulletin* 117 (11), 1534–1553.)
- Mulch, A., Teyssier, C., Cosca, M. A., Vennemann, T. W., Dec. 2006. Thermomechanical analysis of strain localization in a ductile detachment zone. *Journal of Geophysical Research* 111 (B12), B12405.)
- Muraoka, H., Takahashi, M., 2010. Geothermal Systems Constrained by the Sumatran Fault and its Pull-Apart Basins in Sumatra, Western Indonesia. *Proceedings World Geothermal Congress*.)
- Naldrett, A. J., 1966. Talc-Carbonate Alteration of some Serpentinized Ultramafic Rocks south of Timmins, Ontario. *Journal of Petrology* 7 (3), 489–499.
- Nordgulen, A., Barnes, C. G., Yoshinobu, A. S., Frost, C., Prestvik, T., Austrheim, H., Anderson, H. S., Marko, W. T., McArthur, K., 2008. Pre-Scandian tectonic and magmatic evolution of the Helgeland Nappe Complex, Uppermost Allochthon.)
- Nordgulen, O., Barnes, C., Yoshinobu, A., Frost, C., Prestvik, T., Austrheim, H., Anderson, H., Marko, W., McArthur, K., 2011. Eurogranites 2011: Magmatism and Tectonics in the Uppermost Allochthon, central Norway. Internal publication of the Norwegian Geological Survey, 67.

- Norton, M. G., Apr. 1986. Late Caledonide Extension in western Norway: A response to extreme crustal thickening. *Tectonics* 5 (2), 195–204.)
- O’Hanley, D., 1996. *Serpentinites: Records of tectonic and petrological history*. Vol. 277. Oxford University Press New York.
- Okland, I., Huang, S., Dahle, H., Thorseth, I., Pedersen, R., Jul. 2012. Low temperature alteration of serpentinitized ultramafic rock and implications for microbial life. *Chemical Geology* 318–319, 75–87.)
- Olerud, S., 1990. Undersøkelse av talk-magnesitt forekomster ved Hundøyran påLeka.)
- Oliver, N. H. S., Cartwright, I., Wall, V. J., Golding, S. D., Sep. 1993. Regional carbonate alteration of the crust by mantle-derived magmatic fluids, Tamil Nadu, South India. *Journal of Metamorphic Geology* 11 (5), 705–720.)
- Osmundsen, P., Andersen, T., Mar. 2001. The middle Devonian basins of western Norway: sedimentary response to large-scale transtensional tectonics? *Tectonophysics* 332 (1–2), 51–68.)
- Osmundsen, P., Andersen, T., Markussen, S., Jun. 1998. Tectonics and sedimentation in the hangingwall of a major extensional detachment: the Devonian Kvamshesten Basin, western Norway. *Basin Research* 10 (2), 213–234.)
- Osmundsen, P. T., Braathen, A., Sommaruga, A., Skilbrei, J. R., Nordgulen, O. y., Roberts, D., Andersen, T. B., Olesen, O., Mosar, J., 2005. Metamorphic core complexes and gneiss-cored culminations along the Mid-Norwegian margin: an overview and some current ideas. *Norwegian Petroleum Society Special Publications* 12, 29–41.)
- Padrón-Navarta, J. A., Sánchez-Vizcaíno, V. L., Hermann, J., Connolly, J. A., Garrido, C. J., Gómez-Pugnaire, M. T., Marchesi, C., Sep. 2013. Tschermak’s substitution in antigorite and consequences for phase relations and water liberation in high-grade serpentinites. *Lithos* 178, 186–196.)
- Park, A.-H. A., Fan, L.-S., Nov. 2004. Mineral sequestration: physically activated dissolution of serpentine and pH swing process. *Chemical Engineering Science* 59 (22–23), 5241–5247.)
- Pascal, C., Ebbing, J., Skilbrei, J., 2007. Interplay between the Scandes and the Transscandinavian Igneous Belt: integrated thermo-rheological and potential field modelling of the Central Scandes. *Norwegian Journal of Geology* 87, 3 – 12.)
- Passchier, C. W., Trouw, R. A. J., 2005. *Microtectonics*, 2nd Edition. Springer.
- Pasteris, J. D., 1981. Occurrence of graphite in serpentinitized olivines in kimberlite. *Geology* 9 (8), 356.)
- Paukert, A. N., Matter, J. M., Kelemen, P. B., Shock, E. L., Havig, J. R., Nov. 2012. Reaction path modeling of enhanced in situ CO₂ mineralization for carbon sequestration in the peridotite of the Samail Ophiolite, Sultanate of Oman. *Chemical Geology* 330–331, 86–100.)
- Paulick, H., Bach, W., Godard, M., De Hoog, J., Suhr, G., Harvey, J., 2006. Geochemistry of abyssal peridotites (Mid-Atlantic Ridge, 15°20’N, ODP Leg 209): Implications for fluid/rock interaction in slow spreading environments. *Chemical Geology* 234 (3), 179–210.
- Pedersen, R., 1992. Constraints on Magma Chamber Processes Operating Close to The Petrological Moho: Evidence from the Layered Ultramafic Rocks of the Leka Ophiolite Complex.
- Pedersen, R., Furnes, H., Dunning, G., 1988. Some Norwegian ophiolite complexes reconsidered. *Norges Geologisk Undersøkelse* 3, 80–85.

- Pedersen, R.-B., Johannesen, G. M., Boyd, R., Jul. 1993. Stratiform platinum-group element mineralizations in the ultramafic cumulates of the Leka ophiolite complex, central Norway. *Economic Geology* 88 (4), 782–803.
- Picazo, S., Cannat, M., Delacour, A., Escartín, J., Rouméjon, S., Silant'ev, S., Sep. 2012. Deformation associated with the denudation of mantle-derived rocks at the Mid-Atlantic Ridge 13–15N: The role of magmatic injections and hydrothermal alteration. *Geochemistry, Geophysics, Geosystems* 13 (9).)
- Pineau, F., Javoy, M., Kornprobst, J., Apr. 1987. Primary Igneous Graphite in Ultramafic Xenoliths: II Isotopic Composition of the Carbonaceous Phases Present in Xenoliths and Host Lava at Tissemt (Eggr, Algerian Sahara). *Journal of Petrology* 28 (2), 313–322.)
- Pluhar, C., Coe, R., Lewis, J., Monastero, F., Glen, J., Oct. 2006. Fault block kinematics at a releasing stepover of the Eastern California shear zone: Partitioning of rotation style in and around the Coso geothermal area and nascent metamorphic core complex. *Earth and Planetary Science Letters* 250 (1–2), 134–163.)
- Plumlee, G., 1998. United States Geological Survey Certificate of Analysis: Basalt, Columbia River, BCR-2.)
- Plümper, O., Piazzolo, S., Austrheim, H., Aug. 2012. Olivine Pseudomorphs after Serpentinized Orthopyroxene Record Transient Oceanic Lithospheric Mantle Dehydration (Leka Ophiolite Complex, Norway). *Journal of Petrology* 53 (9), 1943–1968.
- Pohl, W., Jun. 1990. Genesis of magnesite deposits – models and trends. *Geologische Rundschau* 79 (2), 291–299.)
- Prestvik, T., 1972. Alpine-type mafic and ultramafic rocks of Leka, Nord-Trøndelag. *Norges Geologisk Undersøkelse* 273, 23–34.
- Prestvik, T., 1974. Supracrustal Rocks of Leka, Nord-Trøndelag. *Norges Geologisk Undersøkelse* 311, 65–87.)
- Prestvik, T., 1980. The Caledonian ophiolite complex of Leka, north central Norway. In: *Ophiolites: Proceedings, International Ophiolite Symposium, Cyprus*. pp. 555–566.
- Reid, K., May 2004. Magmatic processes in the Tosenfjord region, north-central Norway: implications for the evolution of the Helgeland Nappe complex.)
- Rey, P., Burg, J. P., Casey, M., 1997. The Scandinavian Caledonides and their relationship to the Variscan belt. *Geological Society, London, Special Publications* 121 (1), 179–200.)
- Roberts, D., Apr. 2003. The Scandinavian Caledonides: event chronology, palaeogeographic settings and likely modern analogues. *Tectonophysics* 365 (1–4), 283–299.
- Roberts, D., Gee, D. G., 1985. An introduction to the structure of the Scandinavian Caledonides. *The Caledonide Orogen, Scandinavia and Related Areas*, 55–68.
- Roberts, D., Melezhik, V. M., Haldal, T., 2002. Carbonate formations and early NW-directed thrusting in the highest allochthons of the Norwegian Caledonides: evidence of a Laurentian ancestry. *Journal of the Geological Society*.)
- Roberts, D., Nordgulen, O. y., Melezhik, V., 2007. The Uppermost Allochthon in the Scandinavian Caledonides: From a Laurentian ancestry through Taconian orogeny to Scandian crustal growth on Baltica. *Geological Society of America Memoirs* 200, 357–377.)
- Robinson, P. T., Malpas, J., Zhou, M.-F., Ash, C., Yang, J.-S., Bai, W.-J., 2005. Geochemistry and Origin of Listwanites in the Sartohay and Luobusa Ophiolites, China. *International Geology Review* 47 (2), 177–202.

- Rollinson, H. R., 1993. Using Geochemical Data: Evaluation, Presentation, Interpretation., 352.)
- Saal, A. E., Hauri, E. H., Langmuir, C. H., Perfit, M. R., Oct. 2002. Vapour undersaturation in primitive mid-ocean-ridge basalt and the volatile content of Earth's upper mantle. *Nature* 419 (6906), 451–5.)
- Säntti, J., Kontinen, A., Sorjonen-Ward, P., Johanson, B., Pakkanen, L., Jun. 2006. Metamorphism and Chromite in Serpentinized and Carbonate-Silica-Altered Peridotites of the Paleoproterozoic Outokumpu-Jormua Ophiolite Belt, eastern Finland. *International Geology Review* 48 (6), 494–546.)
- Sato, M., Valenza, M., 1980. Oxygen fugacities of the layered series of the Skaergaard intrusion, East Greenland. *American Journal of Science* 280-A, 134–158.)
- Scambelluri, M., Fiebig, J., Malaspina, N., Müntener, O., Pettke, T., Jul. 2004. Serpentinite Subduction: Implications for Fluid Processes and Trace-Element Recycling. *International Geology Review* 46 (7), 595–613.
- Schandl, E. S., Naldrett, A. J., 1992. CO₂ metasomatism of serpentinites, south of Timmons, Ontario. *The Canadian Mineralogist* 30 (1), 93–108.)
- Schermerhorn, L., Jan. 1973. What is keratophyre? *Lithos* 6 (1), 1–11.)
- Schulze, R. K., Hill, M. A., Field, R. D., Papin, P. A., Hanrahan, R. J., Byler, D. D., Dec. 2004. Characterization of carbonated serpentine using XPS and TEM. *Energy Conversion and Management* 45 (20), 3169–3179.)
- Schwarzenbach, E. M., Früh-Green, G. L., Bernasconi, S. M., Alt, J. C., Plas, A., Aug. 2013. Serpentinization and carbon sequestration: A study of two ancient peridotite-hosted hydrothermal systems. *Chemical Geology* 351, 115–133.)
- Seguret, M., Seranne, M., Chauvet, A., Brunel, A., 1989. Collapse basin: A new type of extensional sedimentary basin from the Devonian of Norway. *Geology* 17 (2), 127–130.)
- Seranne, M., 1992. Late Palaeozoic Kinematics of the Møre - Trøndelag Fault Zone and Adjacent Areas, Central Norway. *Norsk geologisk tidsskrift* 72 (2), 141–158.)
- Seranne, M., Seguret, M., Jan. 1987. The Devonian basins of western Norway: tectonics and kinematics of an extending crust. *Geological Society, London, Special Publications* 28 (1), 537–548.
- Shaw, A. M., Behn, M. D., Humphris, S. E., Sohn, R. A., Gregg, P. M., Jan. 2010. Deep pooling of low degree melts and volatile fluxes at the 85E segment of the Gakkel Ridge: Evidence from olivine-hosted melt inclusions and glasses. *Earth and Planetary Science Letters* 289 (3-4), 311–322.)
- Sheppard, S. M., 1980. Isotopic evidence for the origins of water during metamorphic processes in oceanic crust and ophiolite complexes. In: Allègre, C., Aubonin, J. (Eds.), *Orogenic mafic-ultramafic association*. pp. 135–147.)
- Shervais, J. W., Kolesar, P., Andreassen, K., Jan. 2005. A Field and Chemical Study of Serpentinization - Stonyford, California: Chemical Flux and Mass Balance. *International Geology Review* 47 (1), 1–23.)
- Sindre, A., Pedersen, R. B., 1990. Gravimetrisk Undersøkelse av Leka Ofiolittkompleks. *Norges Geologiske Undersøkelse*, 20.
- Slagstad, T., Balling, N., Elvebakk, H., Midttømme, K., Olesen, O., Olsen, L., Pascal, C., Aug. 2009. Heat-flow measurements in Late Palaeoproterozoic to Permian geological provinces in south and central Norway and a new heat-flow map of Fennoscandia and the Norwegian-Greenland Sea. *Tectonophysics* 473 (3-4), 341–361.)

- Souche, A., Beyssac, O., Andersen, T. B., Jul. 2012. Thermal structure of supra-detachment basins: a case study of the Devonian basins of western Norway. *Journal of the Geological Society* 169 (4), 427–434.
- Souche, A., Dabrowski, M., Andersen, T. B., Feb. 2014. Modeling thermal convection in supradetachment basins: example from western Norway. *Geofluids* 14 (1), 58–74.)
- Spear, F. S., 1995. *Metamorphic Phase Equilibria and Pressure-Temperature-Time Paths*. Mineralogical Society of America Washington.
- Steltenpohl, M. G., Carter, B. T., Andresen, A., Zeltner, D. L., Jul. 2009. ⁴⁰Ar/³⁹Ar Thermochronology of Late and Postorogenic Extension in the Caledonides of North-Central Norway. *The Journal of Geology* 117 (4), 399–414.)
- Stephens, M. B., Jan. 1988. The Scandinavian Caledonides: a complexity of collisions. *Geology Today* 4 (1), 20–26.)
- Stephens, M. B., Gee, D. B., 1985. A tectonic model for the evolution of the eugeosynclinal terranes in the central Scandinavian Caledonides. John Wiley & Sons Ltd, New York, pp. 953–978.
- Stephens, M. B., Gee, D. G., 1989. Terranes and polyphase accretionary history in the Scandinavian Caledonides. *Geological Society of America, Special Paper* 230, 17–30.
- Stern, R. J., Gwinn, C. J., 1990. Origin of late precambrian intrusive carbonates, eastern desert of Egypt and Sudan: C, O and Sr isotopic evidence. *Precambrian Research* 46 (3), 259–272.)
- Sturt, B., Andersen, T., Furnes, H., 1985. The Skei Group, Leka: an unconformable clastic sequence overlying the Leka Ophiolite. *The Caledonide Orogen*, 395–405.)
- Svensen, H., Jamtveit, B., Banks, D. A., Karlsen, D., Feb. 2001. Fluids and halogens at the diagenetic-metamorphic boundary: evidence from veins in continental basins, western Norway. *Geofluids* 1 (1), 53–70.)
- Thompson, A. B., Connolly, J. A., Jan. 1992. Migration of metamorphic fluid: some aspects of mass and heat transfer. *Earth-Science Reviews* 32 (1–2), 107–121.)
- Thorsnes, T., Grønlie, A., Løseth, H., Roberts, D., Kozlov, N. E., Ivanov, A. A., Tucker, R. D., Nilsen, B. r., 1991. Tectonostratigraphy in the Velfjord-Tosen region, southwestern part of the Helgeland nappe complex, Central Norwegian Caledonides. *Norges geologiske undersøkelse*.)
- Titus, S., Fossen, H., Pedersen, R., Vigneresse, J., Tikoff, B., Aug. 2002. Pull-apart formation and strike-slip partitioning in an obliquely divergent setting, Leka Ophiolite, Norway. *Tectonophysics* 354 (1–2), 101–119.
- Tollo, R. P., Sep. 2010. From Rodinia to Pangea: The Lithotectonic Record of the Appalachian Region. Vol. 206 of *Geological Society of America Memoirs*. Geological Society of America.)
- Trommsdorff, V., Evans, B., 1974. Alpine metamorphism of peridotitic rocks. *Schweiz Mineral Petrogr Mitt* 54, 333–354.)
- Trull, T., Nadeau, S., Pineau, F., Polve, M., Javoy, M., 1993. C-He systematics in hotspot xenoliths: Implications for mantle carbon contents and carbon recycling. *Earth and Planetary Science Letters* 118 (1), 43–64.)
- Tveit, R., 1989. Vulkanologiske og geokjemiske undersøkelser av submarine vulkanitter på Storøya, Leka. Hovedoppgave i geokjemi, Universitetet i Bergen.)
- Vasconcelos, C., McKenzie, J. A., Warthmann, R., Bernasconi, S. M., 2005. Calibration of the $\delta^{18}\text{O}$ paleothermometer for dolomite precipitated in microbial cultures and natural environments. *Geology* 33 (4), 317.)

- Vils, F., Pelletier, L., Kalt, A., Müntener, O., Ludwig, T., Nov. 2008. The Lithium, Boron and Beryllium content of serpentinized peridotites from ODP Leg 209 (Sites 1272A and 1274A): Implications for lithium and boron budgets of oceanic lithosphere. *Geochimica et Cosmochimica Acta* 72 (22), 5475–5504.
- Whitney, D. L., Evans, B. W., Dec. 2009. Abbreviations for names of rock-forming minerals. *American Mineralogist* 95 (1), 185–187.)
- Wickham, S., Janardhan, A., Stern, R., 1994. Regional carbonate alteration of the crust by mantle-derived magmatic fluids, Tamil Nadu, South India. *The Journal of Geology*.)
- Winter, J. D., 2010. *Principles of Igneous and Metamorphic Petrology*. Prentice Hall.
- Wyllie, A. G., Candela, P. A., Burke, T. M., 1987. Compositional zoning in unusual Zn-rich chromite from the Sykesville district of Maryland and its bearing on the origin of 'ferritchromite'. *American mineralogist* 72, 413–422.)
- Wyllie, P., 1977. Mantle Fluid Compositions Buffered by Carbonates in Peridotite-CO₂-H₂O. *Journal of Geology*.)
- Wyllie, P. J., Nov. 1978. Mantle Fluid Compositions Buffered in Peridotite-CO₂-H₂O by Carbonates, Amphibole, and Phlogopite. *The Journal of Geology* 86 (6), 687–713.)
- Yoshinobu, A. S., Barnes, C. G., Nordgulen, O. y., Prestvik, T., Fanning, M., Pedersen, R., 2002. Ordovician magmatism, deformation, and exhumation in the Caledonides of central Norway: An orphan of the Taconic orogeny? *Geology* 30 (10), 883.
- Zane, A., Sassi, R., Guidotti, C., 1998. New data on metamorphic chlorite as a petrogenetic indicator mineral, with special regard to greenschist-facies rocks. *Canadian mineralogist* 36, 713–726.)
- Zane, A., Weiss, Z., Mar. 1998. A procedure for classifying rock-forming chlorites based on microprobe data. *Rendiconti Lincei* 9 (1), 51–56.)
- Zhang, Y., Zindler, A., 1993. Distribution and evolution of carbon and nitrogen in Earth. *Earth and Planetary Science Letters* 117 (3), 331–345.)
- Zharikov, V. A., Pertsev, N. N., Rusinov, V. L., 2007. Metasomatism and metasomatic rocks. Recommendations by the IUGS subcommission on the systematics of metamorphic rocks, 9.)

Appendices

MICROPROBE RESULTS

Table 6: Microprobe analysis of olivine

Rock Type	Peridotite (tectonite)		Peridotite (cumulate)							
Sample nr	LE-12-01		LE-13-02				LE-13-05			
Mineral	Ol	Ol	Ol	Ol	Ol	Ol	Ol	Ol	Ol	Ol
wt%										
SiO ₂	40,65	40,82	41,64	41,84	41,49	41,30	41,41	41,95	41,62	41,98
TiO ₂	0,01	0,00	0,00	0,02	0,00	0,01	0,00	0,00	0,00	0,00
Cr ₂ O ₃	0,00	0,01	0,01	0,00	0,00	0,00	0,00	0,05	0,06	0,05
Al ₂ O ₃	0,00	0,03	0,00	0,00	0,01	0,00	0,03	0,02	0,00	0,00
FeO	9,12	9,15	7,99	7,83	8,07	9,63	8,95	7,46	6,73	7,45
MnO	0,17	0,26	0,22	0,22	0,19	0,23	0,21	0,41	0,38	0,42
NiO	0,42	0,37	0,26	0,24	0,20	0,27	0,30	0,09	0,10	0,09
MgO	49,32	49,29	49,81	50,33	50,39	49,39	49,38	51,04	51,92	51,26
CaO	0,02	0,02	0,02	0,03	0,02	0,05	0,06	0,02	0,01	0,04
Na ₂ O	0,02	0,00	0,00	0,02	0,00	0,03	0,01	0,01	0,01	0,00
K ₂ O	0,00	0,03	0,01	0,01	0,01	0,00	0,00	0,00	0,01	0,00
Total	99,73	99,99	99,96	100,53	100,37	100,91	100,35	101,04	100,83	101,30
Oxygen p.f.u	4	4	4	4	4	4	4	4	4	4
Si	1,00	1,00	1,02	1,01	1,01	1,00	1,01	1,01	1,00	1,01
Ti	0,00	0,00	0,00	0,00	0,00	0,00	0,00	0,00	0,00	0,00
Cr	0,00	0,00	0,00	0,00	0,00	0,00	0,00	0,00	0,00	0,00
Al	0,00	0,00	0,00	0,00	0,00	0,00	0,00	0,00	0,00	0,00
Fe _(tot)	0,19	0,19	0,16	0,16	0,16	0,20	0,18	0,15	0,13	0,15
Mn	0,00	0,01	0,00	0,00	0,00	0,00	0,00	0,01	0,01	0,01
Ni	0,01	0,01	0,01	0,00	0,00	0,01	0,01	0,00	0,00	0,00
Mg	1,80	1,80	1,81	1,82	1,82	1,79	1,79	1,83	1,86	1,83
Ca	0,00	0,00	0,00	0,00	0,00	0,00	0,00	0,00	0,00	0,00
Na	0,00	0,00	0,00	0,00	0,00	0,00	0,00	0,00	0,00	0,00
K	0,00	0,00	0,00	0,00	0,00	0,00	0,00	0,00	0,00	0,00
Total	3,00	3,00	3,00	3,00	3,00	3,00	3,00	3,00	3,00	3,00
Mg#*	0,90	0,90	0,92	0,92	0,92	0,90	0,91	0,92	0,93	0,92

*Mg#: Mg²⁺/(Mg²⁺ + Fe²⁺)

Table 7: Microprobe analysis of serpentine

Rock Type	Peridotite (tectonite)				Peridotite (cumulate)				
Sample nr	LE-12-01				LE-13-02				
Mineral	srp (matrix)		srp (vein)		srp (matrix)		srp (vein)		srp + brc
wt%									
SiO ₂	42,85	43,61	40,96	40,76	43,04	43,04	43,40	43,59	37,65
TiO ₂	0,00	0,00	0,00	0,00	0,00	0,00	0,01	0,01	0,01
Cr ₂ O ₃	0,30	0,07	0,00	0,00	0,11	0,11	0,00	0,03	0,02
Al ₂ O ₃	1,34	0,92	0,03	0,25	1,54	1,54	1,42	1,66	0,00
FeO	3,10	2,37	5,73	6,54	2,40	2,40	1,81	2,08	4,21
MnO	0,00	0,03	0,13	0,16	0,04	0,04	0,05	0,03	0,09
NiO	0,16	0,12	0,00	0,03	0,04	0,04	0,05	0,03	0,21
MgO	38,16	38,48	37,21	36,08	39,05	39,05	39,54	39,46	39,84
CaO	0,06	0,00	0,07	0,08	0,02	0,02	0,02	0,00	0,04
Na ₂ O	0,02	0,02	0,00	0,03	0,03	0,03	0,00	0,01	0,03
K ₂ O	0,01	0,00	0,02	0,06	0,00	0,00	0,00	0,00	0,00
Total	85,997	85,63	84,15	83,98	86,27	86,27	86,304	86,88	82,01
Calculated with	5(O) and 4(OH)								
Si	2,05	2,09	2,02	2,03	2,04	2,04	2,05	2,05	1,87
Ti	0,00	0,00	0,00	0,00	0,00	0,00	0,00	0,00	0,00
Cr	0,01	0,00	0,00	0,00	0,00	0,00	0,00	0,00	0,00
Al	0,08	0,05	0,00	0,01	0,09	0,09	0,08	0,09	0,00
Fe ³⁺	0,00	0,00	0,00	0,00	0,00	0,00	0,00	0,00	0,00
Fe ²⁺	0,12	0,09	0,24	0,27	0,10	0,10	0,07	0,08	0,17
Mn	0,00	0,00	0,01	0,01	0,00	0,00	0,00	0,00	0,00
Ni	0,01	0,00	0,00	0,00	0,00	0,00	0,00	0,00	0,01
Mg	2,73	2,75	2,73	2,67	2,76	2,76	2,80	2,77	2,94
Ca	0,00	0,00	0,00	0,00	0,00	0,00	0,00	0,00	0,00
Na	0,00	0,00	0,00	0,00	0,00	0,00	0,00	0,00	0,00
K	0,00	0,00	0,00	0,00	0,00	0,00	0,00	0,00	0,00
Total	5,00	5,00	5,00	5,00	5,00	5,00	5,00	5,00	5,00
Mg#	0,96	0,97	0,92	0,91	0,97	0,97	0,98	0,97	0,95

Table 8: Microprobe analysis of serpentine

Rock Type	Peridotite (cumulate)					Serpentinite					
Sample nr	LE-13-01		LE-13-05			LE-11-02					
Mineral	srp (vein)		srp (matrix)			srp (matrix)					
wt%											
SiO ₂	40,66	40,38	44,72	44,55	44,41	44,08	43,03	45,28	42,99	44,72	
TiO ₂	0,01	0,00	0,00	0,00	0,00	0,00	0,01	0,02	0,00	0,02	
Cr ₂ O ₃	0,00	0,00	0,02	0,07	0,04	0,03	0,07	0,02	0,26	0,09	
Al ₂ O ₃	0,02	3,03	0,28	0,51	0,63	0,52	1,23	0,01	1,48	0,33	
FeO	1,85	2,60	1,88	1,42	1,96	3,93	5,80	3,70	5,81	5,74	
MnO	0,07	0,02	0,03	0,02	0,06	0,05	0,09	0,02	0,06	0,03	
NiO	0,03	0,07	0,07	0,06	0,01	0,20	0,22	0,14	0,25	0,24	
MgO	40,04	37,55	40,12	40,00	40,19	38,10	36,72	39,13	36,91	37,32	
CaO	0,03	0,03	0,00	0,01	0,00	0,01	0,01	0,02	0,00	0,02	
Na ₂ O	0,00	0,02	0,00	0,00	0,03	0,00	0,02	0,04	0,01	0,00	
K ₂ O	0,00	0,01	0,00	0,02	0,00	0,03	0,00	0,00	0,00	0,00	
Total	82,71	83,71	87,11	86,66	87,32	86,94	87,19	88,39	87,76	88,52	
Calculated with	5(O) and 4(OH)										
Si	1,99	1,97	2,10	2,10	2,08	2,10	2,06	2,12	2,05	2,11	
Ti	0,00	0,00	0,00	0,00	0,00	0,00	0,00	0,00	0,00	0,00	
Cr	0,00	0,00	0,00	0,00	0,00	0,00	0,00	0,00	0,01	0,00	
Al	0,00	0,18	0,02	0,03	0,03	0,03	0,07	0,00	0,08	0,02	
Fe ³⁺	0,00	0,00	0,00	0,00	0,00	0,00	0,00	0,00	0,00	0,00	
Fe ²⁺	0,08	0,11	0,07	0,06	0,08	0,16	0,23	0,15	0,23	0,23	
Mn	0,00	0,00	0,00	0,00	0,00	0,00	0,00	0,00	0,00	0,00	
Ni	0,00	0,00	0,00	0,00	0,00	0,01	0,01	0,01	0,01	0,01	
Mg	2,92	2,74	2,81	2,81	2,80	2,70	2,62	2,73	2,62	2,63	
Ca	0,00	0,00	0,00	0,00	0,00	0,00	0,00	0,00	0,00	0,00	
Na	0,00	0,00	0,00	0,00	0,00	0,00	0,00	0,00	0,00	0,00	
K	0,00	0,00	0,00	0,00	0,00	0,00	0,00	0,00	0,00	0,00	
Total	5,00	5,00	5,00	5,00	5,00	5,00	5,00	5,00	5,00	5,00	
Mg#	0,98	0,96	0,97	0,98	0,97	0,94	0,92	0,95	0,92	0,92	

Table 9: Microprobe analysis of serpentine

Rock Type	Serpentinite		Talc-carbonate group one			
Sample nr	LE-11-02		LE-12-02		LE-13-04	
Mineral	srp (matrix)		srp (vein)		srp	
wt%						
SiO ₂	44,78	45,13	45,75	40,61	42,88	42,78
TiO ₂	0,01	0,00	0,00	0,00	0,00	0,00
Cr ₂ O ₃	0,00	0,04	0,24	0,27	0,02	0,05
Al ₂ O ₃	0,08	0,03	2,49	3,82	1,28	1,20
FeO	5,75	5,49	7,88	8,94	7,82	7,96
MnO	0,07	0,04	0,06	0,01	0,03	0,05
NiO	0,27	0,16	0,16	0,14	0,10	0,10
MgO	37,30	37,57	31,94	32,81	34,68	34,58
CaO	0,00	0,01	0,01	0,03	0,02	0,02
Na ₂ O	0,00	0,02	0,00	0,00	0,03	0,03
K ₂ O	0,01	0,00	0,03	0,02	0,01	0,01
Total	88,28	88,48	88,55	86,64	86,86	86,78
Calculated with	5(O) and 4(OH)					
Si	2,12	2,13	2,21	1,99	2,09	2,08
Ti	0,00	0,00	0,00	0,00	0,00	0,00
Cr	0,00	0,00	0,01	0,01	0,00	0,00
Al	0,01	0,00	0,14	0,22	0,07	0,07
Fe ³⁺	0,00	0,00	0,00	0,00	0,00	0,00
Fe ²⁺	0,23	0,22	0,32	0,37	0,32	0,32
Mn	0,00	0,00	0,00	0,00	0,00	0,00
Ni	0,01	0,01	0,01	0,01	0,00	0,00
Mg	2,63	2,64	2,30	2,40	2,51	2,51
Ca	0,00	0,00	0,00	0,00	0,00	0,00
Na	0,00	0,00	0,00	0,00	0,00	0,00
K	0,00	0,00	0,00	0,00	0,00	0,00
Total	5,00	5,00	5,00	5,00	5,00	5,00
Mg#	0,92	0,92	0,88	0,87	0,88	0,89

Table 10: Microprobe analysis of talc

Rock Type	Talc-carbonate group one							Talc-carbonate group 2	
Sample nr	LE-11-01				LE-12-02		LE-13-04		LE-13-03
Mineral	Talc	Talc	Talc	Talc	Talc	Talc	Talc	Talc	Talc
wt%									
SiO ₂	63,69	63,02	63,05	62,40	63,10	61,69	63,20	62,85	62,07
TiO ₂	0,02	0,00	0,01	0,00	0,00	0,00	0,02	0,00	0,00
Cr ₂ O ₃	0,05	0,04	0,00	0,07	0,03	0,02	0,02	0,01	0,07
Al ₂ O ₃	0,08	0,01	0,03	0,14	0,03	0,07	0,04	0,07	0,12
FeO	2,66	2,86	2,12	3,06	3,14	3,23	2,47	2,39	4,81
MnO	0,02	0,00	0,03	0,03	0,04	0,00	0,00	0,00	0,01
NiO	0,39	0,34	0,29	0,32	0,21	0,24	0,11	0,10	0,06
MgO	30,28	29,27	29,70	29,12	29,31	28,90	29,58	28,86	28,13
CaO	0,00	0,02	0,01	0,02	0,04	0,02	0,04	0,04	0,05
Na ₂ O	0,01	0,02	0,03	0,04	0,00	0,04	0,02	0,03	0,04
K ₂ O	0,00	0,00	0,00	0,00	0,01	0,00	0,00	0,02	0,00
Total	97,20	95,60	95,27	95,18	95,89	94,21	95,50	94,36	95,36
Calculated with	20(O) and 4(OH)								
Si	10,28	10,37	10,37	10,37	10,35	10,30	10,38	10,46	10,31
Ti	0,00	0,00	0,00	0,00	0,00	0,00	0,00	0,00	0,00
Cr	0,01	0,00	0,00	0,00	0,00	0,00	0,00	0,00	0,01
Al	0,02	0,00	0,01	0,01	0,01	0,01	0,01	0,01	0,03
Fe ³⁺	0,00	0,00	0,00	0,00	0,00	0,00	0,00	0,00	0,00
Fe ²⁺	0,36	0,39	0,29	0,29	0,43	0,45	0,34	0,33	0,42
Mn	0,00	0,00	0,00	0,00	0,01	0,00	0,00	0,00	0,00
Ni	0,05	0,05	0,04	0,04	0,03	0,03	0,01	0,01	0,04
Mg	7,28	7,18	7,28	7,28	7,17	7,19	7,24	7,16	7,17
Ca	0,00	0,00	0,00	0,00	0,01	0,00	0,01	0,01	0,00
Na	0,00	0,01	0,01	0,01	0,00	0,01	0,01	0,01	0,01
K	0,00	0,00	0,00	0,00	0,00	0,00	0,00	0,00	0,00
Total	18,00	18,00	18,00	18,00	18,00	18,00	18,00	18,00	18,00
Mg#	0,95	0,95	0,96	0,96	0,94	0,94	0,96	0,96	0,94

Table 11: Microprobe analysis of carbonate. Dol = dolomite, Mgs = magnesite and Cal = calcite. Because of low concentrations (<0.01 wt.%) the elements SrO, P₂O₅, BaO, Cl and SO₃ are omitted from the table.

Rock Type	Peridotite (tectonite)		Peridotite (cumulate)			Serpentinite			
Sample nr	LE-12-01	LE-13-01	LE-13-01	LE-13-02	LE-13-02	LE-11-02	LE-11-02	LE-11-02	LE-11-02
Mineral	Cal	Dol	Dol	Dol	Dol	Mgs	Mgs	Mgs	Mgs
wt%									
SiO ₂	0,27	0,35	0,58	0,05	0,09	0,03	0,03	0,07	0,00
FeO	0,11	0,79	0,84	0,91	0,74	5,65	5,43	4,57	6,11
MnO	0,03	0,17	0,15	0,22	0,15	0,54	0,57	0,51	0,68
MgO	0,24	21,50	21,18	20,94	21,09	42,93	43,25	44,03	42,83
CaO	56,20	29,99	29,73	30,69	30,82	0,11	0,12	0,15	0,17
Na ₂ O	0,00	0,01	0,00	0,00	0,00	0,00	0,01	0,00	0,00
Total	56,85	52,78	52,48	52,81	52,89	49,25	49,42	49,33	49,79
Si	0,00	0,01	0,02	0,00	0,00	0,00	0,00	0,00	0,00
Fe ³⁺	0,00	0,00	0,00	0,00	0,00	0,00	0,00	0,00	0,00
Fe ²⁺	0,00	0,02	0,02	0,02	0,02	0,07	0,07	0,05	0,07
Mn	0,00	0,00	0,00	0,01	0,00	0,01	0,01	0,01	0,01
Mg	0,01	0,98	0,97	0,96	0,96	0,92	0,93	0,94	0,92
Ca	0,99	0,98	0,98	1,01	1,01	0,00	0,00	0,00	0,00
Na	0,00	0,00	0,00	0,00	0,00	0,00	0,00	0,00	0,00
Total	2,00	4,00	4,00	4,00	4,00	2,00	2,00	2,00	2,00
Mg#	0,86	0,98	0,98	0,98	0,98	0,93	0,93	0,95	0,93

Table 12: Microprobe analysis of carbonate. Dol = dolomite, Mgs = magnesite and Cal = calcite. Because of low concentrations (<0.01 wt.%) the elements SrO, P₂O₅, BaO, Cl and SO₃ are omitted from the table.

Rock Type	Talc-carbonate group one									
Sample nr	LE-11-01					LE-12-02				
Mineral	Dol		Mgs			Fe-mgs			Fe-mgs	
wt%										
SiO ₂	0,92	1,40	0,07	0,05	0,00	0,06	0,03	0,08	0,00	0,73
FeO	1,13	1,53	1,31	4,12	3,91	3,37	12,29	13,07	12,26	12,80
MnO	0,26	0,24	0,32	0,84	0,83	0,70	0,15	0,05	0,06	0,26
MgO	20,84	21,33	20,95	44,30	44,65	44,81	38,75	37,54	38,25	37,76
CaO	30,03	29,61	29,64	0,21	0,22	0,15	0,26	0,29	0,42	0,28
Na ₂ O	0,02	0,03	0,00	0,04	0,03	0,01	0,00	0,01	0,00	0,02
Total	53,20	54,14	52,29	49,52	49,64	49,10	51,47	51,02	50,99	51,84
Si	0,03	0,04	0,00	0,00	0,00	0,00	0,00	0,00	0,00	0,01
Fe ³⁺	0,00	0,00	0,00	0,00	0,00	0,00	0,00	0,00	0,00	0,00
Fe ²⁺	0,03	0,04	0,03	0,05	0,05	0,04	0,15	0,16	0,15	0,16
Mn	0,01	0,01	0,01	0,01	0,01	0,01	0,00	0,00	0,00	0,00
Mg	0,95	0,96	0,97	0,94	0,94	0,95	0,84	0,83	0,84	0,82
Ca	0,98	0,96	0,99	0,00	0,00	0,00	0,00	0,00	0,01	0,00
Na	0,00	0,00	0,00	0,00	0,00	0,00	0,00	0,00	0,00	0,00
Total	4,00	4,00	4,00	2,00	2,00	2,00	2,00	2,00	2,00	2,00
Mg#	0,97	0,96	0,97	0,95	0,95	0,96	0,85	0,84	0,85	0,84

Table 13: Microprobe analysis of carbonate. Dol = dolomite, Mgs = magnesite and Cal = calcite. Because of low concentrations (<0.01 wt.%) the elements SrO, P₂O₅, BaO, Cl and SO₃ are omitted from the table.

Rock Type	Talc-carbonate group one			Talc-carbonate group two		
Sample nr	LE-13-04			LE-13-03		
Mineral	Fe-mgs		Dol	Dol		
wt%						
SiO ₂	0,02	0,00	0,05	0,02	0,03	0,00
FeO	8,25	11,09	9,42	2,21	3,57	3,55
MnO	0,81	0,04	0,26	0,40	0,32	0,28
MgO	40,40	39,06	39,71	19,40	18,51	18,26
CaO	0,31	0,21	0,49	30,39	31,07	31,09
Na ₂ O	0,00	0,01	0,00	0,00	0,01	0,02
Total	49,79	50,41	49,94	52,42	53,51	53,19
Si	0,00	0,00	0,00	0,00	0,00	0,00
Fe ³⁺	0,00	0,00	0,00	0,00	0,00	0,00
Fe ²⁺	0,10	0,14	0,12	0,06	0,09	0,09
Mn	0,01	0,00	0,00	0,01	0,01	0,01
Mg	0,88	0,86	0,87	0,91	0,86	0,85
Ca	0,01	0,00	0,01	1,02	1,04	1,05
Na	0,00	0,00	0,00	0,00	0,00	0,00
Total	2,00	2,00	2,00	4,00	4,00	4,00
Mg#	0,90	0,86	0,88	0,94	0,90	0,90

Table 14: Microprobe analysis of spinel. Ftc = ferritchromite, mag = magnetite.

Rock Type	Peridotite (tectonite)		Peridotite (cumulate)		Serpentinite		
Sample nr	LE-12-01		LE-13-05		LE-11-02		
Mineral	Ftc	Cr-Spinel	Ftc	Mag	Ftc	Ftc	
wt%							
SiO ₂	0,66	0,02	0,04	0,14	0,04	0,58	0,02
TiO ₂	0,35	0,31	0,31	0,26	0,02	0,40	0,26
Cr ₂ O ₃	28,59	40,58	40,68	33,22	1,76	30,37	17,78
Al ₂ O ₃	0,31	23,24	22,73	0,65	0,01	0,12	0,04
FeO (tot)	62,61	24,47	24,58	54,99	90,90	63,18	76,19
MnO	0,74	1,04	1,05	2,42	0,21	0,60	0,33
NiO	0,43	0,07	0,05	0,11	0,10	0,14	0,31
MgO	2,43	9,59	9,75	4,55	1,48	0,63	0,17
CaO	0,01	0,01	0,00	0,02	0,01	0,03	0,02
V ₂ O ₃	0,11	0,18	0,20	0,07	0,02	0,15	0,15
ZnO	0,30	1,37	1,11	0,43	0,00	0,41	0,18
Total	96,55	100,88	100,50	96,85	94,53	96,58	95,45
Si	0,03	0,00	0,00	0,01	0,00	0,02	0,00
Ti	0,01	0,00	0,01	0,01	0,00	0,01	0,01
Cr	0,84	1,00	1,00	0,95	0,05	0,90	0,53
Al	0,01	0,85	0,84	0,03	0,00	0,01	0,00
Fe ³⁺	1,08	0,13	0,14	0,99	1,94	1,02	1,44
Fe ²⁺	0,86	0,50	0,50	0,68	0,91	0,96	0,97
Mn	0,02	0,03	0,03	0,07	0,01	0,02	0,01
Ni	0,01	0,00	0,00	0,00	0,00	0,00	0,01
Mg	0,13	0,44	0,45	0,25	0,08	0,04	0,01
Ca	0,00	0,00	0,00	0,00	0,00	0,00	0,00
V	0,00	0,00	0,01	0,00	0,00	0,00	0,00
Zn	0,01	0,03	0,03	0,01	0,00	0,01	0,01
Total	3,00	3,00	3,00	3,00	3,00	3,00	3,00
Fe ³⁺ #*	0,56	0,07	0,07	0,50	0,97	0,53	0,73
Cr#**	0,98	0,54	0,54	0,97	1,00	0,99	1,00

*Fe³⁺ / (Fe³⁺ + Cr + Al)

**Cr / (Cr + Al)

Table 15: Microprobe analysis of spinel. Cr-Mag = chromium rich magnetite, ftc = ferritchromite, mag = magnetite.

Rock Type	Talc-carbonate group one						
Sample nr	LE-11-01		LE-12-02		LE-13-04		
Mineral	Ftc		Ftc	Ftc	Cr-spinel	Ftc	
wt%							
SiO ₂	0,63	0,13	0,05	3,44	0,00	0,02	0,03
TiO ₂	0,44	0,37	0,29	0,20	0,07	0,22	0,20
Cr ₂ O ₃	15,29	11,99	33,15	22,59	35,32	27,40	29,96
Al ₂ O ₃	0,07	0,09	0,16	0,38	25,03	0,11	0,46
FeO	77,15	81,65	60,82	63,27	34,71	66,71	63,65
MnO	0,09	0,08	0,24	0,16	0,26	0,22	0,24
NiO	0,24	0,14	0,07	0,08	0,04	0,09	0,06
MgO	0,31	0,26	0,29	3,39	4,08	0,27	0,30
CaO	0,00	0,00	0,01	0,79	0,02	0,02	0,03
V ₂ O ₃	0,46	0,43	0,13	0,12	0,17	0,28	0,25
ZnO	0,12	0,13	0,43	0,21	0,61	0,28	0,32
Total	94,81	95,27	95,64	94,61	100,32	95,61	95,50
Si	0,02	0,01	0,00	0,13	0,00	0,00	0,00
Ti	0,01	0,01	0,01	0,01	0,00	0,01	0,01
Cr	0,46	0,36	1,00	0,66	0,90	0,82	0,90
Al	0,00	0,00	0,01	0,02	0,95	0,01	0,02
Fe ³⁺	1,45	1,59	0,97	1,05	0,15	1,15	1,06
Fe ²⁺	1,01	0,99	0,97	0,90	0,78	0,97	0,97
Mn	0,00	0,00	0,01	0,01	0,01	0,01	0,01
Ni	0,01	0,00	0,00	0,00	0,00	0,00	0,00
Mg	0,02	0,02	0,02	0,19	0,20	0,02	0,02
Ca	0,00	0,00	0,00	0,03	0,00	0,00	0,00
V	0,01	0,01	0,00	0,00	0,00	0,01	0,01
Zn	0,00	0,00	0,01	0,01	0,01	0,01	0,01
Total	3,00	3,00	3,00	3,00	3,00	3,00	3,00
Fe ³⁺ #	0,76	0,82	0,49	0,61	0,07	0,58	0,54
Cr#**	0,99	1,00	0,99	0,98	0,49	0,99	0,98

*Fe³⁺ / (Fe³⁺ + Cr + Al)

**Cr / (Cr + Al)

Table 16: Mineral analysis of clinopyroxene (Wood & Banno Norm) and chlorite.

Rock Type	Peridotite		Talc-carbonate group one		Talc-carbonate group two	
Sample nr	LE-12-01		LE-12-02		LE-13-03	
Mineral	Cpx	Cpx	Chl	Chl	Chl	Chl
wt%						
SiO ₂	53,14	53,56	37,69	37,15	31,96	32,02
TiO ₂	0,10	0,09	0,00	0,01	0,02	0,02
Cr ₂ O ₃	1,00	0,95	1,22	1,49	1,58	1,93
Al ₂ O ₃	2,67	2,68	7,47	7,41	13,87	13,28
FeO	2,19	2,20	8,78	8,79	8,36	9,07
MnO	0,11	0,05	0,00	0,05	0,06	0,07
NiO	0,02	0,07	0,12	0,13	0,09	0,10
MgO	17,30	17,60	31,96	31,93	29,94	29,67
CaO	24,57	23,89	0,04	0,01	0,05	0,06
Na ₂ O	0,28	0,32	0,01	0,01	0,01	0,03
K ₂ O	0,00	0,02	0,04	0,00	0,04	0,03
Total	99,99	100,42	87,32	86,98	85,97	86,27
Calculated with 20(O)16(OH)						
Si	1,90	1,91	13,22	13,09	11,34	11,38
Ti	0,00	0,00	0,00	0,00	0,00	0,01
Cr	0,03	0,03	0,34	0,41	0,44	0,54
Al	0,11	0,11	3,09	3,08	5,80	5,56
Fe ³⁺	0,07	0,05	0,00	0,00	0,00	0,00
Fe ²⁺	0,00	0,01	2,58	2,59	2,48	2,70
Mn	0,00	0,00	0,00	0,02	0,02	0,02
Ni	0,00	0,00	0,03	0,04	0,03	0,02
Mg	0,92	0,94	16,71	16,77	15,84	15,72
Ca	0,94	0,91	0,01	0,00	0,02	0,02
Na	0,02	0,02	0,01	0,01	0,01	0,02
K	0,00	0,00	0,02	0,00	0,02	0,01
Total	4,00	4,00	36,00	36,00	36,00	36,00

SAMPLE LOCALITIES

Table 17: Sample localities with GPS coordinates

Sample	GPS Coordinate	Lithology
LE-11-01	N65°05.544 E11°40.602	Talc-carbonate
LE-11-02	N65°05.544 E11°40.602	Serpentine
LE-12-01	N65°05.580 E11°40.558	Partly altered peridotite from the mantle tectonite
LE-12-02	N65°05.544 E11°39.792	Talc-carbonate
LE-13-01	N65°05.421 E11°40.243	Partly altered peridotite from the cumulate section
LE-13-02	N65°05.440 E11°40.235	Partly altered peridotite from the cumulate section
LE-13-03	N65°05.231 E11°39.821	Blueish talc-carbonate
LE-13-04	N65°05.231 E11°39.821	Talc-carbonate
LE-13-05	N65°05.554 E11°40.614	Partly altered peridotite from the cumulate section